UNIVERSITÉ DU QUÉBEC À MONTRÉAL

OSCILLATIONS MILLÉNAIRES DES CONDITIONS HYDROGRAPHIQUES D'ISFJORDEN, OUEST DU SPITZBERG, AU COURS DE L'HOLOCÈNE, EN RELATION AVEC LA DYNAMIQUE DE LA DÉRIVE NORD-ATLANTIQUE

MÉMOIRE
PRÉSENTÉ
COMME EXIGENCE PARTIELLE
DE LA MAÎTRISE EN SCIENCES DE LA TERRE

PAR
CAMILLE BRICE

AOÛT 2019

UNIVERSITÉ DU QUÉBEC À MONTRÉAL
Service des bibliothèques

Avertissement

REMERCIEMENTS

Je tiens à remercier en premier lieu ma directrice Anne de Vernal qui m'a aidée, guidée et encouragée depuis le baccalauréat jusqu'à aujourd'hui. Je la remercie d'avoir toujours été présente pour me soutenir tout au long de mon cheminement académique, surtout durant les moments les plus difficiles. Toutes les opportunités qu'elle m'a offertes, entre les expéditions en mer et les congrès à l'international, m'ont énormément formée et ont transformé cette maîtrise en une expérience inoubliable. Merci aussi à mon codirecteur Pierre Francus de m'avoir accueillie dans son laboratoire à Québec. Je dois le remercier pour ses connaissances en sédimentologie et pour le partage de ces dernières avec moi. Un grand merci à Matthias Forwick sans qui mon stage à Tromsø n'aurait jamais eu lieu. Mon séjour en Norvège m'a permise de me former en laboratoire, mais aussi de vivre une belle aventure à l'international. Je remercie Matthias d'avoir pris le temps, malgré son horaire très chargé, de m'accueillir et de m'aider durant ce temps et aussi tout au long de mon projet.

Merci à tous les merveilleux étudiants et membres ArcTrain et Geotop. Merci d'avoir écouté mes présentations orales et regardé mes posters à toutes les années. Mais surtout, je n'oublierai pas tous les congrès, les pots, les partys d'Halloween, les Annual Meetings... qui ont été dans les meilleurs moments de ma maîtrise, durant lesquels j'ai fêté et rencontré des personnes incroyables. Merci à mes amis tripeux de plein air et de roches avec qui je peux toujours partir à l'aventure. Une belle pensée pour Dominique (et Miette évidemment) qui rend ma vie beaucoup plus fun et agréable.

Comment survivre dans le laboratoire de micropaléontologie sans la magnifique dame Estelle ? Un énorme merci à cette incroyable responsable de lab qui nous a gardé en vie et en ordre les dernières années, mais surtout un merci à ma grande amie d'être dans ma vie et sans qui le 7e étage serait vraiment plus plate. Et finalement, je pense à ma merveilleuse amie Jade. Celle avec qui j'ai eu la chance de partager le laboratoire et les microscopes pendant d'innombrables heures, à mimer les dinokystes, à danser dans l'habit de HF ou encore à rire jusqu'à en pleurer. Je la remercie pour m'avoir aidée tant pendant le bacc. que pendant la maîtrise, en me rappelant quel est mon objectif, en relisant mes textes ou simplement en étant une amie.

Un grand merci à ma famille de toujours m'encourager dans mes démarches et d'être présente et fière de moi. Un merci spécial à ma sœur Marie-Hélène et à Kevin de m'avoir grandement aidé dans mes analyses statistiques. Sans leur générosité et leur patience, je n'aurais pas pu réaliser tout ce que je voulais pour mon projet. Et pour terminer, le plus grand des mercis à ma belle Alice. Merci d'avoir fait des allers-retours Québec-Montréal, merci pour tes incalculables visites dans mon bureau, merci d'accepter mes sautes d'humeur, merci d'être aussi drôle. Bref, merci de faire partie de ma vie.

AVANT-PROPOS

Ce projet de recherche s'inscrit dans le cadre d'une collaboration avec l'Université de Tromsø (UiT), l'Institut de recherche polaire de Corée (KOPRI), l'Institut National de la Recherche Scientifique et l'Université du Québec à Montréal. Le prélèvement de la carotte à l'étude HH16-1205-GC a été fait à bord du navire de recherche Helmer Hanssen de l'UiT par Matthias Forwick (UiT) et Seung-Il Nam (KOPRI). Les analyses granulométriques ainsi que les analyses sur le carbone organique ont été réalisées par Seung-Il Nam. J'ai contribué au projet en réalisant les mesures géochimiques et physiques, la description lithologique et les analyses palynologiques.

Le mémoire a été construit sous forme d'article scientifique et sera soumis à la revue *Boreas* prochainement. L'article, soit le chapitre 1 du mémoire, est donc rédigé en anglais et a été construit selon les normes de la revue.

TABLES DES MATIÈRES

LISTE DES FIGURES

LISTE DES TABLEAUX

LISTE DES ABRÉVIATIONS

AMOC
: *Atlantic meridional overturning circulation*
Circulation méridienne de retournement de l'Atlantique

AMS
: *Accelerator mass spectrometry*
spectrométrie de masse par accélération

BP
: *Before present*
Avant l'actuel

Cal. a
: *Calibrated year*
Année calibrée

cf.
: *Confer*
Se reporter à

e.g.
: *Exempli gratia*
Par exemple

ca.
: *Circa*
Près de

LISTE DES SYMBOLES

~	*Environ*
°C	Degrés Celcius
cm	centimètre
psu	Unité de salinité (*practical unit salinity*)
SI	Unité de susceptibilité magnétique, valeurs exprimées en masse spécifique
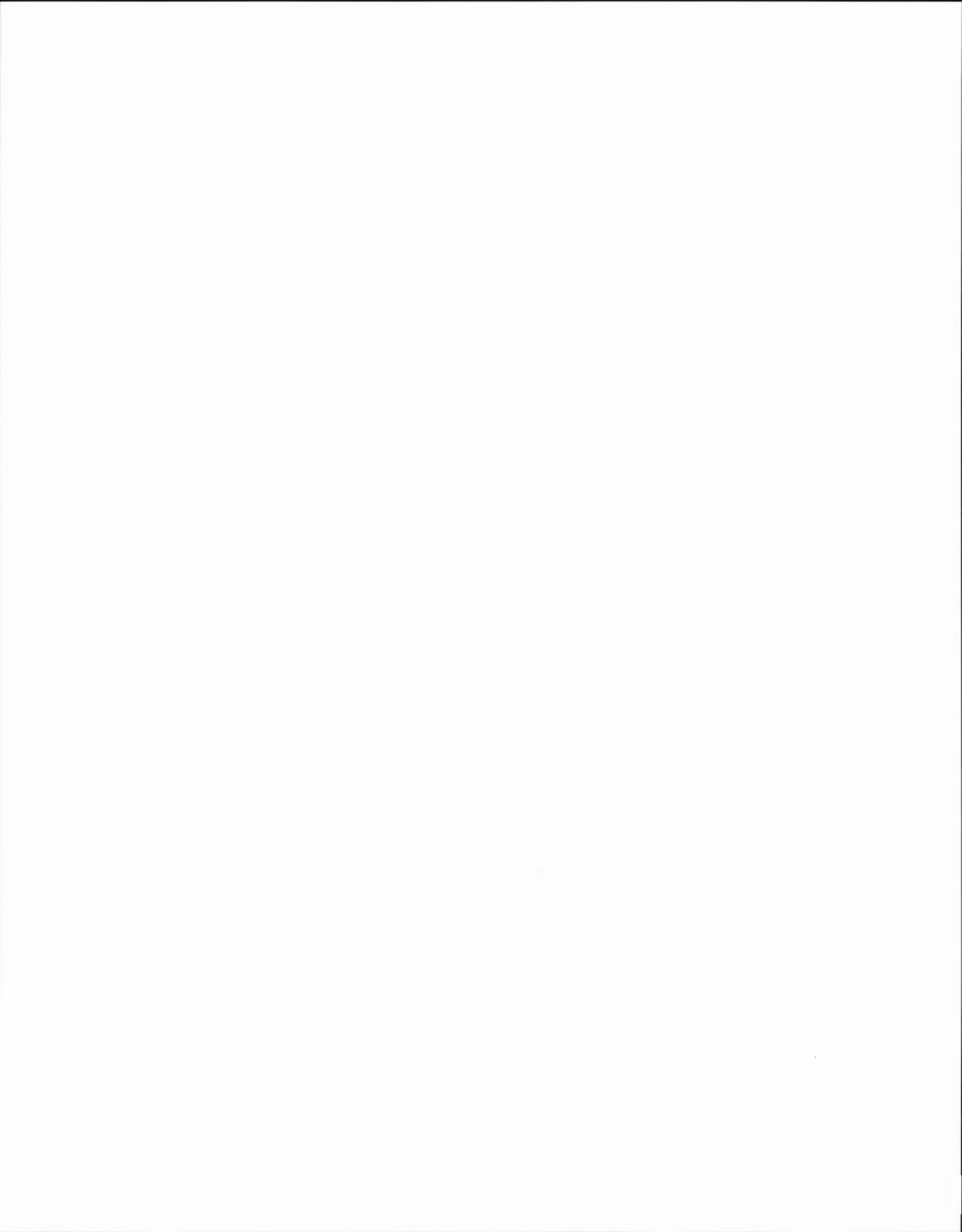
RÉSUMÉ

Les fjords de la côte Ouest du Spitzberg sont des endroits reliant le milieu continental au milieu marin qui enregistrent ainsi l'interaction entre les eaux atlantiques, la glace de mer et les glaciers. Les branches les plus nordiques de la dérive nord-atlantique transportent jusque dans l'Océan Arctique un flux de chaleur, qui limite l'étendue de glace de mer et contrôle le bilan d'énergie entre l'océan et l'atmosphère. L'étude d'une archive sédimentaire (la carotte HH16-1205-GC) du plus grand système de fjord du Spitzberg, Isfjorden, a permis de retracer les variations des conditions hydroclimatiques au cours des derniers 6800 ans.

La période couverte par l'enregistrement couvre de l'Holocène moyen à supérieur qui se caractérise par un refroidissement graduel. Deux phases de refroidissement plus marqués sont enregistrées. Un environnement de glaciers proximaux avec une activité glaciaire importante, des eaux stratifiées mais aussi une productivité primaire élevée caractérisent une première phase de 1000 ans de la carotte, soit de ~ 6800 à 5800 ans BP. À ~ 4000 ans BP, la précipitation de manganèse indique que le milieu devient plus anoxique, probablement en relation avec une diminution de l'intensité du courant profond dans le fjord. Les eaux atlantiques formant la masse d'eau intermédiaire à profonde à cet endroit, la diminution de son advection dans le fjord pourrait avoir causé une anoxie du milieu. Durant l'intervalle de 2000-1200 ans BP, l'augmentation en abondance de deux espèces de dinokystes phototrophes, soit *Spiniferites elongatus* et *Impagidinium pallidum*, révèle un environnement légèrement plus chaud et salin. Durant cette même période, l'environnement redevient aussi plus oxygéné.

Superposées au refroidissement à long terme de l'Holocène, des oscillations des conditions hydrographiques et de la composition des sédiments sont enregistrées. Ces oscillations sont d'échelle millénaire, les périodes variant entre 1100 et 1500 ans. Le couvert de glace présente la variabilité la plus distincte, avec une périodicité d'environ 1250 ans qui est aussi présente dans l'abondance relative d'*Operculodinium centrocarpum* et dans les ratios géochimiques K/Ti et K/Al. Des analyses par ondelettes ont confirmé ce mode de variabilié et indiquent que les oscillations varient légèrement de l'Holocène moyen à l'Holocène supérieur et sembleraient associées à des changements de régime de la dérive nord-atlantique.

INTRODUCTION

Plusieurs études récentes ont démontré que l'Arctique est la région la plus sensible aux variations climatiques actuelles (IPCC, 2014). Différents mécanismes de rétroactions provoquent un réchauffement deux fois plus rapide que la moyenne globale; ce phénomène est nommé l'amplicification arctique (Serreze and Barry, 2011). Le réchauffement accéléré de l'Arctique a des répercussions directes sur le système climatique du globe. Des expériences de modélisation tentent de reproduire ce phénomène, d'évaluer la responsabilité de l'activité humaine et ainsi de prévoir quel sera le climat dans le futur. Toutefois, la variabilité climatique naturelle, en particulier dans les hautes latitudes, reste mal comprise. C'est pourquoi l'étude de l'évolution du climat des régions nordiques au cours de l'Holocène est importante (e.g., Renssen *et al.*, 2005). Les enregistrements instrumentaux étant trop brefs pour comprendre comment le système climatique répond aux grands changements des forçages naturels et anthropiques, des enregistrements de longue durée à partir de traceurs indirects du climat sont très utiles.

Les eaux nord-atlantiques, relativement chaudes et salées, proviennent des basses latitudes et sont transportées vers le nord pour atteindre l'Océan Arctique via le détroit de Fram et la mer de Barents (figure 1.1). Elles représentent la plus importante source de chaleur de l'Océan Arctique (Aagaard *et al.*, 1985). Une variation de l'intensité ou des propriétés de ces masses d'eau influencent donc grandement le climat de la région arctique. En effet, les eaux nord-atlantiques contrôlent en majeure partie les limites du couvert de glace, lui même modifiant l'albedo et les échanges de chaleur entre l'océan et l'atmosphère.

L'archipel de Svalbard, situé entre le détroit de Fram et la mer de Barents, est au centre des interactions entre les eaux atlantiques, les eaux arctiques et la limite de la glace de mer. La marge ouest du Spitzberg, la plus grande île de l'archipel, est sous l'influence directe de ces masses d'eau puisque que les courants Ouest (atlantique) et Est (arctique) du Spitzberg la longent (figure 1.1). Par conséquent, les fjords situés sur la côte ouest du Spitzberg sont des zones d'étude particulièrement intéressantes. Les enregistrements sédimentaires qu'ils renferment fournissent de l'information sur les apports en eau atlantique, la variation de la glace de mer et la position des glaciers continentaux adjacent s'il y a lieu. L'interaction océan-glaciers peut entraîner une réponse climatique régionale (Hald *et al.*, 2011). De plus, les forts apports en sédiment dans les fjords, dus à l'érosion continentale, permettent des enregistrements sédimentaires à haute résolution (Svendsen *et al.*, 1992; Hald *et al.*, 2004, 2011; Forwick et Vorren, 2007, 2009; Baeten *et al.*, 2010; Forwick *et al.*, 2010; Rasmussen *et al.*, 2012).

Plusieurs études ont été réalisées dans les fjords de Svalbard notamment afin de caractériser la dernière déglaciation de la calotte glaciaire Svalbard et de la mer de Barents (Hald *et al.*, 2004, 2011; Forwick *et al.*, 2010; Baeten *et al.*, 2010; Rasmussen *et al.*, 2012; Bartels *et al.*, 2017, 2018). Les fjords représentent en effet les principales voies de drainage des glaciers (Ottesen *et al.*, 2007). Les reconstitutions ont essentiellement été faites à partir de traceurs des masses d'eau profondes et intermédiaires, par exemple les populations de foraminifères (Kucera, 2007; Jorissen *et al.*, 2007). Les données concernant les conditions des eaux de surface sont beaucoup plus limitées ainsi que les connaissances sur les échanges entre les différentes masses de la colonne d'eau. De plus, les enregistrements remontant jusqu'à la déglaciation montrent de grands changements océaniques, qui peuvent masquer des fluctuations plus subtiles.

Dans cette perspective, ce mémoire a pour objectif de reconstituer les conditions océaniques et climatiques d'Isfjorden, le système de fjords le plus important de Svalbard, au cours de l'Holocène moyen et supérieur. Une approche multi-traceurs a été utilisée afin de pouvoir retracer l'histoire glaciaire du Spitzberg, reconstruire les conditions des eaux de profondeur et de surface du fjord pour, par la suite, identifier les liens entre la dynamique de glaciers et de la glace de mer, et des conditions océaniques de l'Atlantique Nord. L'analyse d'une carotte de sédiment prélevée dans le centre d'Isfjorden a permis de réaliser les mesures. L'évolution de la dynamique des glaciers et des masses d'eau profondes a pu être retracée par des analyses non-destructives des propriétés physico-chimiques des sédiments. Les intruments utilisés incluent un scanneur de fluorescence à rayon-X (XRF) mesurant la composition géochimique et le *Multi Sensor Core Logger* (MSCL) pour déterminer la densité et la susceptibilité magnétique. Des analyses destructives telles que la granulométrie et la palynologie ont aussi été réalisées. Les reconstitutions des conditions des eaux de surface ont été faites à l'aide de la technique des analogues modernes (*Modern Analogues Technique*; MAT; Guiot et de Vernal, 2007) à partir d'assemblages de kystes de dinoflagellées (dinokystes). Ces derniers sont des protistes algaires hétérotrophes et/ou phototrophes vivant pour la plupart dans la partie sommitale de la colonne d'eau. Durant leur cycle de vie, certaines espèces forment un kystecomposé de matière organique réfractaire. Les assemblages de dinokystes réflètent la distribution des dinoflagellés et ainsi les paramètres hydrographiques de surface de la colonne d'eau, incluant la température, la salinité, la productivité primaire et le couvert de glace de mer.

Ce projet vise dans un premier temps à amener de nouvelles données paléocéanographiques en zone arctique afin d'augmenter le résolution spatiale et ainsi améliorer les reconstitutions régionales. Il vise dans un deuxième temps à étudier les interactions entre milieux continentaux et marins ainsi qu'entre les masses d'eau à l'aide de l'utilisation de plusieurs indicateurs géochimiques, paléoécologiques et

physiques. L'application de cette approche méthodologique est notamment aussi une contribution dans le domaine car elle permet d'évaluer le comportement de chaque indicateur paéloclimatique utilisé face aux mêmes variations enregistrées.

CHAPITRE I

MILLENNIAL-SCALE OSCILLATIONS OF HYDROGRAPHIC CONDITIONS IN ISFJORDEN, WEST SPITSBERGEN, DURING THE HOLOCENE, IN RELATION TO THE NORTH-ATLANTIC DRIFT DYNAMICS

Camille Brice[1]*, Anne de Vernal[1], Pierre Francus[2], Matthias Forwick[3], Seung-Il Nam[4]

[1] GEOTOP-UQAM, CP 8888 Montréal, H3C 3P8, Canada

[2] Institut National de la Recherche Scientifique, Centre Eau Terre et Environnement, Québec, G1K 9A9, Canada

[3] University of Tromsø, Department of Geology, N-9037, Norway

[4] Korea Polar Research Institute , Incheon 406-840, Republic of Korea

* Corresponding author

ABSTRACT

A high resolution sedimentary record from Isfjorden, West Spitsbergen, was studied to provide insights on the changes in ocean conditions and glacial dynamics of Arctic fjords linked to Atlantic waters inflow during the Holocene. Palynological and sedimentological analysis of core HH16-1205-GC from central Isfjorden allowed to reconstruct sea surface conditions and sedimentary regimes of the last ~6.8 ka. Beside a gradual cooling characterizing the Holocene, two transitions marked the record, one at ~6.8 cal. ka BP and the other at ~4.0 cal. ka BP. Glacial erosion from the inner part of the fjord with an important sea ice cover characterized the first hundred years of the record. Abundant cyst of *Pentapharsodinium dalei* reveals that stratified waters with relatively high productivity also characterized the interval spanning 6.8-6.4 cal. ka BP. During the transition from mid to late-Holocene at about 4.0 cal. ka BP, there was a reduction in water mass oxygenation, likely caused by stratification. From 2.0 to 1.2 cal. ka BP, the geochemical data recorded large amplitude variations while the increase of *Impagidinium pallidum* and *Spiniferites elongatus* in the dinocyst assemblages suggests enhanced Atlantic water inflow. Beside the cold pulses mentioned above, a general cooling trend is observed with general SST decrease from 2.5 to 1.5°C and primary productivity decreases from 750 to 650 gC m^{-2} a^{-1}. Although the reconstructions show noisy variations, the smoothed curves reveal oscillations of sea ice cover, summer temperature and salinity with a millennial pacing. Wavelets analysis and cross-wavelet analysis on K/Ti ratio coupled with sea ice confirmed a relatively strong signal of a 1100 to 1500-year cycle in this record.

Keywords: Fjord, Glaciers, Spitsbergen, Holocene, North Atlantic Drift

1.1 Introduction

Ocean circulation in the North Atlantic Ocean plays a determinant role in the climate system. Warm and saline Atlantic water (AW) transported through the Fram Strait and the Barents Sea by the North Atlantic Drift (NAD) is the principal heat source of the Arctic Ocean (Aagaard et al., 1985). Therefore, the NAD partly controls the sea ice extent, which in turn is a major component on the Northern Hemisphere climate notably because of the ice albedo feedback (e.g., Serreze and Barry, 2011). Furthermore, interaction with sea ice affects salinity and hence the Atlantic Meridional Overturning Circulation (AMOC; e.g., Rudels et al., 1996; Dieckmann and Hellmer, 2010).

The archipelago of Svalbard is located between the Fram Strait and the Barents Sea (76-80°N), in an area making the transition between the Atlantic Ocean and Arctic Ocean (figure 1.1). The Svalbard climate is highly dependent upon the NAD, which flows along its western margin. Any change of the NAD strength and thermal properties, which directly influence the climate, sea ice distribution and glaciers dynamic. Thus, Svalbard is ideally located for studying past climate and ocean hydrography variations in order to better understand the role of NAD on climate-ice-ocean interactions.

Simultaneous reconstructions of ocean and land conditions from marine and terrestrial proxies are possible from the analyses of Arctic fjords sedimentary records. The fjords of western Svalbard are characterized by high temperature and salinity gradients largely determined by inflow of warm and saline North Atlantic waters relative to fresh and cold waters from continental glacier runoff and Arctic coastal waters. Moreover, fjords are characterized by rapid sediment accumulations allowing for high temporal resolution recordings (Svendsen et al., 1992; Hald et al., 2004; Forwick and Vorren, 2007, 2009; Beaten et al., 2010; Rasmussen et al., 2012).

Several studies have been conducted on the western and northern shelves and fjords of Svalbard to investigate the ice sheet dynamic during late Weichselian of the Svalbard/Barents Sea Ice Sheet (SBSIS; Elverhøi et al., 1995; Andersson et al., 2000; Landvik et al., 2005; Ottesen et al., 2007). They suggest that the SBSIS was drained rapidly by fast-flowing ice-streams that filled the fjords. Other studies rather focussed on the deglaciation and Postglacial from the shelf and slope records, which led to reconstruct abrupt and high amplitude changes in hydrological conditions notably in the AW advection (Koç et al., 2002; Rasmussen et al., 2007; Slùbowska-Woldengen et al., 2007). Similar studies conducted in fjords have provided additional information on the response of glaciers to AW variations during the Postglacial (Svendsen and Mangerud, 1997; Forwick and Vorren, 2009, 2010; Beaten et al., 2010; Skirbekk et al., 2010; Hald et al., 2004, 2011; Rasmussen et al., 2012; Bartels et al., 2017). All these studies suggest that the deglaciation was marked by harsh conditions until the warmer period of the Bølling-Allerød that lasted from 14.5 to 12.6 cal. ka BP and was followed by the Younger Dryas (YD) cooling until 11.5 cal. ka BP (Svendsen and Mangerud, 1997; Koç et al., 2002; Rasmussen et al., 2007; Slùbowska-Woldengen et al., 2007; Forwick and Vorren, 2009, 2010; Beaten et al., 2010; Skirbekk et al., 2010; Hald et al., 2011; Rasmussen et al., 2012; Bartels et al., 2017). The early Holocene, starting after the YD, was characterized by optimal conditions until 7.0 cal. ka BP followed by a gradual cooling (Ibid). A transition toward colder conditions marked the beginning of the mid-Holocene (Ibid) and the late-Holocene after 4.0 cal. ka BP (Jennings et al., 2004; Skirbekk et al., 2010; Rasmussen et al., 2012; Svendsen and Mangerud, 1997; Beaten et al., 2010). Such regional paleoclimate inferences were mostly based on reconstructions of paleoceanographical conditions in intermediate and bottom waters, based on benthic foraminifer records (Koç et al., 2002; Rasmussen et al., 2007; Slùbowska-Woldengen et al., 2007; Hald et al., 2004, 2011; Rasmussen et al., 2012; Bartels et al., 2017) with only rare studies of documenting the conditions in the surface layer (Rigual-Hernández et al., 2018). In contrast to the relatively well documented cooling trend characterizing the Postglacial in the

northeast North Atlantic, the millennial climate variability of the Holocene is debated (cf. Debret et al., 2007). Many records show millennial-scale signals in the North-Atlantic region (Bond et al., 1997, 2001; Campbell et al., 1998; Bianchi and McCave, 1999; Klitgaard-Kristensen et al., 2001; Schulz and Paul, 2002; Sarnthein et al., 2003; Giraudeau et al., 2010; Werner et al., 2013), but the nature and origin of the variability is unclear (e.g., Debret et al., 2007; Goslin et al, 2018).

In this paper, we aim at reconstructing past AW variations and glaciers dynamic since the mid-Holocene in central Isfjorden. Multi-proxy analysis on a marine sediment core allowed acquisition of data documenting surface and bottom water conditions as well as glacial activity. Oceanographic parameters at the surface, such as sea surface temperature (SST), sea surface salinity (SSS), productivity and sea ice cover, were estimated based on dinocyst assemblages. Physical properties and geochemical content of the sediment were also measured, providing information on the source of detrital material from erosion, bottom water properties and currents.

1.2   Study area

1.2.1   Physiographic setting

Svalbard is an archipelago located in the Arctic, between 74 and 81°N, and 10 and 35°E (figure 1.1A). It is circled by the Arctic Ocean to the north, the Fram Strait to the west and the Barents Sea to the east. About 60% of Svalbard is covered by glaciers (Hagen et al., 1993, 2003), with many outlet glaciers terminating in the sea. Spitsbergen is the largest island of Svalbard; it represents more than half of the archipelago total area. It is mountainous and its northern and western coasts are composed a large glacially eroded fjords. In these subpolar fjords, sea ice forms during fall-winter and breaks up during summer (Howe et al., 2010). There are also

some coastal areas that are characterized by low-lying bedrock plains often blanketed by raised beaches (Ingolfsson, 2011).

The Isfjorden fjord system is the largest and has the second biggest drainage basin of Spitsbergen (Hagen et al., 1993). It is located in the middle of the western coast of the island (78-79°N; 13-17°E; figure 1.1B). The system is about 100 km long and is composed of the trunk fjord Isfjorden and of thirteen tributary fjords. There are nine tidewater glaciers that terminate into the fjord system. The ice coverage is about 40% of the total fjord system area. Nevertheless, it is the fjord system with the smallest glacier cover of Spitsbergen, relative to its size (Forwick and Vorren, 2009). The mouth of Isfjorden is about 10 km wide and its deepest point is 455 m in the Svensksunddypet (Nilsen et al., 2008). The Isfjorden mouth is wide and has no shallow sill. It is therefore connected directly to the shelf and slope area along West Spitsbergen allowing ocean waters to penetrate into the fjord easily.

1.2.2 Geology

Devonian to Paleogene sedimentary rocks dominate the geology of the Isfjorden system (figure 1.1C; Dallmann et al., 2002). Sandstone, siltstone and shale are observed along the central part of the fjord. The inner part of Isfjorden is composed of limestone, chert, and silicified limestone and sandstone. Metamorphic rocks of the Neoproterozoic, phyllite and schist, occupy the mouth of the fjord. There are intrusive rocks, mostly granite from Caledonian age, north-east of the fjord. Unconsolidated Quaternary marine and glaciofluvial sediments were deposited in the valleys and along the rivers flowing into the fjord (Dallmann et al., 2002).

1.2.3 Oceanography

Two main water masses influence the archipelago of Svalbard, the relatively warm and saline Atlantic water (AW) and the cold Arctic water. The east coast of Svalbard

is dominated by the East Spitsbergen Current (ESC), carrying the Arctic water (figure 1.1B). It comes from the Arctic Ocean and flows southward along the coasts of Nordaustlandet and Spitsbergen, turns around the island and continues flowing northward. The AW (T > 3°C, S > 34.9 psu) is brought by the West Spitsbergen Current (WSC) that flows northward along the continental slope of the west Spitsbergen margin. The WSC is a northern extension of the North Atlantic Drift, a surface current. At the latitude of Spitsbergen (~79°N), AW has lost an important quantity of heat causing the water mass to be denser and dive to the subsurface (Nilsen et al., 2008).

The Isfjorden hydrography is composed of water masses of external and local origins (Fig 1.2). Two external water masses are advected in the system, the AW from the WSC and the Arctic-type water (ArW), which consists in Arctic waters freshened by fjords outflows carried northward along the Spitsbergen coast by the Coastal Current (CC), a modified extension of the ESC. Further off the coast, the WSC flows next to the CC, the Arctic front separating both currents (Loeng, 1991). The AW can reach the fjord mouth but after crossing the CC, leading to the modification of the water mass. Hence, the AW entering the fjord mixes with the ArW, which results in temperature and salinity decrease thus forming the so-called Transformed Atlantic Water (TAW; T > 1°C, S >34.7 psu) (Svendsen et al., 2002; Nilsen et al., 2008). The TAW flows into the fjord through its southern part, below the ArW, and exits in the north (Slùbowska-Woldengen et al., 2007; Nilsen et al., 2008; Rasmussen et al., 2012). The intensity of the AW inflow varies annually and the water is more saline and warmer during summer (Svendsen et al., 2002).

Surface waters (SW; T > 1°C) are mostly local and come from glacial melt and river runoff during spring and summer. They occupy the surface layer that decrease in thickness towards the mouth of the fjord (figure 1.2). Autumn and winter cooling of SW forms local waters (LW; T < 1°C) without notable change in salinity. The winter

cooled waters (WCW; T < -0.5°C, S > 34.4 psu) are also local water masses that forms from brine formation and/or intense cooling of AW. When the WCW become denser than TAW it sinks to the bottom of the fjord. Strong formation of WCW can lead to enhanced inflow of AW the following summer (Nilsen et al., 2008; Rasmussen et al., 2012).

The sea ice cover in the Isfjorden system is seasonal. It forms in winter in the tributary fjords and the inner fjord and stars to break up between April and July. Nine tidewater glaciers drain into the tributary fjords. Generally, the outer part of the fjord is ice free throughout the year (Svendsen et al., 2002; Nilsen et al., 2008; Forwick et al., 2009; Rasmussen et al., 2012).

1.3   Methodology

The 465 cm long gravity core HH16-1205-GC (78°20.813'N, 015°17.11'E) was retrieved from 259 m water depth in central Isfjorden during an expedition onboard the R/V Helmer Hanssen of the University of Tromsø in July 2016.

1.3.1   Sedimentology

Before opening the core, the physical properties were measured using a GEOTEK Multisensor Core Logger (MSCL) at every centimeter along the core. The properties we measured include the bulk density, obtained from gamma rays ^{137}Cs source, magnetic susceptibility, P-wave velocity and amplitude to calculate the fractional porosity. The temperature as well as the diameter of the core was also measured. X-rays photographs were taken of the whole-core sections and on half sections after core opening. A lithological description of the sediments included the visible

variations in grain-size, fossil and clast content, bioturbation, colour and sedimentary structures. Colour information is based on the Munsell Soil Colour Charts.

Half sections were scanned with an Avaatech X-ray Fluorescence (XRF) core scanner for acquiring the geochemical composition of the sediment in a non-destructive way. The XRF core scanner has a rhodium tube permitting the measurement of relative concentration of element between Mg and U. The acquisition of data was made at 10 mm intervals with an exposure time of 10 seconds at a voltage of 10 kV and a current of 1000 µA for Al, Si, S, Cl, K, Ca, Ti, Mn and Fe and at 30kV and 2000 µA with a Pb-thick filter for Rb, Sr and Zr. The XRF data are expressed as counts per time. In order to minimize the matrix effect such as variations in intensities due to uneven surface or a thin water film (Tjallingii et al., 2007; Weltje & Tjallingii, 2008), data are interpreted as elemental ratios rather than absolute values.

After non-destructive measurements, the core HH16-1205-GC was subsampled at every 5 cm and was shipped to the Korean Polar Research Institute (KOPRI) for grain-size analysis. The samples were dried and ~300 mg was collected and treated with 35% H_2O_2 to decompose organic matter. After rinsing with distilled water, the samples were treated with an ultrasonic vibrator for 15 seconds in order to keep them in suspension and facilitate dispersion. Grain-size analysis was then performed at Korea Institute of Geoscience and Mineral Resources, Daejeon, Korea (KIGAM) using a Mastersizer 2000 laser analyzer. It provides the grain-size percentage for several size categories and calculates the percentage of clay, silt, and sand, and median grain size of samples. Grain-size percentage were analysed with the software GRADISTAT (Blott and Pye, 2001) to calculate the mean, the sorting and the distribution mode with different statistic methods.

1.3.2   Chronology

The chronology of core HH16-1205-GC is based on accelerator mass spectrometry (AMS) ^{14}C dates from mixed benthic foraminifers tests and bivalve shells. Radiocarbon dating was performed on the mini radiocarbon dating System (MICADAS) instrument of Alfred Wegener Institute (AWI) in Bremerhaven. The AMS ^{14}C dates are reported using the Libby half-life of 5568 years. A calibration was made using the Marine13 calibration curve (Reimer et al. 2013) with an additional correction (ΔR) of 90 ± 35 for the regional air-sea reservoir (Mangerud and Gulliksen 1975). The age-depth model was computed with the software Bacon 2.2 (Blaauw and Christen, 2011) run under R (R Core Team, 2016). Bacon relies on a Bayesian approach and applies a high number of iterations to create the 'best model' within a confidence interval.

1.3.3   Microfossils analysis

The core HH16-1205-GC was also subsampled at 5 cm intervals for palynological analysis. Each sample was processed according to the standard protocol of de Vernal et al. (2010). One to 2 g were collected and sieved at 106 μm and 10 μm. The dried fraction > 106 μm, mainly composed of detrital material, was weighed and used as a proxy for ice rafting deposition and for hand-picking of biogenic carbonate. The 10-106 μm fraction was used for palynological preparations, which consisted in chemical treatment with HCl (10%) and HF (49%) to dissolve carbonate and silica particles respectively. The residues were mounted on microscope slides with glycerin gelatin. *Lycopodium clavatum* spore tablets were added to the samples to estimate palynomorph concentration (e.g., Mertens et al. 2009).

The palynological analysis consisted of counts and identification of all palynomorphs on the slides, including pollen grains, spores, dinocysts, *Halodinium* and foraminifer organic linings. The observations were made with an optical microscope in

transmitted light at magnifications of X400 to X1000. Reworked pre-Quaternary dinocysts, pollen grains, spores and acritarchs were also counted. A minimum of 300 dinocysts were counted and identified in each sample. The nomenclature of dinocysts follows that of Rochon et al. (1999) and Radi et al. (2013). The relative abundance of dinocyst taxa was expressed as percentages vs. counted dinocysts. Pollen grains and spores were used to quantify terrestrial inputs and reworked palynomorphs as indicators of erosion of old sedimentary material, subsequent transport and re-sedimentation. The concentration of palynomorphs is expressed as number of specimens per gram of sediment. Fluxes were also estimated using sedimentation rates based on ^{14}C dating and the density calculated from MSCL measurements.

1.3.4 Reconstruction of sea surface conditions

Sea surface temperature (SST; °C) in winter and summer, sea surface salinity (SSS; psu) in winter and summer, sea ice cover (months per year >50%) and primary productivity ($gC/m^2/a^1$) were reconstructed from dinocyst assemblages based on the application of modern analogue technique (MAT; Guiot and de Vernal, 2007) using the updated database of the Northern Hemisphere, which includes 1968 reference sites and 71 taxa (de Vernal et al., subm.). MAT is a software package running under R (R Core Team, 2016). The reconstructions were made from the five best modern analogue sites as identified from the calculation of the distance (inversely proportional to the similarity) after log-transformation of percentage data. In the case of the n = 1968 database, the threshold distance for good analogues is 1.2. The sea surface conditions at the five selected modern analogue sites lead to define the maximum, minimum and most probable values associated to the assemblage, which corresponds to the average weighted value inversely to the distance. The distance can be used as indicator of the quality of the reconstruction: the lowest is the distance, the highest is the similarity of the modern analogue situation, and therefore the best is the reliability of the estimate. Tests to evaluate the accuracy of the approach indicate that

errors of prediction are ± 1.4 months/year for the sea ice cover, ± 1.1°C and ± 1.6°C for winter and summer SSTs, ± 2.6 for SSS, and ± 55 gC/m^2/a for productivity.

1.3.5   Time-series analysis and quantitative treatment

Multivariate analysis were made using the R package 'vegan' (Oksanen et al., 2018) in order to extract common trends between dinocyst populations, sea surface parameters and geochemical composition of the sediment. Principal component analysis (PCA) was first applied on the all data. This method use the Euclidean distance and the relationships detected are linear (Borcard et al., 2011). Prior to the analysis, geochemical and environmental data were standardized. Because PCA is a linear method and considers double zeros as resemblances, it is not adapted for species abundance data (Borcard, 2011). Hellinger transformation (Legendre and Gallagher, 2001) of the species abundance data was made to remove this problem. PCA was also applied on a combination of environmental and chemical variables. Redundancy analysis (RDA; Legendre and Gallagher, 2001) was necessary when comparing these data with the dinocyst assemblages, because the percentages of species depend upon the other variables. RDA is a multivariate multiple linear regression followed by a PCA of the table of fitted values. It seeks linear combinations of the explanatory variables (here, sea surface condition or geochemical composition) that explain the variation of the response matrix (dinocyst percentages) (Borcard, 2011).

For estimating the frequency spectrum of our data, we used the Lomb-Scargle periodogram (Lomb, 1976; Scargle, 1982), which is a method for detecting periodic signals on uneven sampled time series. The application for the algorithm was done with the R package 'lomb' (Ruf, 1999). P-values for the highest peak in the periodogram are computed from the exponential distribution.

Wavelets analysis was also done with the R package 'WaveletComp' (Roesch and Schmidbauer, 2018). Since wavelets analysis requires evenly spaced time series, our data was first interpolated using a Fast Fourier Transformation. No detrending was made on the data for the analysis. Wavelets analysis was performed with a time resolution of 1 unit time, a frequency resolution of 1/100, and the 'white.noise' method with 10 simulations. The same arguments were used for cross-wavelets analysis between sedimentological and palynological data, except that the frequency resolution was 1/50 and 5 simulations were made.

1.4 Results

1.4.1 Chronology

The chronology of core HH16-1205-GC was established based on 6 radiocarbon dates of benthic and planktonic foraminifera tests, and bivalve shells (figure 1.3; table 1). The resulting curve revealed relatively constant and high sedimentation rate throughout the core. Hence, it allows extrapolations at the bottom and top of the core. The sedimentation rates varies between 0.055 and 0.095 cm a^{-1}, with a mean rate of ~0.7 cm a^{-1}. The time resolution of our analyses are ~ 10 years for non-destructive analyses and ~ 50 years for palynology and grain size.

1.4.2 Physical properties

The sediment of the whole core HH16-1205-GC is mainly composed of silt and clay. At the bottom of the core slightly coarser material than at the top was recovered, with a median size between 6 and 7.5 μm that decreases to ~5.5 μm towards the top (figure 1.4). The percentage of silt gradually decreases from 65 to ~57 % while the percentage of clay increases from ~33 to 40 % (see supplementary material in Brice

et al., 2019). Sand is nearly absent, varying between 0 and 1%. Some layers containing sand (9-12%) are observed at *ca*. 6.2 and *ca*. 4.4 cal. ka BP.

The grain size distribution mode led to distinguish different sections in the core (figure 1.4). At the bottom of the core, the modes vary between 8.2 and 9.4 µm with peaks at 11.8 µm. At *ca*. 4000 cal. ka BP, there is a transition toward lower values of 8.2 µm with some drops to 7 µm. The distribution mode is 7 µm from *ca*. 2.2 to 1.2 cal. ka BP. In the uppermost interval, from 1.2 to 0.4 cal. ka BP, values are fluctuating between 8.2 and 7 µm.

Bulk density and magnetic susceptibility are generally stable along the core. A slight decrease trend is nevertheless observed with density decreasing from 1.55 to 1.45 g cm^{-3} and magnetic susceptibility from 20 to 13 x 10^{-5} SI upward. Magnetic susceptibly records some variations with high values of 23 x 10^{-5} SI at *ca*. 5.3 cal. ka BP and lower values at 4.3 cal. ka BP. A significant decrease in both bulk density and magnetic susceptibility is recorded from *ca*. 1.25 to 1.1 cal. ka BP with minimum of 1.35 g cm^{-3} and 12 x 10^{-5} SI respectively.

1.4.3   Geochemistry

Measurements of organic carbon reveal high values, which may suggest high productivity and/or low organic matter oxydation. The total organic carbon (TOC) fluctuates between 2 and 2.75% throughout the core with a very slight decreasing trend upward. The Corg:N ratios vary around 10 until 3.0 cal. ka BP and increases gradually to 14-15 afterward. Such Corg:N values indicate a mix origin of the organic carbon with a slight drift toward continental values in the upper half of the core (Meyers, 1997). The CaCO$_3$ content fluctuate between from 0 and 8% with low values until 3.5 cal. ka BP increasing afterward. Carbonates are mostly of detrital origin as indicated by micropaleontological observations. The δ^{13}C values vary

between -24.5 and -25.1 ‰ throughout the core also suggesting a mixture of terrestrial and marine organic matter (Meyers, 1997).

All results from the XRF core scanner are presented as element log-ratios (figure 1.5) to minimize the matrix effects (Tjallingii et al., 2007; Weltje and Tjallingii, 2008). Eleven elements have used in the study (Al, Si, Cl, K, Ca, Ti, Mn, Fe, Rb, Sr and Zr) and plotted vs. their sum (see supplementary material in Brice et al., 2019) in order to better illustrate elements variations. A Loess regression was applied on ratios with a degree of smoothing of span = 0.15 to mitigate the noise in results (Cleveland and Devlin, 1988). The geochemical composition of sediment at the bottom of the core (6.8-5.8 cal. ka BP) shows very high Sr and Ca values. The high Ca concentrations decrease abruptly upward. The Ca/Ti curve shows the same trend as Ca concentration alone, suggesting that its source might not be detrital. Sr/Ca, which is often used to characterize whether the calcium is detrital or pelagic (Rothwell et al., 2015), reveals oscillations indicating the contribution from both sources. K/Al and Fe/Ti show low values with decreasing trends from the bottom until 5.8 cal. ka BP, when both undergo an important increase. K/Ti reflects grain size variations and presents similar but more tenuous trend than Ca/Ti.

At *ca.* 4.2 cal. ka BP, a sharp change is recorded in Mn. Relatively low and stable values of Mn/Fe characterize the lowest part of the core and increase significantly at 4.2 cal. ka BP. Higher concentrations of Mn, which is a redox-sensitive element (Rothwell et al., 2015), indicate a shift toward low oxygen bottom conditions until ~1.8 cal. ka BP. Large amplitudes oscillations of Mn characterize the last 2 millennia as well as K/Al and Fe/Ti.

In the upper part of the core encompassing the last 2 ka, all elements used in this study show large amplitude variations. In addition to Mn/Fe, K/Al and Fe/Ti, Fe/Ca also varies with similar frequency although the amplitude is lower. The largest

transition is recorded at 1.2 cal. ka BP, when all ratios mentioned above record a sharp increase.

1.4.4 Palynology

1.4.4.1 Dinocysts and palynomorphs

Palynological counts revealed high dinocyst concentrations ranging between 10,000 and 30,000 cysts/g (figure 1.6). The dinocysts fluxes thus ranging between 1000 and 5000 specimens/cm²/a, up to 10 000 specimens/cm²/a at 6.65 cal. ka BP indicate high productivity. The highest values are recorded at the bottom of the core with fluxes gradually decreasing going upward. The cysts of *Halodinium* sp., which belongs to ciliates and mostly occurs in coastal estuarine environments (Gurdebeke, et al. 2018), is also abundant throughout the core (2000-12,000 specimens/g) and also suggest high productivity. Low occurrence of pollen grains and spores (~ 100 specimens/g) is consistent with the geographical setting of the surrounding environment characterized by arctic tundra and glaciers. The concentrations of foraminifera linings range from 1000 to 8000 linings/g. Pollen grains, spores, *Halodinium* sp. and foraminifera linings concentrations show a similar decreasing trend upward as the dinocysts adundance. *Pediastrum* colonies are present but occasionnally, between 0 and 400 individuals/g, and do not show any trend. Reworked palynomorphs abundance is low, ranging from 500 to 3500 specimens/g.

Islandinium minutum largely dominates the dinocysts assemblage of the whole core, with relative abundances varying between 40 and 80%. This is not surprising since *Islandinium minutum* is a species associated with cold conditions (cf. de Vernal et al., 2013), typical of Arctic fjords (Grøsfjeld et al., 2009). Other taxa such as *Brigantedinium* spp., the cyst of *Pentapharsodinium dalei*, *Spiniferites elongatus*, *Operculodinium centrocarpum* and *Impagidinium pallidum* are also present. The lowest few cm of the core, which represents less than a hundred years, are mostly

composed of heterotrophic taxa *Islandinium minutum* and *Brigantedinium* spp, corresponding to ~90% of the assemblage. Above, from *ca.* 6.7 to 6.5 cal. ka BP, there is an abundance peak of the cyst of *Pentapharsodinium dalei*, up to 47%. At 6.5 cal. ka BP, cyst of *Pentapharsodinium dalei* drops to 20% while *Islandinium minutum* increased to >60%. Following this interval, the assemblages show relatively uniform assemblages dominated by *Islandinium minutum* (75%) and *Brigantedinium* spp. (15%), accompanied by *Impagidinium pallidum*, *Operculodinium centrocarpum* and *Spiniferites elongatus*. Between 4.8 and 3.6 cal. ka BP, an increase is recorded in relative abundance of *Brigantedinium* spp (30-40%) at the expense of *Islandinium minutum* (~60%). The interval spanning 2.0-1.3 cal. ka BP is characterized by an increase in the phototrophic taxa *Spiniferites elongatus* (9-13%) and *Impagidinium pallidum* (4-7 %), and a small decrease of *Islandinium minutum* (50%). Both *Spiniferites elongatus* and *Impagidinium pallidum* are characteristic of surface sediment from the Nordic seas under the influence of relatively warm and saline AW (Bonnet et al., 2010). From 1.3 cal. ka BP to present, the assemblages are similar to those of the interval from 6.5 to 2.0 cal. ka BP.

1.4.4.2 Sea surface conditions reconstructions

The application of MAT yielded reconstructions with five close analogues for every sample. The distance between fossil spectra and modern analogues never exceeded the value of 0.35. The analogues come from different areas, including the Baffin Bay and the Fram Strait, which results in noisy estimates of sea-surface parameters. A Loess regression was applied to the reconstructed sea surface conditions in order to better visualize the trends, with a degree of smoothing of span=0.15. Yet, the smoothed MAT results (figure 1.7) revealed fairly stable sea surface conditions along the study interval, although cyclical variation can be observed.

The base of the core (6.8-6.7 cal. ka BP) starts with a sharp increase in spring and summer sea surface productivity, from 300 to 950, and from 500 to 1100 gC/m^2/a,

respectively. Summer SST shows an increase from 0 to 4.5 °C while winter SST remained steady close to the freezing point. The SSS decrease from 31 to 30.5 in summer and 33.5 to 32 in winter. Sea ice cover is ~9.5 months/year at the bottom of the core but immediately decrease to 7 months/year after. All maximum or minimum values in surface parameters are recorded between 6.7 and 6.6 cal. ka BP, which coincides with maximum percentages of the cyst of *Pentapharsodinium dalei*.

High fluctuations are recorded in summer SST, SSS and in productivity between 6.6 and 6.2 cal. ka BP. During that period, winter and summer SSS increase to ~33.2 and ~32.4 psu respectively, summer SST decrease to 2.3°C and productivity to 750 gC/m²/a. Sea ice cover seems more stable, but decreased to 6 months/year until 6.2 cal. ka BP. Afterward, sea surface conditions show mainly stable values, except the sea ice cover recording very high amplitude and frequency variations, between 5 and 9 months/year until the top of the core. Winter and summer SSS have close values until *ca.* 3.6 cal. ka BP, when summer SSS decreases to ~32 psu and winter SSS increases to ~33.5 psu. Summer SST shows a decreasing trend throughout the core, from ~2.5 to ~1.5 °C. A decreasing trend is also observed for summer productivity, from ~ 750 to ~ 650 psu. A more distinct cooling is recorded in the last hundred years since about 700 years ago .

1.4.5 Statistical analysis

1.4.5.1 Multivariate analysis

Principal component analysis applied on the XRF sum ratios led to identify 3 principals poles (see supplementary material). The first pole groups all detrital elements, including Si, Al, K, Ti, Rb and Zr. The second one is composed of Fe, Mn and Cl. Ca and Sr are forming the last pole.

PCA made on the chemical data and sea surface conditions revealed similar variance between sea ice cover and the ratios Ca/Ti and K/Ti with negative scores of the axis 1 explaining 30% of the total variance (figure 1.8a). All other variables have positive axis 1 values. Sea ice cover is opposed to the other sea surface parameters on both axis. The same situation is observed for Ca/Ti and K/Ti compared to all other ratios. PC 1 seems to explain more the XRF data as their values are larger. Ca/Ti and K/Ti are the ratios that show the highest values at the bottom of the core, which is likely reflected on the first axis. PC 2 possibly represents the temperature since SSTs are rather aligned along that axis and all water parameters increase when it is positive except sea ice cover.

Redundancy analysis was also made on dinocysts assemblage and XRF ratios. The RDA model could only explain 21% of the total variance, which is the amount of variance of the species explained by the XRF data. However, RDA axes 1 and 2 are statistically significant and therefore show relevant information. The biplot (figure 1.8c) shows three general groups of variables. On RDA axis 1 (12% variance explained), the cysts of *Pentapharsodinium dalei* and the ratios K/Ti and Ca/Ti are grouped together on the positive side. *Spiniferites elongatus*, *Brigantedinium* spp., Sr/Ca and K/Al are located on the opposite side. The group mainly composed of Mn/Fe, Fe/Ti and *Islandinium minutum* is rather expressed by the RDA axis 2 since it is more or less on the zero value of the first axis.

1.4.5.2 Spectral analysis

The application of the algorithm Lomb-Scargle periodogram highlighted different oscillations within the time series (figure 1.9). Two strong signals were detected for periods around 1260 and 1580. In the XRF data, there is a periodicity of 1269 years for K/Al and K/Ti and of 1587 years for Fe/Ti. The analysis of the relative abundance of *Operculodinium centrocarpum* highlighted a periodicity of 1582 years. When smoothing the sea ice cover estimates, the Lomb-Scargle periodogram revealed a

periodicity of 1265 years. The same cycle was detected in dinocysts concentrations. Oscillations with similar periods are also discernible from the analyses of the other sea surface parameters, but they are not as clear.

Distinct periodic signals have also been identified for several parameters using the wavelets analysis (figure 1.10). Sea ice cover exhibits a stable cycle of ~1300 years between 6.8 and 2.0 cal. ka BP. Another clear and straightforward signal is also detected with a periodicity of 150 years. Both winter SST and SSS have a clear 1300-year cycle and a 'wavy' 150-year cycle throughout the core. Similar oscillations between sea ice cover, winter SSS and SST are not surprising since these parameters correlate together. A period of ~1300 years is also observed in the relative abundance of *Operculodinium centrocarpum* from 6.8 to 1.5 cal. ka BP. Dinocyst concentrations show a periodicity of ~ 1700 years, during the mid-Holocene. At *ca.* 3.5 cal. ka BP, the periodicity decreases to ~1500 years. Three XRF ratios showed interesting but less clear signals. Fe/Ti exhibits an oscillation with a period of ~ 1300 years over the last 3.5 ka. K/Ti have a decreasing periodicity from ~1500 years at the base of the core to ~1100 years in the upper part of the sequence. Results for K/Al show a weak periodicity of ~1100 years but a stronger one seems to occur at ~700 years.

Cross-wavelets analysis on K/Ti coupled with the sea ice cover revealed a very clear and stable periodic signal of ~1200 years. Both parameters are in opposite phase until 4.0 cal. ka BP, but are in phase after 3.0 cal. ka BP. A cycle with a period of 1500 years until 4.0 cal. ka BP in Fe/Ti appears to be in opposite phase with SST. From 4.0 cal. ka BP to present both Fe/Ti and SST are clearly in phase with a 1200-year cycle.

1.5   Discussion

1.5.1   Holocene transitions and major changes

1.5.1.1   Mid-Holocene transition (6.8 – 5.8 cal. ka BP)

Very high concentrations of Ca, as well as relatively high concentrations of Sr characterize the bottom of the core. The highest content of these elements are observed at ~6.8 cal. ka BP. However, the provenance of high Ca and Sr concentrations is not clear. Similarity between Ca variations and Ca/Ti ratio usually suggests non-detrital origin, but low $CaCO_3$ content contradicts XRF indicators. An explanation might be a change in the main source of detrital sediments. The bedrock of the inner part of the fjord, north-east of the study site, is mainly carbonate rocks and evaporites. Hence, during the mid Holocene transition, sediments were probably coming from this region, which was occupied by fast-flowing ice streams during the last deglaciation (Ottesen, 2007). Glaciers from central Spitsbergen were probably more proximal to our site. The glaciers would have then gradually retracted, becoming distal, thus resulting in decreased input of sediments from this area, hence Ca and Sr content in our core. High values of K/Ti can support this hypothesis since the highest values were recorded at the bottom of the core. K/Ti has been used as a proxy for identifying continental (K) vs. ocean (Ti) sediment provenance in Iceland region (Richter et al., 2006). Isostasy could have also played a role in the changes of sedimentary source as well as glacial activity, which could explain the apparent contradiction in the XRF data. The results from MAT suggest quasi-perennial sea ice cover (8-9 months/a) at the base of the core followed by very rapid decrease down to ~ 6.6 months/a at *ca.* 6.2 cal. ka BP. This would be compatible with a change in the sedimentary regime.

Very high percentages of the cyst of *Pentapharsodinium dalei* were recorded between 6.7 and 6.5 cal. ka BP. With percentage going up from 3 to 47 % and then going

down to almost zero, this interval reveals a very abrupt and brief change in sea surface conditions. The cyst of *Pentapharsodinium dalei* is common in Arctic and sub-Arctic regions that occur in a wide range of salinity condition (e.g. Matthiessen et al., 2005; de Vernal et al., 2013). It was used as an indicator of stratification in surface water related to supply of freshwater from glaciers, as well as indicator of high primary productivity in Svalbard fjords (Grøsfjeld, 2009). The dominance of this species in the dinocyst assemblage is also consistent with the geochemical results suggesting that the inner part of the fjords may have deliver meltwater with high nutrient content to the study site.

The major changes recorded at the basis of the core, might have started before 6.8 cal. ka BP. It is therefore difficult to fully describe the changes without the recovery of older material. Nevertheless, the results from XRF and palynology point to a transition during an interval marked by cold conditions and ice proximal environment (figure 1.11). This interval at the transition between early and mid-Holocene has been defined by a change in the foraminiferal fauna interpreted as a cooling in many studies of the northern North Atlantic(Hald et al., 2004; Jennings et al., 2004; Beaten et al., 2010; Skirbekk et al., 2010; Rasmussen et al. 2012). The strong influence of AW during the early Holocene has been suggested for the Svalbard shelf and slope (Slùbowska et al., 2005; Slùbowska-Woldengen et al., 2007, 2008; Rasmussen et al., 2007; 2012; Skirbekk et al., 2010) while the onset of the regional cooling started right after at *ca.* 9.0 ka BP (Birks, 1991; Wohlfarth et al., 1995; Sarnthein et al., 2003; Hald et al., 2004; Rasmussen et al., 2007; Forwick et al., 2009). Another cooling occurred at *ca.* 7.4-7.2 cal. ka BP, when the inflow of AW diminished, leading to a cold environment with lower salinity. Skirbekk et al. (2010) reconstructed a cooling in Kongsfjorden during this period although productivity and diversity remained high. The authors concluded that minor reduction of AW inflow caused a reduction of the salinity. This cooling over Svalbard was apparently more important in the surface water (Sarnthein et al., 2003) than in subsurface waters which remained under the

AW influence (Slùbowska et al., 2005; Slùbowska-Woldengen et al., 2007, 2008; Rasmussen et al., 2007; 2012). The abundance of *Pentapharsodinium dalei* in our record at around 6.6 cal. ka BP also points to high productivity and low salinity. Increased glacial activity during mid-Holocene was revealed by IRD in central Isfjorden (9.0-4.0 cal. ka BP; Forwick et al., 2009) and in the tributary fjord Billefjorden at 7.9 cal. ka BP (7930-5460 cal. ka BP; Beaten et al., 2010). Even though ice rafting does not confirm the influence of surrounding tidewater glaciers, the timing of high IRD content in other Svalbard records and the high Ca concentration in core HH16-1205-GC support the hypothesis of enhanced glacial activity at regional scale.

1.5.1.2 Mid-Late Holocene transition (4.4 – 3.8 cal. ka BP).

The grain size have led to identify a shift at 4.0 cal. ka BP. There is a high peak in the median size, followed by a decrease observed in the percentage of silt and in the grain size distribution mode. This is mainly caused by a peak followed by a decrease in the sand content. Various XRF ratios also indicate changes in sediment chemistry at that time. The ratio Mn/Fe, which increased sharply at ~4.2 cal. ka BP, points to a modification in the oxygenation of the water mass. As Mn and Fe are redox-sensitive, an increase in Mn/Fe indicates a switch to low oxygen bottom conditions (Rothwell, 2015). Stratification of the water column, a more permanent sea ice cover or a change in the bottom current can prevent water masses from mixing, thus causing a reduction of bottom water ventilation. The Fe/Ti ratio, which can be used to identify variations in sediment delivery (Rothwell, 2015), shows an important shift at ~4.4 cal. ka BP. Between 4.4 and 4.2 cal. ka BP, a major jump is also observed in K/Al. Hence, all sgeochemical data points toward a change in bottom water conditions between 4.4 and 4.0 cal. ka BP. Changes in sea surface conditions also occurred following this interval. At *ca.* 3.8 cal. ka BP, the seasonal contrasts of SSS increased while sea ice cover decreased significantly. Dinocysts assemblages, which were dominated by

Islandinium minutum (~80%) record an increase of *Brigantedinium* spp., from ~15 to 40% between 4.8 and 3.8 cal. ka BP. When co-dominant, these two species reflect cold conditions and the presence of Arctic Water (e.g., Matthiessen et al., 2005; Grøsfjeld et al., 2009; de Vernal et al., 2013).

The transition between the mid and late-Holocene at ~4.0 cal. ka BP has been described as another cooling step in the gradual Holocene cooling at the scale of the northeastern North Atlantic and around Svalbard area (Jennings et al., 2004; Skirbekk et al., 2010; Rasmussen et al., 2012). In Isfjorden fjord system, it has been suggested that the glaciers in Billefjorden area started the regrowth (Svendsen and Mangerud, 1997; Beaten et al., 2010). Forwick and Vorren (2009) observed a diminution of the IRD flux at 4.0 cal. ka BP which they associate to enhanced formation of fast ice and denser sea ice cover. Reduced drift of iceberg can have been caused by the entrapment of icebergs close to the calving fronts in the tributaries fjords. However, the study from Hald et al. (2004) rather suggests a reduced tidewater glaciation during the late Holocene in Van Mijenfjorden, a fjord located about 100 km to the north of Isfjorden.

Physical and chemical data in our study core highlight an important change in the sedimentary regime (figure 1.11). The main cause is however unclear. Reduction of bottom currents, denser sea ice and/or stratification are the most probable candidates. The interval between 4.4 and 3.8 cal. ka BP is characterized by dense sea ice cover for 7-8 months/year and likely corresponds to a cooling event. A few hundred years gap is observed between the changes in recorded by geochemical tracers and those of sea surface conditions. Hence, there seems to be a relationship in the climatic and oceanic variations as suggesteded by Forwick and Vorren (2009), but with a notable delay.

1.5.1.3 From 2.0 cal. ka BP to present.

The time interval between 2.0 and 1.2 cal. ka BP was marked by an increase in the phototrophic taxa *Spiniferites elongatus* and *Impagidinium pallidum*. The occurrence of these species at the expense of *Islandinium minutum* indicates more oceanic conditions and lesser sea ice cover thus suggestingenhanced influence of AW (e.g., Bonnet 2011; de Vernal et al., 2013). Summer SST gained ~1°C while sea ice cover reduced by ~ 1.5 months/year during this interval. With an offset of ~300 years, a change is also observed in most geocheminal ratios, especially Mn/Fe, K/Al and Fe/Ti, which dropped between 1.7 and 1.2 cal. ka BP. The fluctuations in dinocysts assemblage and geochemical content may be connected and linked to an intensification of the AW advection. The preservation of foraminifera in Isfjorden improved also by 2.0 cal. ka BP as the proportion of calcareous species, the concentration of agglutinated species and the overall diversity all increased (Rasmussen et al., 2012). This indicates periodical increased influence of AW in bottom waters. However, while Rasmussen et al. (2012) deduced dominant AW in bottom and subsurface waters over the last 2 kas from foraminiferal assembages, our dinocyst data rather show a transition to colder conditions at the surface after *ca.* 1.2 cal. ka BP. Sea ice cover gradually increased to 8.5 months/year, thus preventing AW to reach the surface. Corg:N also indicates a slight shift toward more continental values since 1.6 cal. ka BP.

1.5.2 Mode of variability

1.5.2.1 Mid-late Holocene cooling trend

Following early Holocene warm interval, a general cooling with stepwise transitions has been documented by many studies over the Nordic Seas (Koç et al., 2002; Sarnthein et al., 2003, Andersen et al., 2004; Hald et al., 2004; Slùbowska et al., 2005; Rasmussen et al., 2007, 2012; Forwick and Vorren, 2009; Werner et al., 2013). The cooling phases have been dated around 8.2, 7.0 and 4.0-5.0 cal. ka BP.

Bulk density and magnetic susceptibility measured in core HH16-1205-GC show a decreasing trend toward the top, which may either be from compaction of the deeper sediments or from changes in climate conditions. However, grain size analysis also revealed a decrease in median grain size. Summer SST decreased by about 1°C on the average, while sea ice cover gained *ca.* 1 month/a coverage during the mid-late Holocene. Hence, we can consider that Isfjorden also underwent a gradual cooling over the last 7 kas.

1.5.2.2 Millennial-scale cycles

Variations with two major periods have been identified from the Lomb-Scargle analysis performed on sea surface parameters and geochemical data. Sea ice cover reconstruction, percentage of *Operculodinium centrocarpum* and ratios K/Ti and K/Al all show a cyclicity with ~ 1270-year period. A ~ 1590-year period is also detected from the dinocyst concentrations and the ratio Fe/Ti. Wavelets analysis confirmed a strong variability with a pacing around 1300 years, particularly well expressed during the mid-Holocene for sea ice cover, winter SST and K/Ti. On the opposite, Fe/Ti and dinocyst concentration rather show variations with ~1300-year period during the late Holocene. Cross-wavelets analysis of K/Ti versus sea ice cover showed a common periodicity of ~ 1100 years over the entire 7 kas. However, even though the periodicity remained the same, there is a change in the phasing between the two proxies at *ca.* 3500 cal. ka BP. A similar phenomenon is observed in the Fe/Ti versus winter SST. The cyclicity started with 1500 years and slowly decreases to 1200 years, with a change in the phasing at around 4.0 cal. ka BP. The shift in the phasing between the sea surface conditions and chemical composition is synchronised with the second cooling phase described earlier. During the mid-Holocene, both types of indicators are in phase, but they totally change to anti-phase oscillation during the late Holocene. The reason for this change in phasing is however unknown.

Other studies from the North Atlantic region have reported a ~1500-year cycle during the Holocene (Bond et al., 1997; Bianchi and McCave, 1999; Campbell et al., 1998; Mayewski et al., 1997; Sarnthein et al., 2003). However, the periodicities are not constant during the whole period, with cycles apparently shorter during the early Holocene. On the western continental margin of the Barents Sea, a periodicity of 1000-1350 years was identified over the Holocene, except in the early Holocene marked by cycles of ~900 years (Sarnthein et al., 2003). Debret et al. (2007) performed wavelet analysis on the time series of Bond et al. (2001) and highlighted a cyclicity of 1000 years during the first half of the Holocene whereas the cycles of the last 5500 years were characterized by a period of 1500 years. The 1500-year cycles of the Holocene have been initially compared to the Dansgaard/Oeschger (D-O) oscillations that took place during the last glacial period (Bond et al., 1997; Schulz and Paul, 2002). Bond et al. (1997) regarded them as mini D-O cycles with smaller amplitude signals due to smaller ice volumes. However, the linkage between these cycles as well as their cause remained debatable. The climate oscillations of the Holocene were tentatively attributed to solar activity (Bond et al., 2001), to current intensity of the North Atlantic Deep Water (Bianchi and McCave., 1999) and to atmospheric processes related to the North Atlantic Oscillation (Giraudeau et al., 2000).

During the Holocene, the Isfjorden hydrology was under the influence of local factors such as glaciers and the former SBSIS, but it was also sensitive to AW influx. Variability in sea ice extents and *Operculodinium centrocarpum* percentage reflect fluctuations between cold and relatively mild conditions. Sea ice formation depends upon surface salinity and temperature which can vary with insolation and/or AW advections into the fjord. In Svalbard fjords and on the shelf, *Operculodinium centrocarpum* dominates the offshore regions where AW occupies the surface water (Grøsfjeld et al., 2009). The ratio K/Ti has been used as a tracer of North Atlantic current variations near Iceland (Richter et al., 2006; Hodell et al., 2010) as K can be

linked to continental material and Ti to oceanic/basaltic sources. Hence the K/Ti ratio indicates the relative importance of the deposition of basaltic material transported via North-Atlantic current versus the continental material coming from erosion, runoff and ice-rafting. Richter et al. (2006) associated the K/Ti ratio to the DO cycles in Faeroe Margin sediments. The three proxies, reconstructed sea ice, *Operculodinium centrocarpum* and the K/Ti ratios, present the strongest millennial-scale oscillations of our data set and are all closely related to the North Atlantic drift intensities. Hence, we suggest that the oscillations detected from independent tracers in the core HH16-1205-GC are related to the variations in the strength of the AW drift, which is a component of the AMOC (e.g., Kuhlbrodt et al., 2007). Debret et al. (2007) also concluded that during the last 5.5 kas, the strong 1500-year cycle is related to an oceanic internal variability.

1.5.3   Cross-correlation between sedimentological and palynological data

The concentration of Ca and K in the sediment vary with reconstructed sea ice extent. Principal component analysis shows an opposition between Ca/Ti, K/Ti and sea ice cover on one side and all the others variables on the other side of axis 1. This indicates that Ca, K and sea ice vary inversely to the other parameters, including SST. When focussing on sea surface conditions, it is easy to understand that sea ice cover increases when productivity and temperature decrease. Axis 1 probably represents climate conditions. As for Ca and K that are indicators of continental inputs, the source of Ca is probably the inner part of the fjord that is mainly composed of carbonates rocks (see figure 1 C) and the source of K is the continent crust. The cyst of *Pentapharsodinium dalei* is also covariant with Ca/Ti and K/Ti. Even though the redundancy analysis did not show strong covariance between dinocysts assemblage and XRF data, *Pentapharsodinium dalei* along with Ca and K define the axis 1 of the RDA. *Pentapharsodinium dalei* is known in Svalbard fjords to be associated to fresh water supply and stratified waters. Modern assemblages of dinocysts in an Isfjorden

transect have shown that the highest concentration of *Pentapharsodinium dalei* is found in the inner part of the fjord, where the glaciers are the closest and the freshwater supply most important (Grøsfjeld et al., 2009). The high concentration of *Pentapharsodinium dalei* at our study site suggests an ice-proximal type environment during the interval encompassing 6.7-6.5 cal. ka BP, which is consistent with higher glacial activity.

Dinocyst assemblages, palynomorph concentrations and elemental composition revealed interrelated changes. The major events recorded at about 6.8 and 4.0 cal. ka BP were seen in both sedimentological and palynological data. A temporal offset of few hundred years between the two types of indicators was usually observed. While very high Ca content characterized the 6.8-5.8 cal. ka BP time interval, high abundance of *Pentapharsodinium dalei* was recorded between 6.7 and 6.5 cal. ka BP in the micropaleontological assemblages. A significant increase in Mn indicates a change in bottom water conditions. This change is recorded at 250 cm, which is dated of 4.2 cal. ka BP. A few tens of centimeters above, at 235 cm, which corresponds to 400 years, a change at the surface is reconstructed from dinocysts assemblages suggesting an increased contrast between winter and summer SSS. The discrepancies in the timing of Mn and SSS changes might be real, but it might also be related to the mobility of redox-sensitive metal in the pore waters. There is an important remobilization of Mn in the sediment column during the early diagenesis of suboxic sediments (e.g. Klinkhammer et al., 1982). Mn can diffuse in pore waters through the topmost 5 to 40 cm of marine sediments (e.g. Froelich et al., 1979; Mangini et al., 2001).

Correlation between surface water and bottom water/continental indicators was observed through the millennial-scale oscillations. Cross-wavelets analysis performed on sea ice cover and winter SST versus K/Ti and Fe/Ti respectively highlighted phasing and anti-phasing relationships. Before the late Holocene, sea surface

conditions and XRF ratios had a similar periodicity of ~1200 years, but their oscillations were in anti-phase. During the late Holocene, they change to phase oscillations.

1.6   Conclusion

Cross-correlation between palynological and sedimentological data of core HH16-1205-GC provided a better view of the interactions between continental climate, sea ice extent and ocean circulation. During the last 7 ka, central Isfjorden recorded some large amplitude changes and many subtle variations of relatively small amplitude. First, there is a gradual climate deterioration that is marking the mid and late Holocene. Since the early Holocene optimum, a cooling has been recorded in the Nordic Seas and the Svalbard region (Koç et al., 2002; Hald et al., 2004; Slùbowska-Woldengen et al., 2007; Forwick and Vorren, 2009; Rasmussen et al., 2012; Werner et al., 2013). At the bottom of the study core (~6.8 cal. ka BP), important variations in elemental concentration (Ca, Sr, K) and percentages of the cyst *Pentapharsodinium dalei* indicate a cooling occurred at the transition from early to mid Holocene. The subsequent transition to late Holocene, at ~ 4.0 cal. ka BP, has also been recorded in our core. A major shift in Mn concentration and minor variation in Fe and K highlight a change in the ventilation of bottom water in the fjord. Sea surface salinity also indicates changes in the upper water column. A significant warming in surface water was also recorded between 2.0 and 1.2 cal. ka BP.

Beside Holocene long-term major changes, millennial-scale oscillations characterized the hydrology of the fjord. A relatively strong signal of 1200 to 1500-year periodicity characterizes the palynological data, reconstructed sea surface parameters and geochemical data. Even though fjords are affected by local mechanisms, the

millennial oscillations are likely regional as they seem to be linked with changes in intensity of the North Atlantic Drift. Several studies have detected similar signals in the North Atlantic region. However, the origins of millennial cycles during the Holocene are still unclear. There are two schools of thought in the scientific community: the oscillations have an external origin related to solar forcing (e.g., Bond et al., 2001), or they have an internal origin, such as self-oscillation in the thermohaline circulation (e.g., Broecker et al., 2001; McManus et al., 1999; Giraudeau et al., 2000). Our data cannot provide enough information to suggest a mechanism, but the strong signal detected in *Operculodinium centrocarpum*, sea ice cover and K/Ti is indicating that the oscillations are directly linked to the Atlantic water inflow.

1.7   References

Aagaard, K., Swift, J., & Carmack, E. (1985). Thermohaline circulation in the Arctic Mediterranean seas. Journal of Geophysical Research: Oceans, 90(C3), 4833-4846.

Andersen, C., Koc, N., & Moros, M. (2004). A highly unstable Holocene climate in the subpolar North Atlantic: evidence from diatoms. Quaternary Science Reviews, 23(20-22), 2155-2166.

Andersson, T., Forman, S. L., Ingólfsson, Ó., & Manley, W. F. (2000). Stratigraphic and morphologic constraints on the Weichselian glacial history of northern Prins Karls Forland, western Svalbard. Geografiska Annaler: Series A, Physical Geography, 82(4), 455-470.

Baeten, N. J., Forwick, M., Vogt, C., & Vorren, T. O. (2010). Late Weichselian and Holocene sedimentary environments and glacial activity in Billefjorden, Svalbard. Geological Society, London, Special Publications, 344(1), 207-223.

Bartels, M., Titschack, J., Fahl, K., Stein, R., Seidenkrantz, M.-S., Hillaire-Marcel, C., & Hebbeln, D. (2017). Atlantic Water advection vs. glacier dynamics in northern Spitsbergen since early deglaciation. Climate of the Past, 13(12), 1717-1749.

Bianchi, G. G., & McCave, I. N. (1999). Holocene periodicity in North Atlantic climate and deep-ocean flow south of Iceland. Nature, 397(6719), 515.

Birks, H. H. (1991). Holocene vegetational history and climatic change in west Spitsbergen-plant macrofossils from Skardtjørna, an Arctic lake. The Holocene, 1(3), 209-218.

Blaauw, M., & Christen, J. A. (2011). Flexible paleoclimate age-depth models using an autoregressive gamma process. Bayesian analysis, 6(3), 457-474.

Blott, S. J., & Pye, K. (2001). GRADISTAT: a grain size distribution and statistics package for the analysis of unconsolidated sediments. Earth surface processes and Landforms, 26(11), 1237-1248.

Bond, G., Kromer, B., Beer, J., Muscheler, R., Evans, M. N., Showers, W., . . . Bonani, G. (2001). Persistent solar influence on North Atlantic climate during the Holocene. science, 294(5549), 2130-2136.

Bond, G., Showers, W., Cheseby, M., Lotti, R., Almasi, P., Priore, P., . . . Bonani, G. (1997). A pervasive millennial-scale cycle in North Atlantic Holocene and glacial climates. science, 278(5341), 1257-1266.

Bonnet, S., de Vernal, A., Hillaire-Marcel, C., Radi, T., & Husum, K. (2010). Variability of sea-surface temperature and sea-ice cover in the Fram Strait over the last two millennia. *Marine Micropaleontology*, 74(3-4), 59-74.

Borcard, D., Gillet, F., & Legendre, P. (2011). Spatial analysis of ecological data Numerical ecology with R (pp. 227-292): Springer.

Brice, C., de Vernal, A., Francus, P., Forwick, M., & Nam, S.-I. (2019). *Oscillations millénaires des conditions hydrographiques d'Isfjorden, ouest du Spitzberg, au cours de l'Holocène, en relation avec la dynamique de la dérive Nord-Atlantique.* (Maîtrise), Université du Québec à Montréal, Montréal.

Broecker, W. S., Sutherland, S., & Peng, T.-H. (1999). A possible 20th-century slowdown of Southern Ocean deep water formation. *science*, 286(5442), 1132-1135.

Campbell, I. D., Campbell, C., Apps, M. J., Rutter, N. W., & Bush, A. B. (1998). Late Holocene~ 1500 a climatic periodicities and their implications. *Geology*, 26(5), 471-473.

Cleveland, W. S., & Devlin, S. J. (1988). Locally weighted regression: an approach to regression analysis by local fitting. Journal of the American statistical association, 83(403), 596-610.

Dallmann, W. K. (2002). Bedrock map of Svalbard and Jan Mayen (Vol. 33): Norsk polarinstitutt.

de Vernal, A., Bilodeau, G., & Henry, M. (2010). *Techniques de préparation et d'analyses en micropaléontologie.* Les Cahiers du Geotop. Université du Québec à Montréal.

de Vernal, A., Radi, T., Zaragosi, S., Van Nieuwenhove, N., Rochon, A. Allan, E., De Schepper, S., Eynaud, F., Head, M., Limoges, A.,Londeix, L., Marret, F., Matthiessen, J., Penaud, A., Pospelova, V., Price, A. Richerol, T. (subm.). Distribution of common modern dinocyst taxa in surface sediments of the Northern Hemisphere in relation to environmental parameters: the updated n=1968 database. *Marine Micropaleontology*, subm.

de Vernal, A., Rochon, A., Fréchette, B., Henry, M., Radi, T., & Solignac, S. (2013). Reconstructing past sea ice cover of the Northern Hemisphere from dinocyst assemblages: status of the approach. *Quaternary Science Reviews*, 79, 122-134.

Debret, M., Bout-Roumazeilles, V., Grousset, F., Desmet, M., McManus, J. F., Massei, N., . . . Trentesaux, A. (2007). The origin of the 1500-year climate cycles in Holocene North-Atlantic records. *Climate of the Past Discussions*, 3(2), 679-692.

Dieckmann, G. S., & Hellmer, H. H. (2010). The importance of sea ice: an overview. *Sea ice*, 2, 1-22.

Elverhøi, A., Andersen, E. S., Dokken, T., Hebbeln, D., Spielhagen, R., Svendsen, J. I., . . . Forsberg, C. F. (1995). The growth and decay of the Late Weichselian ice sheet in western Svalbard and adjacent areas based on provenance studies of marine sediments. *Quaternary Research*, 44(3), 303-316.

Forwick, M., & Vorren, T. O. (2007). Holocene mass-transport activity and climate in outer Isfjorden, Spitsbergen: marine and subsurface evidence. *The Holocene*, 17(6), 707-716.

Forwick, M., & Vorren, T. O. (2009). Late Weichselian and Holocene sedimentary environments and ice rafting in Isfjorden, Spitsbergen. *Palaeogeography, Palaeoclimatology, Palaeoecology*, 280(1-2), 258-274.

Forwick, M., Vorren, T. O., Hald, M., Korsun, S., Roh, Y., Vogt, C., & Yoo, K.-C. (2010). Spatial and temporal influence of glaciers and rivers on the sedimentary environment in Sassenfjorden and Tempelfjorden, Spitsbergen. *Geological Society, London, Special Publications*, 344(1), 163-193.

Froelich, P. N., Klinkhammer, G., Bender, M. L., Luedtke, N., Heath, G. R., Cullen, D., . . . Maynard, V. (1979). Early oxidation of organic matter in pelagic sediments of the eastern equatorial Atlantic: suboxic diagenesis. *Geochimica et cosmochimica acta*, 43(7), 1075-1090.

Giraudeau, J., Grelaud, M., Solignac, S., Andrews, J., Moros, M., & Jansen, E. (2010). Millennial-scale variability in Atlantic water advection to the Nordic Seas derived from Holocene coccolith concentration records. *Quaternary Science Reviews*, 29(9-10), 1276-1287.

Goslin, J., Fruergaard, M., Sander, L., Gałka, M., Menviel, L., Monkenbusch, J., . . . Clemmensen, L. B. (2018). Holocene centennial to millennial shifts in North-Atlantic storminess and ocean dynamics. *Scientific reports*, 8(1), 12778.

Grøsfjeld, K., Harland, R., & Howe, J. (2009). Dinoflagellate cyst assemblages inshore and offshore Svalbard reflecting their modern hydrography and climate. *Norwegian Journal of Geology/Norsk Geologisk Forening*, 89.

Guiot, J., & de Vernal, A. (2007). Chapter thirteen transfer functions: methods for quantitative paleoceanography based on microfossils. Developments in marine geology, 1, 523-563.

Gurdebeke, P. R., Mertens, K. N., Takano, Y., Yamaguchi, A., Bogus, K., Dunthorn, M., . . . Louwye, S. (2018). The affiliation of Hexasterias problematica and Halodinium verrucatum sp. nov. to ciliate cysts based on molecular phylogeny and cyst wall composition. *European journal of protistology*, 66, 115-135.

Hagen, J. O., Kohler, J., Melvold, K., & Winther, J. G. (2003). Glaciers in Svalbard: mass balance, runoff and freshwater flux. *Polar Research*, 22(2), 145-159.

Hagen, J. O., Liestøl, O., Roland, E., & Jørgensen, T. (1993). Glacier atlas of Svalbard and Jan Mayen.

Hald, M., Ebbesen, H., Forwick, M., Godtliebsen, F., Khomenko, L., Korsun, S., . . . Vorren, T. O. (2004). Holocene paleoceanography and glacial history of the West Spitsbergen area, Euro-Arctic margin. *Quaternary Science Reviews*, 23(20-22), 2075-2088.

Hodell, D. A., Evans, H. F., Channell, J. E., & Curtis, J. H. (2010). Phase relationships of North Atlantic ice-rafted debris and surface-deep climate proxies during the last glacial period. *Quaternary Science Reviews*, 29(27-28), 3875-3886.

Ingólfsson, Ó. (2011). Fingerprints of Quaternary glaciations on Svalbard. *Geological Society, London, Special Publications*, 354(1), 15-31.

Jennings, A. E., Weiner, N. J., Helgadottir, G., & Andrews, J. T. (2004). Modern foraminiferal faunas of the southwestern to northern Iceland shelf: oceanographic and environmental controls. *The Journal of Foraminiferal Research*, 34(3), 180-207.

Klinkhammer, G., Heggie, D., & Graham, D. (1982). Metal diagenesis in oxic marine sediments. *Earth and Planetary Science Letters*, 61(2), 211-219.

Klitgaard - Kristensen, D., Sejrup, H., & Haflidason, H. (2001). The last 18 ka fluctuations in Norwegian Sea surface conditions and implications for the magnitude of climatic change: evidence from the North Sea. *Paleoceanography*, 16(5), 455-467.

Koç, N., Klitgaard-Kristensen, D., Hasle, K., Forsberg, C. F., & Solheim, A. (2002). Late glacial palaeoceanography of Hinlopen Strait, northern Svalbard. *Polar Research*, 21(2), 307-314.

Kuhlbrodt, T., Griesel, A., Montoya, M., Levermann, A., Hofmann, M., & Rahmstorf, S. (2007). On the driving processes of the Atlantic meridional overturning circulation. *Reviews of Geophysics*, 45(2).

Landvik, J. Y., Ingólfsson, Ó., Mienert, J., Lehman, S. J., Solheim, A., Elverhøi, A., & Ottesen, D. (2005). Rethinking Late Weichselian ice-sheet dynamics in coastal NW Svalbard. *Boreas*, 34(1), 7-24.

Legendre, P., & Gallagher, E. D. (2001). Ecologically meaningful transformations for ordination of species data. *Oecologia*, 129(2), 271-280.

Loeng, H. (1991). Features of the physical oceanographic conditions of the Barents Sea. *Polar Research*, 10(1), 5-18.

Lomb, N. R. (1976). Least-squares frequency analysis of unequally spaced data. *Astrophysics and space science*, 39(2), 447-462.

Mangerud, J., & Gulliksen, S. (1975). Apparent radiocarbon ages of recent marine shells from Norway, Spitsbergen, and Arctic Canada. *Quaternary Research*, 5(2), 263-273.

Mangini, A., Jung, M., & Laukenmann, S. (2001). What do we learn from peaks of uranium and of manganese in deep sea sediments? *Marine Geology*, 177(1-2), 63-78.

Mayewski, P. A., Meeker, L. D., Twickler, M. S., Whitlow, S., Yang, Q., Lyons, W. B., & Prentice, M. (1997). Major features and forcing of high‑latitude northern hemisphere atmospheric circulation using a 110,000‑year‑long glaciochemical series. *Journal of Geophysical Research: Oceans*, 102(C12), 26345-26366.

McManus, J. F., Oppo, D. W., & Cullen, J. L. (1999). A 0.5-million-year record of millennial-scale climate variability in the North Atlantic. *science*, 283(5404), 971-975.

Meyers, P. A. (1997). Organic geochemical proxies of paleoceanographic, paleolimnologic, and paleoclimatic processes. *Organic geochemistry*, 27(5-6), 213-250.

Mudie, P. J., & Rochon, A. (2001). Distribution of dinoflagellate cysts in the Canadian Arctic marine region. *Journal of Quaternary Science*: Published for the Quaternary Research Association, 16(7), 603-620.

Nilsen, F., Cottier, F., Skogseth, R., & Mattsson, S. (2008). Fjord–shelf exchanges controlled by ice and brine production: The interannual variation of Atlantic Water in Isfjorden, Svalbard. *Continental Shelf Research*, 28(14), 1838-1853.

Oksanen, J., Blanchet, F. G., Friendly, M., Kindt, R., Legendre, P., McGlinn, . . . Wagner, H. (2018). vegan: Community Ecology Package (Version R package version 2.5-3). Retrieved from https://CRAN.R-project.org/package=vegan

Ottesen, D., Dowdeswell, J. A., Landvik, J. Y., & Mienert, J. (2007). Dynamics of the Late Weichselian ice sheet on Svalbard inferred from high-resolution sea-floor morphology. *Boreas*, 36(3), 286-306.

Radi, T., Bonnet, S., Cormier, M.-A., De Vernal, A., Durantou, L., Faubert, É., . . . Rochon, A. (2013). Operational taxonomy and (paleo-) autecology of round, brown, spiny dinoflagellate cysts from the Quaternary of high northern latitudes. *Marine Micropaleontology*, 98, 41-57.

Rasmussen, T. L., Forwick, M., & Mackensen, A. (2012). Reconstruction of inflow of Atlantic Water to Isfjorden, Svalbard during the Holocene: Correlation to climate and seasonality. *Marine Micropaleontology*, 94-95, 80-90.

Rasmussen, T. L., Thomsen, E., Ślubowska, M. A., Jessen, S., Solheim, A., & Koç, N. (2007). Paleoceanographic evolution of the SW Svalbard margin (76°N) since 20,000 14C a BP. *Quaternary Research*, 67(01), 100-114.

Reimer, P. J., Bard, E., Bayliss, A., Beck, J. W., Blackwell, P. G., Ramsey, C. B., . . . Friedrich, M. (2013). IntCal13 and Marine13 radiocarbon age calibration curves 0–50,000 years cal BP. *Radiocarbon*, 55(4), 1869-1887.

Richter, T. O., Van der Gaast, S., Koster, B., Vaars, A., Gieles, R., de Stigter, H. C., . . . van Weering, T. C. (2006). The Avaatech XRF Core Scanner: technical description and applications to NE Atlantic sediments. *Geological Society, London, Special Publications*, 267(1), 39-50.

Rigual-Hernández, A. S., Colmenero-Hidalgo, E., Martrat, B., Bárcena, M. A., de Vernal, A., Sierro, F. J., ... Lucchi, R. G. (2017). Svalbard ice-sheet decay after the Last Glacial Maximum: New insights from micropalaeontological and organic biomarker

paleoceanographical reconstructions. *Palaeogeography, Palaeoclimatology, Palaeoecology*, 465, 225-236.

Rochon, A., Vernal, A. d., Turon, J.-L., Matthießen, J., & Head, M. (1999). Distribution of recent dinoflagellate cysts in surface sediments from the North Atlantic Ocean and adjacent seas in relation to sea-surface parameters. *American Association of Stratigraphic Palynologists Contribution Series*, 35, 1-146.

Roesch, A., & Schmidbauer, H. (2018). WaveletComp: Computational Wavelet Analysis: R package version 1.1. Retrieved from https://CRAN.R-project.org/package=WaveletComp

Rothwell, R. G. (2015). Twenty years of XRF core scanning marine sediments: what do geochemical proxies tell us? Micro-XRF Studies of Sediment Cores (pp. 25-102): *Springer*.

Rudels, B., Anderson, L., & Jones, E. (1996). Formation and evolution of the surface mixed layer and halocline of the Arctic Ocean. *Journal of Geophysical Research: Oceans*, 101(C4), 8807-8821.

Ruf, T. (1999). The Lomb-Scargle Periodogram in Biological Rhythm Research: Analysis of Incomplete and Unequally Spaced Time-Series. *Biological Rhythm Research*, 30, 178-201.

Sarnthein, M., Van Kreveld, S., Erlenkeuser, H., Grootes, P., Kucera, M., Pflaumann, U., & Schulz, M. (2003). Centennial - to - millennial - scale periodicities of Holocene climate and sediment injections off the western Barents shelf, 75°N. *Boreas*, 32(3), 447-461.

Scargle, J. D. (1982). Studies in astronomical time series analysis. II-Statistical aspects of spectral analysis of unevenly spaced data. *The Astrophysical Journal, 263*, 835-853.

Schulz, M., & Paul, A. (2002). Holocene climate variability on centennial-to-millennial time scales: 1. Climate records from the North-Atlantic realm Climate development and history of the North Atlantic realm (pp. 41-54): *Springer*.

Skirbekk, K., Kristensen, D. K., Rasmussen, T. L., Koç, N., & Forwick, M. (2010). Holocene climate variations at the entrance to a warm Arctic fjord: evidence from Kongsfjorden trough, Svalbard. *Geological Society, London, Special Publications, 344*(1), 289-304.

Ślubowska-Woldengen, M., Koç, N., Rasmussen, T. L., Klitgaard-Kristensen, D., Hald, M., & Jennings, A. E. (2008). Time-slice reconstructions of ocean circulation changes on the continental shelf in the Nordic and Barents Seas during the last 16,000 cal a B.P. *Quaternary Science Reviews, 27*(15-16), 1476-1492.

Ślubowska-Woldengen, M., Rasmussen, T. L., Koç, N., Klitgaard-Kristensen, D., Nilsen, F., & Solheim, A. (2007). Advection of Atlantic Water to the western and northern Svalbard shelf since 17,500cala BP. *Quaternary Science Reviews, 26*(3-4), 463-478.

Ślubowska, M. A., Koç, N., Rasmussen, T. L., & Klitgaard-Kristensen, D. (2005). Changes in the flow of Atlantic water into the Arctic Ocean since the last deglaciation: Evidence from the northern Svalbard continental margin, 80°N. *Paleoceanography, 20*(4), n/a-n/a.

Svendsen, H., Beszczynska-Møller, A., Hagen, J. O., Lefauconnier, B., Tverberg, V., Gerland, S.,... Zajaczkowski, M. (2002). The physical environment of Kongsfjorden–Krossfjorden, an Arctic fjord system in Svalbard. *Polar Research, 21*(1), 133-166.

Svendsen, J. I., & Mangerud, J. (1997). Holocene glacial and climatic variations on Spitsbergen, Svalbard. *The Holocene*, 7(1), 45-57.

Svendsen, J. I., Mangerud, J., Elverhøi, A., Solheim, A., & Schüttenhelm, R. T. (1992). The Late Weichselian glacial maximum on western Spitsbergen inferred from offshore sediment cores. *Marine Geology*, 104(1-4), 1-17.

Tjallingii, R., Röhl, U., Kölling, M., & Bickert, T. (2007). Influence of the water content on X ‐ ray fluorescence core ‐ scanning measurements in soft marine sediments. *Geochemistry, Geophysics, Geosystems*, 8(2).

Weltje, G. J., & Tjallingii, R. (2008). Calibration of XRF core scanners for quantitative geochemical logging of sediment cores: theory and application. *Earth and Planetary Science Letters*, 274(3-4), 423-438.

Werner, K., Spielhagen, R. F., Bauch, D., Hass, H. C., & Kandiano, E. (2013). Atlantic Water advection versus sea-ice advances in the eastern Fram Strait during the last 9 ka: Multiproxy evidence for a two-phase Holocene. *Paleoceanography*, 28(2), 283-295.

Wohlfarth, B., Lemdahl, G., Olsson, S., Persson, T., Snowball, I., Ising, J., & Jones, V. (1995). Early Holocene environment on Bjørnøya (Svalbard) inferred from multidisciplinary lake sediment studies. *Polar Research*, 14(2), 253-275.

Zonneveld, K. A., Marret, F., Versteegh, G. J., Bogus, K., Bonnet, S., Bouimetarhan, I., . . . Edwards, L. (2013). Atlas of modern dinoflagellate cyst distribution based on 2405 data points. *Review of Palaeobotany and Palynology*, 191, 1-197.

Acknowledgments

Tableau 1.1 Radiocarbon dates of core HH16-1205-GC and corresponding calibrated ages. The calibration was made with a ΔR of 90 ± 35 on BACON with the Marine13 calibration curve.

AWI nr.	Sample ID (depth in cm)	14C dates	±	Calibrated years BP ranges		Mean calibrated age BP	Dated material
				1 sigma	2 sigma		
1941.1.1	24-25	1 148	62	553 - 673	508 - 745	624	benthic foram., bivalve shell fragments
1942.1.1	59-60	1 581	60	959 - 1125	905 - 1213	1045	benthic foram., bivalve shell, gastropod
1943.1.1	79-80	2 126	62	1519 - 1696	1416 - 1791	1607	benthic foram., bivalve shell
1944.1.1	144-145	2 582	72	2064 - 2276	1946 - 2329	2153	benthic foram., bivalve shell fragments
1945.1.1	284-285	4 650	78	4657 - 4854	4511 - 4975	4753	benthic foram., bivalve
1946.1.1	374-375	5 693	65	5910 - 6094	5841 - 6168	6006	benthic foram., bivalve
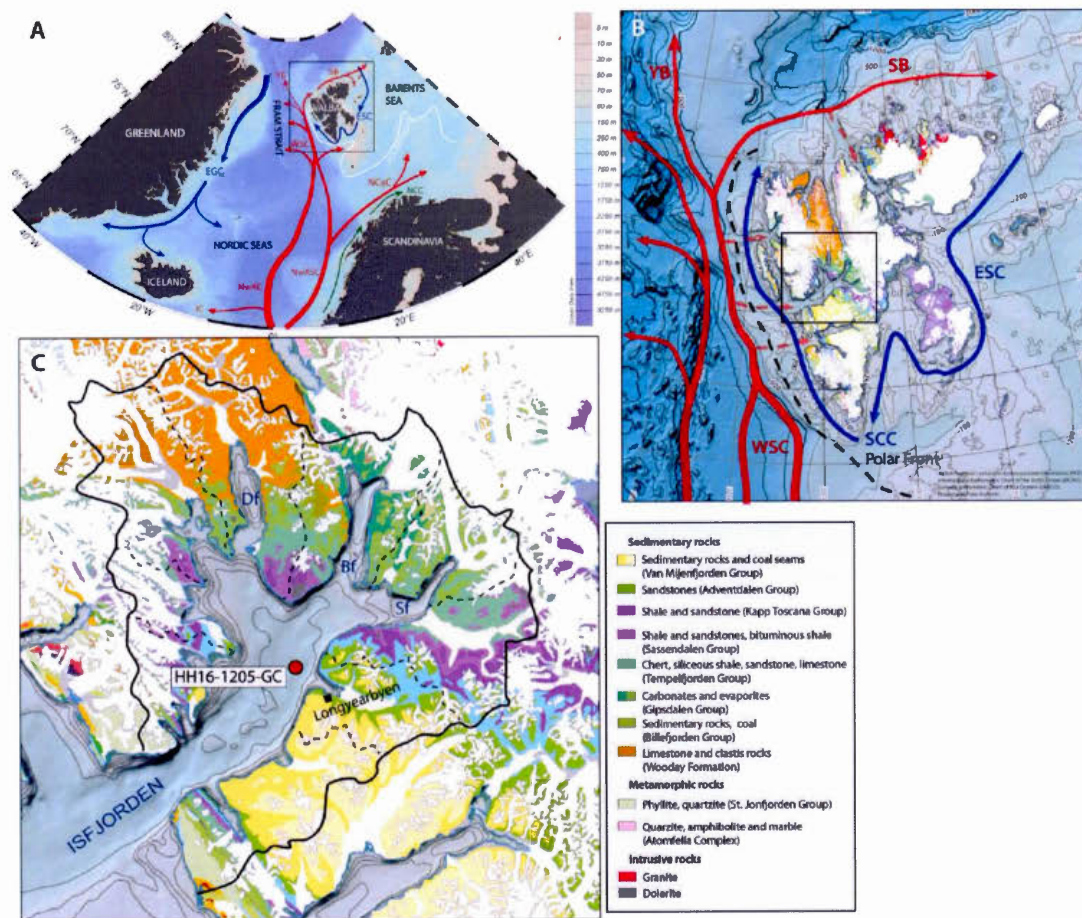
Figure 1. 1   Maps of the study area. A: Map of the North Atlantic. Red arrows represent the North Atlantic drift with Irminger Current (IC), Norwegian Atlantic Current (NwAC), Norwegian Atlantic Slope Current (NwASC), North Cape Current (NCaC), West Spitsbergen Current (WSC), Svalbard Branch (SB) and Yermack Branch (YB). The blue arrows represent the Arctic water flowing via East Spitsbergen Current (ESC) and East Greenland Current (EGC). Green arrows are the Norwegian Coastal Current (NCC). White line indicates the mean position of the Polar Front (Loeng, 1989). B: Geological map of Svalbard (data from Norwegian Polar Institute and International Bathymetric Chart of the Arctic Ocean) with the South Cape Current (SCC). Dashed line represents the general position of the polar

front. C: Geological map of Isfjorden with location of the core. Plain black line is the main watershed boundary; dotted lines are secondary watershed limits. Df: Dicksonfjorden, Bf: Billefjorden, Sf: Sassenfjorden.
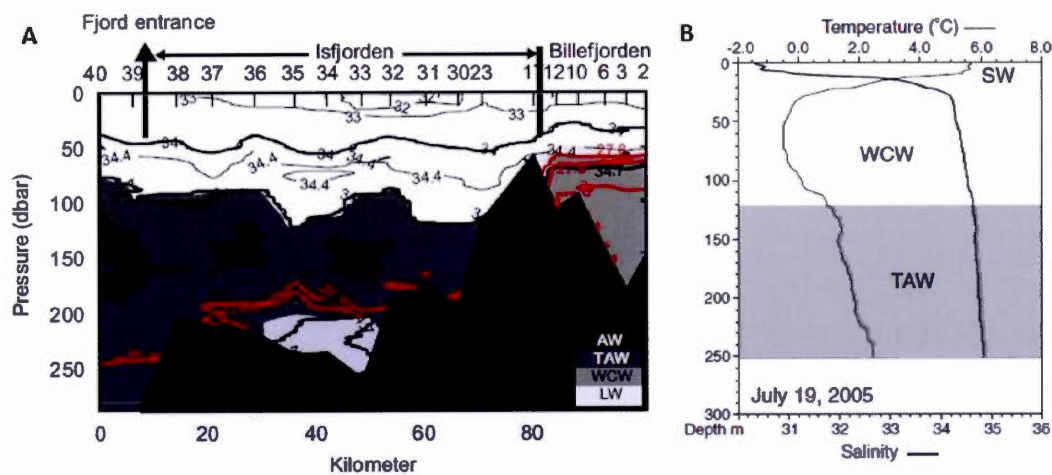
Figure 1. 2   Conductivity, temperature, depth (CTD) profiles of Isfjorden. AW: Atlantic Water, TAW: Transformed Atlantic Water, WCW: Winter Cooled Water, LW: Local Water, SW: Surface Water. A: CTD section from Billefjorden toward Isfjorden mouth along the southern side of the fjord in September 2002. Modified from Nilsen et al. (2008). B: CTD profile taken in 2005 at the site of core JM98-845-PC (78° 20.64′ N; 15° 18.11′ E), close to core HH16-1205-GC site. Modified from Rasmussen et al. (2012).
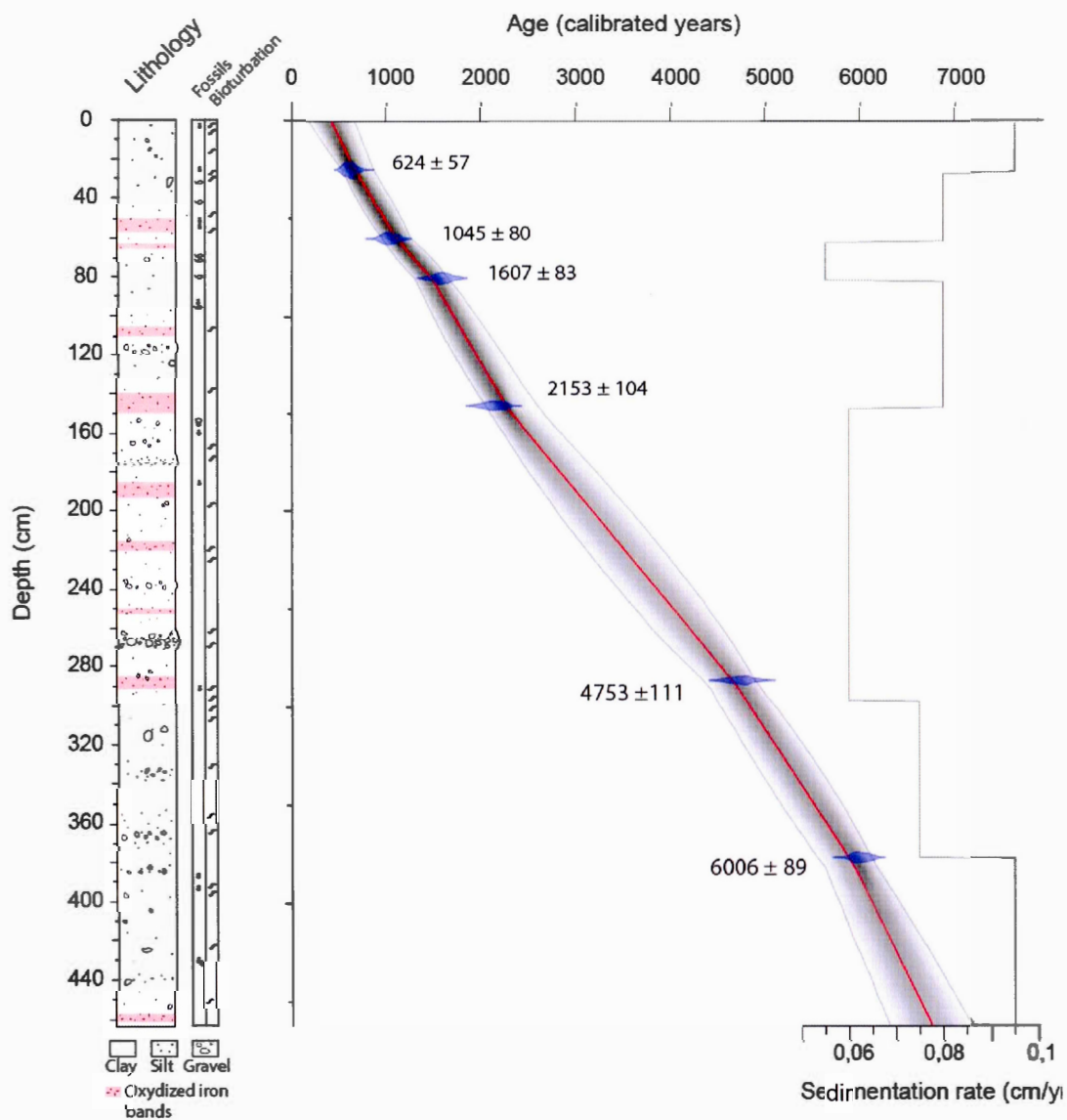
Figure 1. 3   Lithological description, age-depth profile and sedimentation rate of core HH16-1205-GC. Age vs. depth relationship was modeled with R package BACON based on ^{14}C chronological dates.
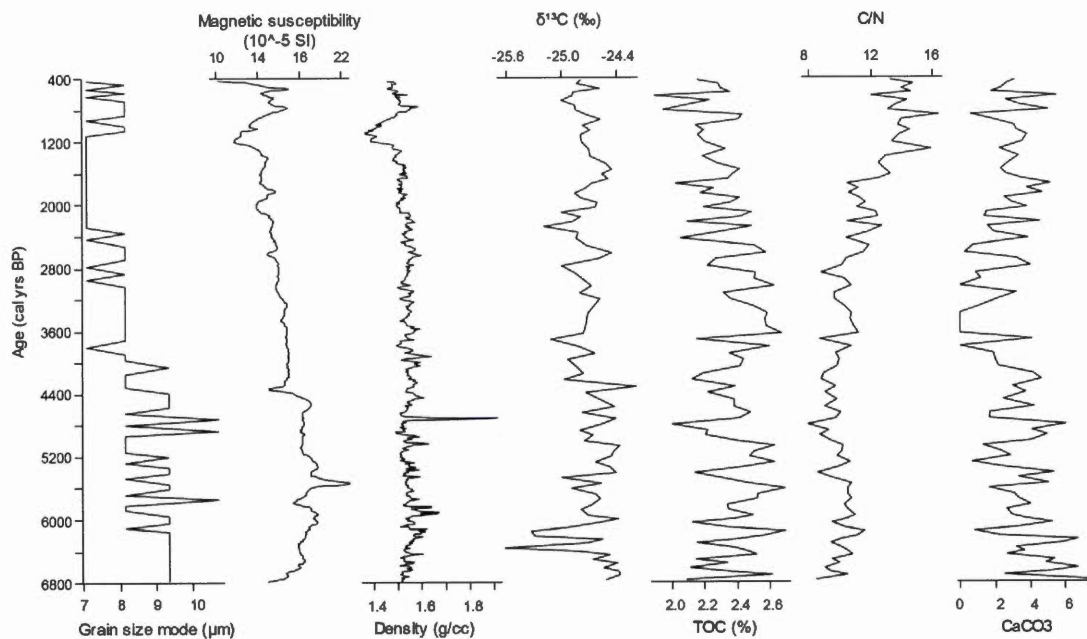
Figure 1. 4 Grain size distribution mode, density and magnetic susceptibility, $\delta^{13}Corg$, percentage of total organic carbon (TOC), ratio of carbon versus nitrogen (C/N) and percentage of carbonates ($CaCO_3$) in bulk sediment of core HH16-1205-GC.
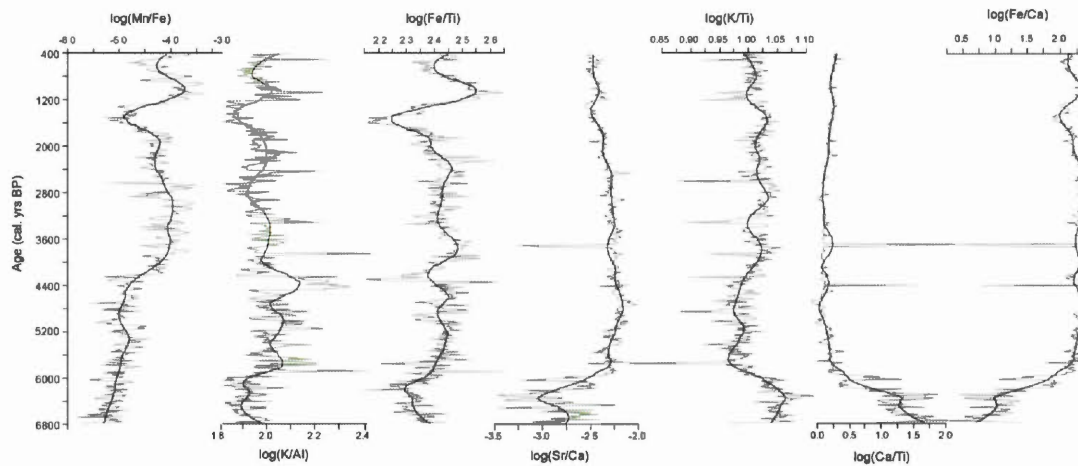
Figure 1. 5 Geochemical content in sediment of core HH16-1205-GC expressed as elements log-ratios.
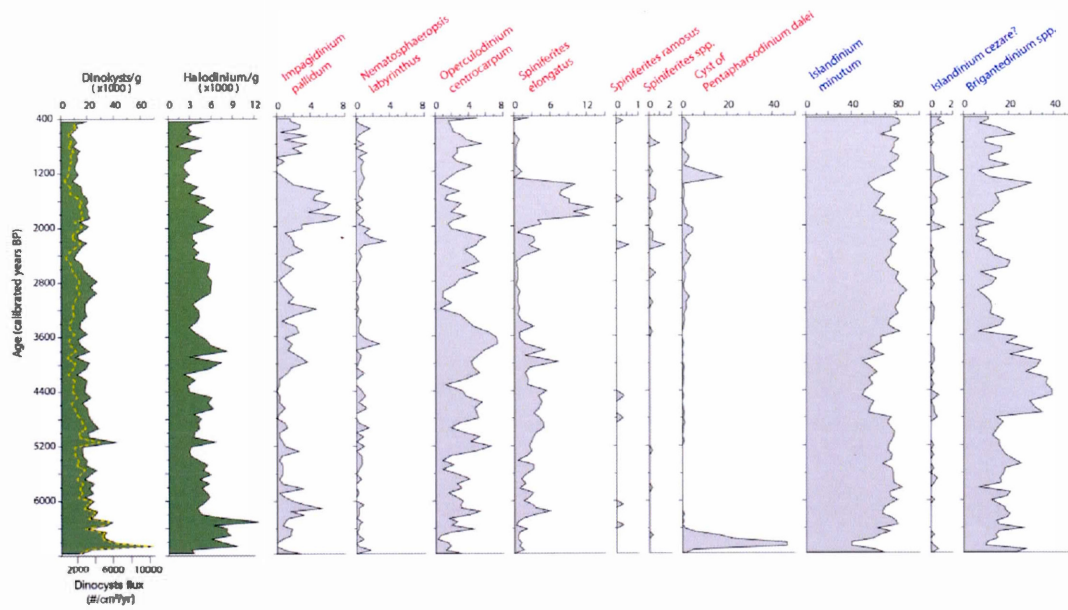
Figure 1. 6 Concentration of dinocysts and *Halodinium* and percentages of the main dinocyst taxa in core HH16-1205-GC. Species written in red are phototrophic and those in blue are heterotrophic.
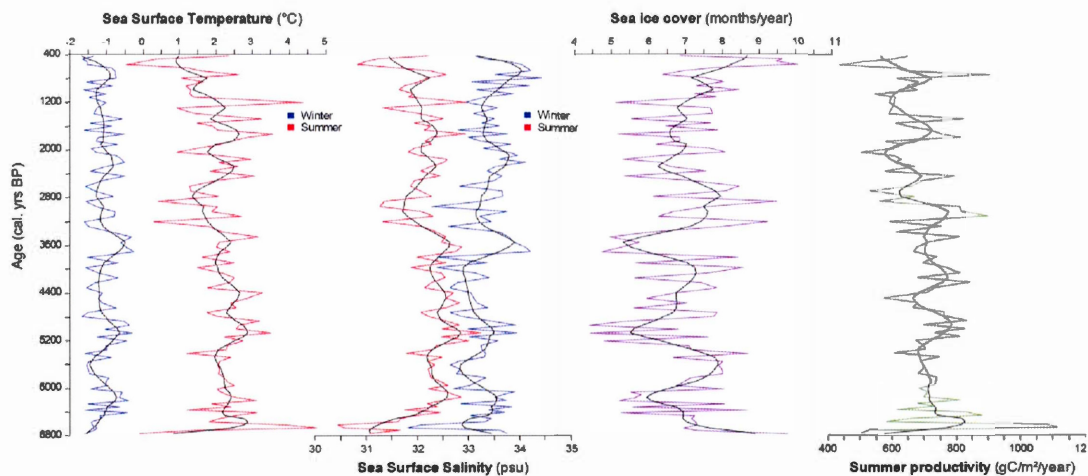
Figure 1. 7   Sea surface conditions reconstructed from the application of MAT to the dinocyst assemblages of core HH16-1205-GC. Sea surface temperatures (SST) in summer and winter are represented by red and blue curves respectively. Summer and winter sea surface salinities are shown by the red and blue curves, sea ice cover and annual productivity are represented by purple and green lines respectively. Black curves correspond to smoothed values after Loess regressions.
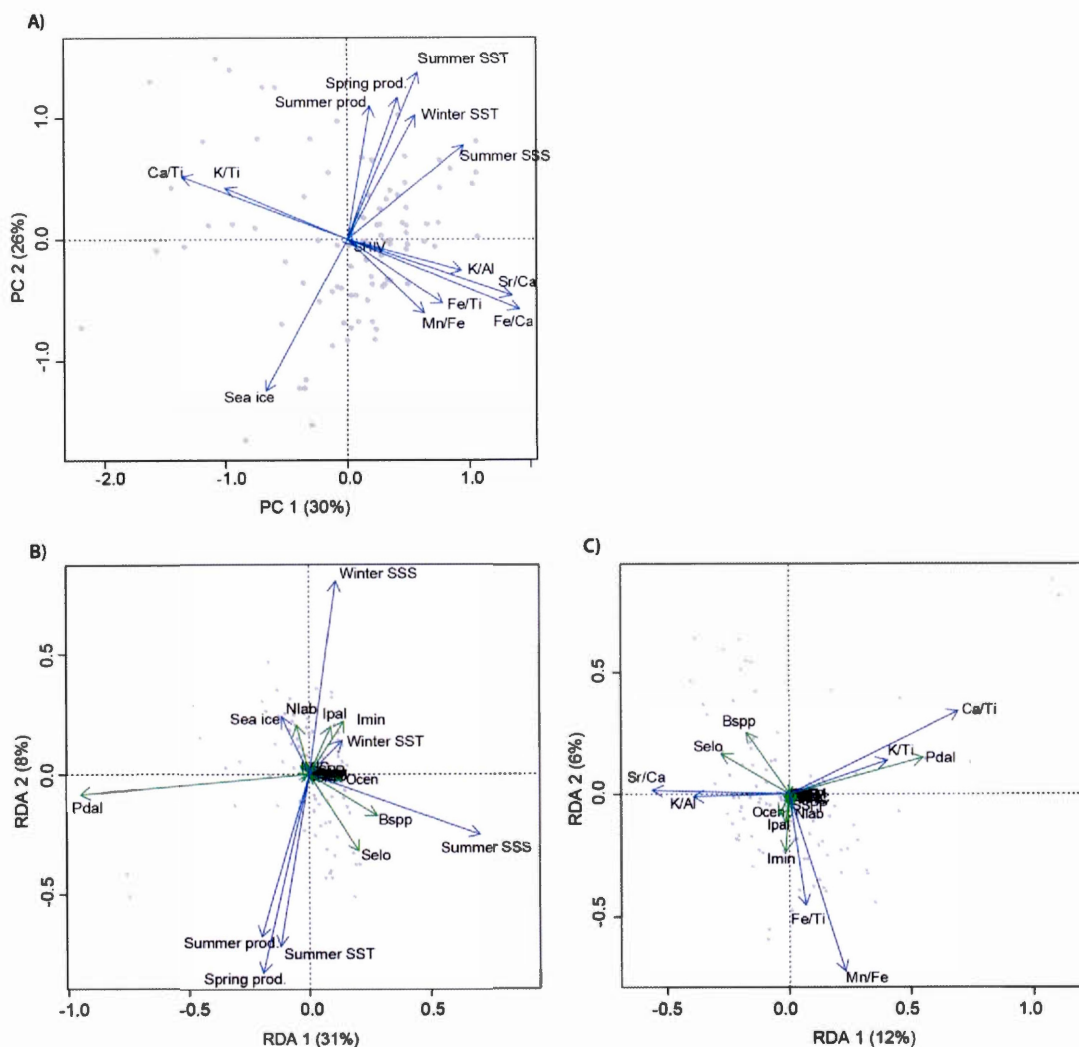
Figure 1. 8   Results pf multivariate analysis of the environmental and geochemical variables, and the dinocyst taxa percentages. A) Principal component analysis of XRF ratios and sea surface parameters. B) Redundancy analysis of sea surface parameters and dinocysts taxa percentages. C) Regression analysis of XRF ratios and dinocyst taxa percentages.
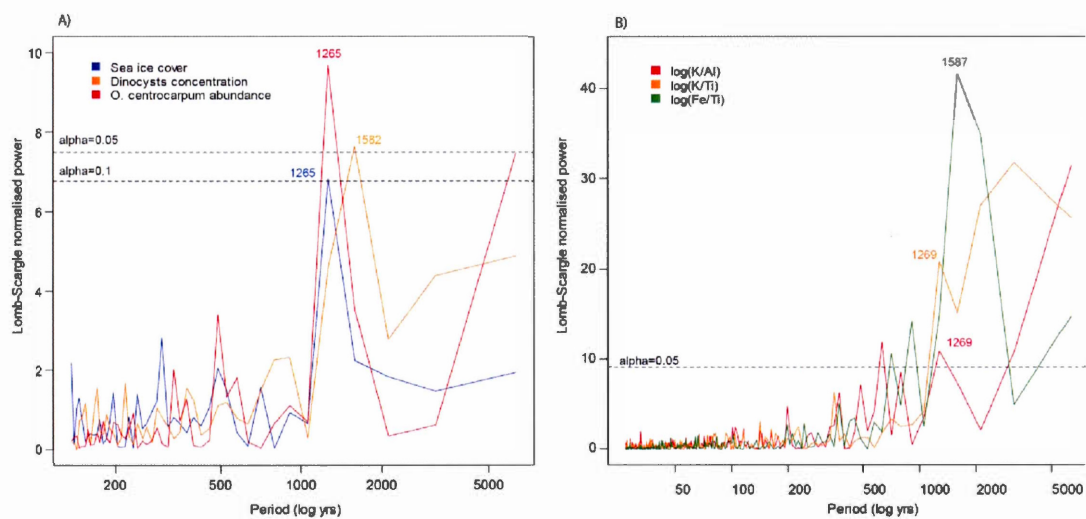
Figure 1. 9   Periodicity of (A) reconstructed sea ice cover, dinocyst concentration and relative abundance of *Operculodinium centrocarpum* and (B) XRF log-ratios K/Al, K/Ti and Fe/Ti computed from a Lomb-Scargle periodogram. Significance levels (alpha) were established at 5% (A and B) and 10% (A). Peak values are 1265 years for sea ice cover and *Operculodinium centrocarpum* and 1582 years for dinocyst concentrations, 1269 years for K/Al and K/Ti and 1587 years for Fe/Ti.
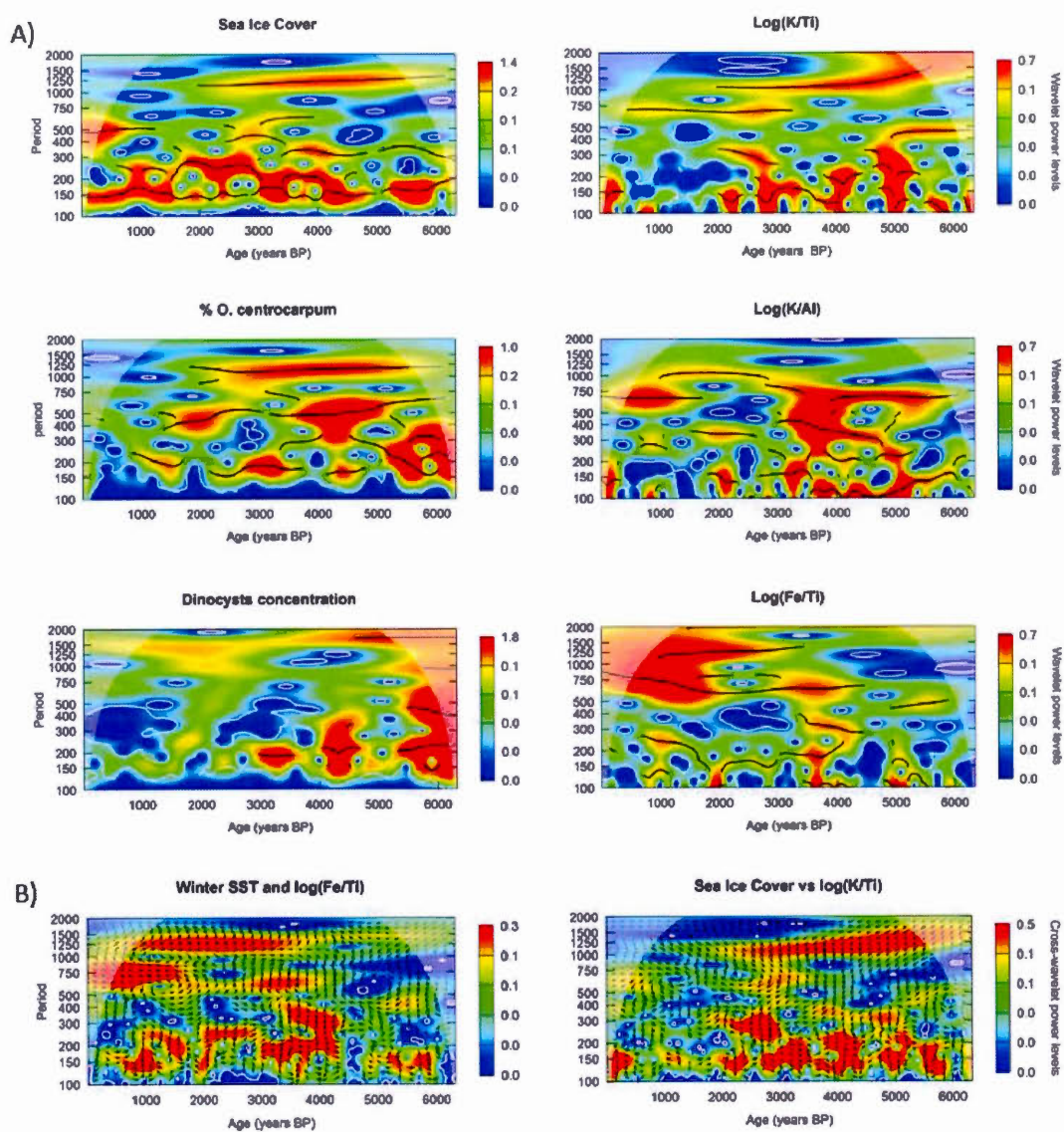
Figure 1. 10 Spectral analysis of the time series. (A) Wavelets analysis applied on MAT reconstructions, palynological results and XRF data. (B) Cross-wavelets analysis between ratios (K/Ti, Fe/Ti) and sea surface conditions.
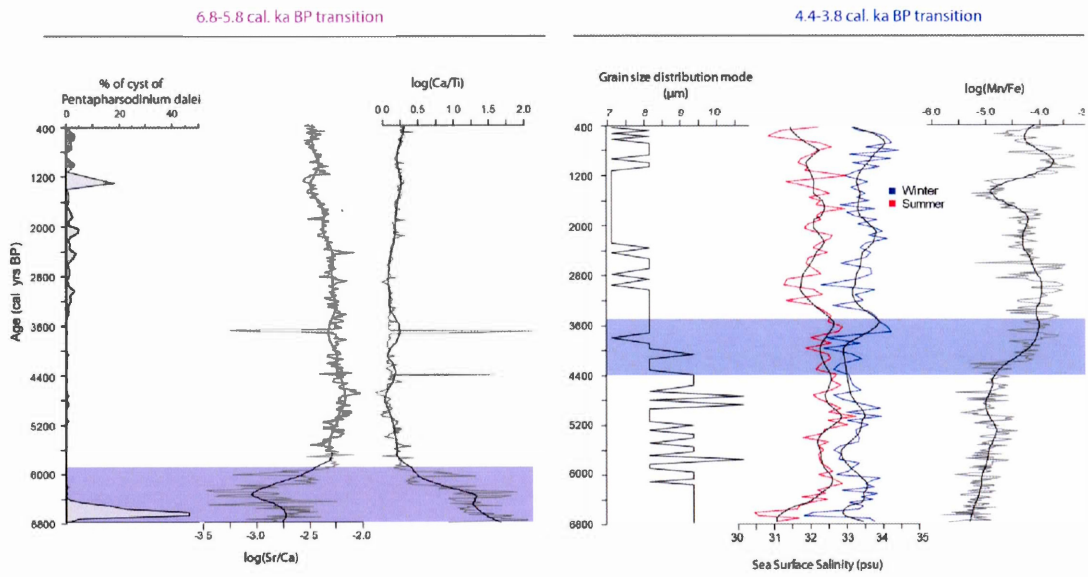
Figure 1. 11   Results of the main proxies characterizing the two majors transitions identified in the record

CONCLUSION

L'analyse de traceurs multiples dans les sédiments de la carotte HH16-1205-GC a permis de retracer les changements et fluctuations caractérisant les conditions climatiques d'Isfjorden au cours des derniers ~6800 ans. Le dénombrement des espèces de kystes de dinoflagellés et la technique des analogues modernes ont fourni des informations sur les conditions des eaux de surface. Les analyses sédimentologiques, tels que la granulométrie, la géochimie et les propriétés physiques, nous ont permis d'identifier la provenance des sédiments et les propriétés des masses d'eau profondes. Le croisement entre ces différents traceurs stratigraphiques permet d'établir des liens entre les masses d'eau, l'activité des glaciers environnants et la glace de mer.

Au cours de l'Holocène moyen et supérieur, le fjord a enregistré un refroidissement graduel entrecoupé de phases de refroidissement plus rapide. Dans la région de Svalbard, ce refroidissement aurait été amorcé au cours de l'Holocène inférieur, suite à l'optimum thermique (Koç *et al.*, 2002; Hald *et al.*, 2004; Slùbowska-Woldengen *et al.*, 2007; Forwick and Vorren, 2009; Rasmussen *et al.*, 2012; Werner *et al.*, 2013). Une diminution ténue mais constante de la densité et de la susceptibilité magnétique des sédiments, ainsi que de la température d'été et de la productivité primaire dans les eaux de surface souligne cette détérioration du climat. L'intervalle 6800-5800 ans calibrés BP est défini par un environnement glacio-marin. Une forte concentration en calcium et strontium dans les sédiments modifie l'ensemble des ratios chimiques. Nous proposons que cet important changement de sédimentation serait due à de l'érosion glaciaire; une activité glaciaire plus intense dans la partie interne du fjord, constituée majoritairement de carbonates, amenerait de fortes quantités de sédiments

riches en calcium et strontium. L'abondance du kyste de *Pentapharsodinium dalei* durant cet intervalle semble indiquer les mêmes conditions. Ce kyste dominant les sédiments actuels de la partie proximale aux glaciers (voir Grøsfjeld *et al.*, 2009) est caractéristique de ce bref intervalle à notre site, soit dans la partie centrale du fjord. *Pentapharsodinium dalei* est associé à des eaux stratifiées et à de la productivité primaire. D'autres études laissent supposer que des conditions relativement chaudes prévalaient avant cette période et qu'un refroidissement aurait débuté vers 7000 ans cal. BP avec l'augmentation de débris glaciaires et un changement dans les populations de foraminifères (Hald *et al.*, 2004, Slùbowska-Woldengen *et al.*, 2007; Skirbekk *et al.*, 2010; Rasmussen *et al.*, 2012). Entre 4400 et 3800 ans BP, un second changement dans l'environnement est enregistré au site HH16-1205-GC. Le manganèse, jusqu'alors peu présent, montre un hausse abrupte, modifiant le ratio Mn/Fe. Il s'agit d'un élément sensible à l'oxydoréduction : lorsque le milieu devient réducteur, la concentration de mangènese augmente. Il y a une diminution notable de la granulométrie, principalement expliquée par la quasi-disparition du sable dans les sédiments. À la surface de la colonne d'eau, la salinité d'hiver et d'été divergent et l'abondance relative de *Brigantedinium* spp. double, passant de ~20 à ~40%. Une diminution de la ventilation dans la colonne caractérise cette période et semble indiquer une modification importante des conditions en profondeur. Des conditions froides à la surface, avec un couvert de glace important sont alors enregistrées. Une advection d'eaux atlantiques plus intense est observée en surface de 2000 à 1200 ans calibrés BP avec l'augmentation des pourcentages de *Spiniferites elongatus* et *Impagidinium pallidum*.

L'utilisation d'analyses spectrales tel que le périodogramme Lomb-Scargle et les analyses par ondelettes ont permis d'identifier des variations cycliques dans les sédiments de la carotte HH16-1205-GC. En effet, des cycles d'échelle millénaire ont été détectés tant à partir des traceurs chimiques que biogéniques. Les analyses spectrales ont révélé des périodicités variant entre 1100 et 1500 ans, selon le traceur

et l'intervalle de temps. Les analyses Lomb-Scargle ont montré deux pics de périodicité, soit à 1260 et à 1580 ans. Les analyses par ondelettes ont confirmé ces cycles millénaires et ont également montré l'évolution des cycles au cours des derniers 6800 ans. De façon générale, la période des oscillations a légèrement diminué entre le début de l'enregistement et aujourd'hui, principalement au moment de la transition de l'Holocène moyen à supérieur. De plus, un changement dans le phasage des traceurs est constaté à ce moment. Avant 3000 ans calibrés BP, l'oscillation du couvert de glace est en anti-phase avec celle de K/Ti. Par la suite, les deux traceurs sont en phase. Le même phénomène est observé entre le température d'hiver et Fe/Ti à l'exception que le changement se produit vers 4000 ans calibrés BP. La cause de ce changement de phase est inconnu mais il souligne néanmoins l'important changement environnemental détecté à la trantion vers l'Holocène supérieur.

L'étude réalisée dans le cadre de cette maîtrise contribue à l'avancée des connaissances dans le domaine de la paléocéanographie arctique en fournissant des données de hautes résolutions temporelles traitant des mécanismes reliant les milieux continentaux et marins. De plus, l'approche par traceurs multiples a aussi offert une contribution méthodologique avec le croisement de données sédimentologiques et paléontologiques amenant un portrait plus complet et stastistiquement plus fiable des reconstitutions climatiques. Les résultats obtenus nous ont ainsi renseignés sur l'environnement d'Isfjorden dans les derniers 7000 ans, mais aussi sur les comportements et les relations entre les divers traceurs utilisés. L'observation des oscillations millénaires a été une contribution significative dans ce projet, cependant la ou les explications de ce phénomène n'ont pas pu être fournies. Une étude approfondie de ce sujet serait très pertinente dans le cadre de la recherche paléocéanographique des régions arctiques et nord-altantiques.

ANNEXE A

RÉSULTATS GÉOCHIMIQUES COMPLÉMENTAIRES

Figure 1 : Ratios des éléments sur la somme. La somme comprend les 11 éléments utilisés dans l'étude, soit Al, Si, Cl, K, Ca, Ti, Mn, Fe, Rb, Sr et Zr

Figure 2 : Analyse par composantes principales des résultats XRF des 11 éléments

Figure 1 : Ratios des éléments sur la somme. La somme comprend les 11 éléments utilisés dans l'étude, soit Al, Si, Cl, K, Ca, Ti, Mn, Fe, Rb, Sr et Zr.
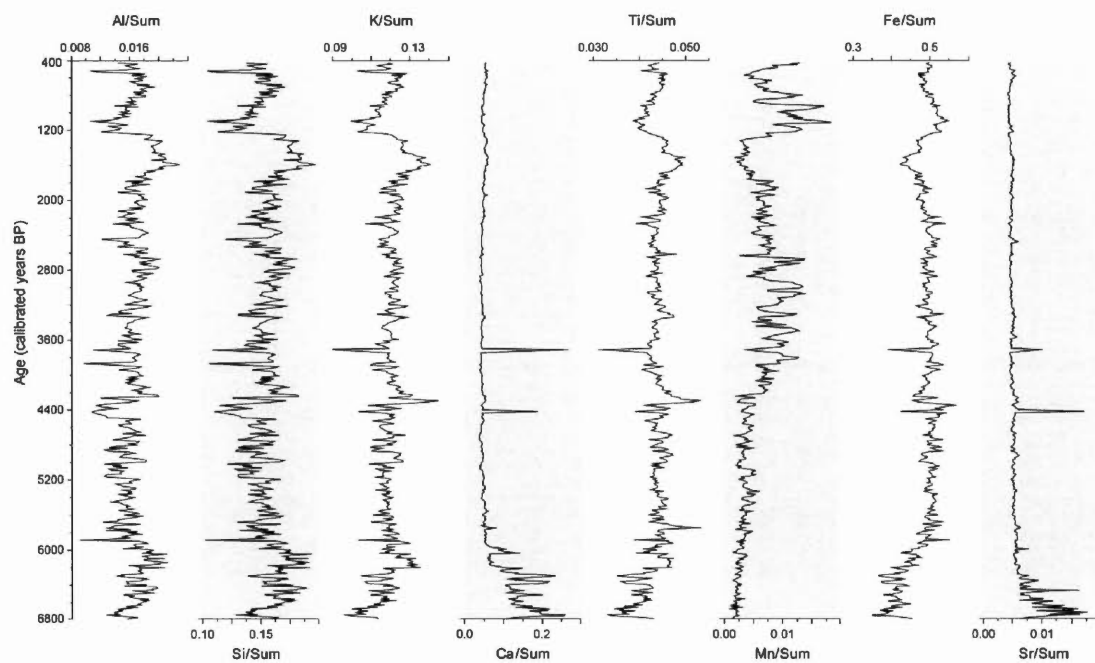
Figure 2 : Analyse par composantes principales des résultats XRF des 11 éléments
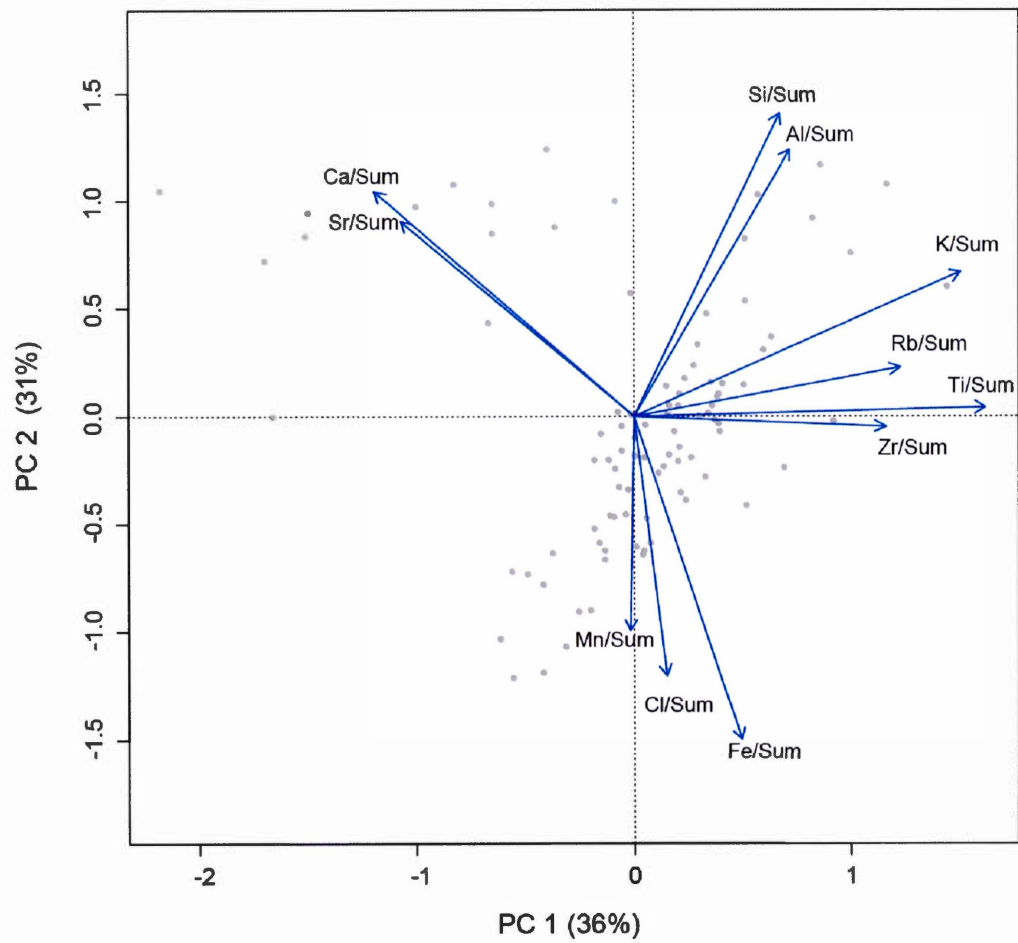
ANNEXE B

RÉSULTATS GRANOLUMÉTRIQUES COMPLÉMENTAIRES

Figure 1 : Taille médiane (en micromètre) et composition en pourcentages de sable, de silt et d'argile des sédiments de la carotte HH16-1205-GC

Figure 1 : Taille médiane (en micromètre) et composition en pourcentages de sable, de silt et d'argile des sédiments de la carotte HH16-1205-GC
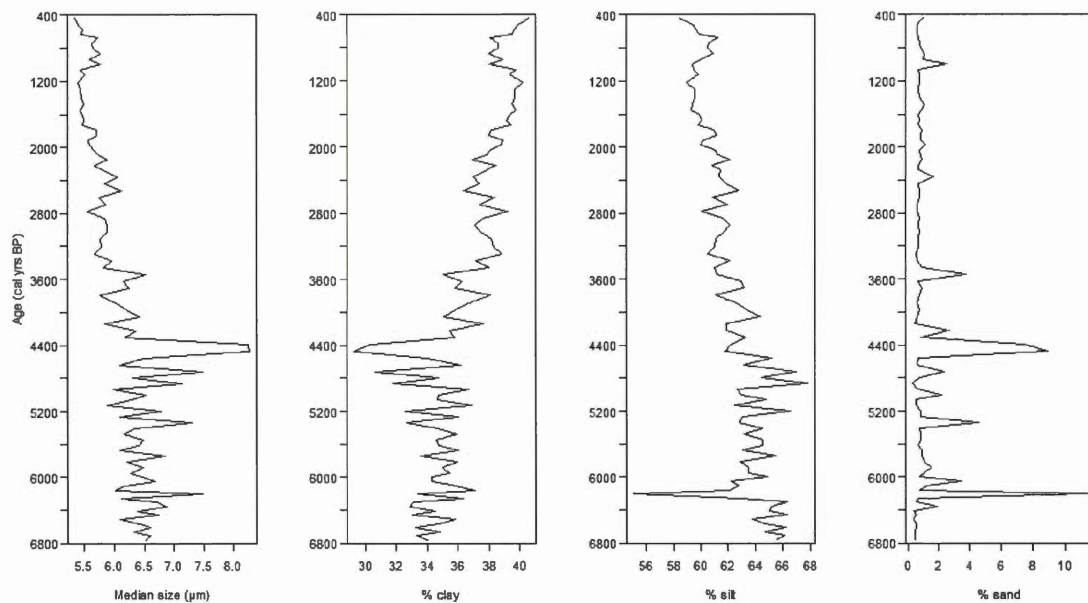
APPENDICE A

RÉSULTATS DES ANALYSES PALYNOLOGIQUES

Tableau A1 : Dénombrement des dinokystes et des autres palynomorphes de la carotte HH16-1205-GC

Tableau A2 : Reconstitutions des conditions des eaux de surface à partir des assemblages de dinokystes de la carotte HH16-1205-GC en utilisant la technique des analogues modernes (n=1968)

Tableau A1 : Dénombrement des dinokystes et des autres palynomorphes de la carotte HH16-1205-GC

Profondeur (cm)	0,5	4,5	9,5	14,5	19,5	24,5	29,5	34,5	39,5	44,5	49,5	54,5
Poids sec (g)	1,6514	2,0337	1,471	1,4321	1,8836	1,7956	1,5399	1,4764	2,2579	2,3894	2,5897	1,8557
Fraction grossière (g)	0,0195	0,0349	0,0249	0,0133	0,0278	0,0262	0,0176	0,0224	0,043	0,0289	0,0311	0,0283
Lycopodes clavatum ajoutés	10679	10679	10679	10679	10679	10679	10679	10679	10679	10679	10679	10679
Dinokystes												
Bitectatodinium tepikiense	0	0	0	0	0	0	1	0	0	0	0	0
Impagidinium pallidum	5	5	9	8	2	11	3	11	6	0	0	3
Impagidinium paradoxum	0	0	0	0	0	0	0	0	0	0	0	0
Impagidinium sphaericum	0	0	0	0	0	0	0	0	0	0	0	0
Nematosphaeropsis labyrinthus	1	0	2	5	3	1	0	3	0	4	1	3
Operculodinium centrocarpum	16	5	6	6	7	10	12	17	8	8	7	8
Spiniferites elongatus	8	0	0	0	0	1	3	2	1	1	1	1
Spiniferites ramosus	0	1	0	0	0	0	0	0	0	0	0	0
Spiniferites spp	0	0	0	0	0	0	1	3	0	0	0	0
Cyst of Pentapharsodinium dalei	4	5	11	10	6	6	7	1	0	4	11	8
Islandinium minutum	244	247	264	217	236	206	263	242	236	222	263	249
Islandinium ? Cezare	3	2	4	1	0	1	0	1	0	0	1	1
Brigantedinium spp.	36	33	23	44	58	71	31	30	52	50	36	36
Selenopemphix quanta	0	0	0	0	2	3	0	0	0	0	0	0
PARC	0	0	0	0	0	0	0	0	0	0	0	0
Palynomorphes												
Somme des dinokystes	**317**	**298**	**319**	**291**	**314**	**310**	**321**	**310**	**303**	**298**	**320**	**309**
Lycopodes	103	137	183	223	240	196	184	243	101	115	104	158
Pollen / Spores	5	8	3	4	7	2	3	1	1	4	6	2
Halodinium	94	88	65	96	113	150	68	39	100	79	80	61
Foraminifera linings	34	33	27	49	36	79	35	35	25	39	30	43
Pediastrum	2	0	0	0	2	1	2	0	1	1	2	2
Reworked palynomorphs	23	56	29	39	38	43	28	28	15	14	32	26
Concentrations												
Dinokysts/g	19902,2	11421,9	12654,9	9730,7	7417,5	9406,5	12098,3	9227,5	14188,8	11581,4	12688,1	11254,4
Pollen+Spores/g	313,9	306,6	119,0	133,8	165,4	60,7	113,1	29,8	46,8	155,5	237,9	72,8
Halodinium/g	5901,6	3372,9	2578,6	3210,1	2669,4	4551,5	2562,9	1160,9	4682,8	3070,2	3172,0	2221,8
Foraminifera linings / g	2134,6	1264,8	1071,1	1638,5	850,4	2397,1	1319,1	1041,8	1170,7	1515,7	1189,5	1566,2
Pediastrum / g	125,6	0,0	0,0	0,0	47,2	30,3	75,4	0,0	46,8	38,9	79,3	72,8
Reworked palynomorphs / g	1444,0	2146,4	1150,4	1304,1	897,7	1304,8	1055,3	833,4	702,4	544,1	1268,8	947,0

	Profondeur (cm)	59,5	64,5	69,5	74,5	79,5	84,5	89,5	94,5	99,5	104,5	109,5	114,5
	Poids sec (g)	2,542	2,9628	2,1984	3,0251	3,0798	2,2644	2,7939	3,0151	2,4977	2,2451	2,8323	2,8694
	Fraction grossière (g)	0,0617	0,0581	0,0293	0,0744	0,0792	0,0267	0,0283	0,0394	0,0433	0,0266	0,0399	0,0315
	Lycopodes clavatum ajoutés	10679	10679	10679	10679	10679	10679	10679	10679	10679	10679	10679	10679
Dinokystes	*Bitectatodinium tepikiense*	0	0	0	0	0	0	0	0	0	0	0	0
	Impagidinium pallidum	0	0	3	6	17	15	14	20	18	12	24	21
	Impagidinium paradoxum	0	0	0	0	0	1	0	0	0	0	0	0
	Impagidinium sphaericum	0	0	0	0	1	0	1	0	0	1	0	0
	Nematosphaeropsis labyrinthus	2	2	3	2	1	1	3	0	2	0	2	3
	Operculodinium centrocarpum	14	8	5	2	9	5	4	10	8	6	12	7
	Spiniferites elongatus	1	4	0	31	24	25	30	29	42	31	40	13
	Spiniferites ramosus	0	0	0	0	0	0	1	0	0	0	0	0
	Spiniferites spp	0	1	0	0	2	2	2	0	0	1	1	0
	Cyst of *Pentapharsodinium dalei*	3	27	55	2	4	4	3	2	5	7	8	4
	Islandinium minutum	230	235	194	168	186	229	216	202	194	210	206	257
	Islandinium ? Cezare	1	1	5	1	0	1	2	2	0	1	1	0
	Brigantedinium spp.	63	21	35	93	63	47	51	51	45	39	26	18
	Selenopemphix quanta	0	0	0	0	0	0	1	1	7	1	0	0
	PARC	0	0	0	0	0	0	0	0	0	0	0	0
	Somme des dinokystes	**314**	**299**	**300**	**305**	**307**	**330**	**328**	**317**	**321**	**309**	**320**	**323**
Palynomorphes	Lycopodes	131	82	171	69	66	81	61	61	66	72	55	85
	Pollen / Spores	5	5	9	1	3	8	3	4	0	3	0	3
	Halodinium	66	66	72	82	56	89	61	90	98	85	73	94
	Foraminifera linings	60	49	35	41	24	34	27	57	43	42	24	46
	Pediastrum	1	2	15	1	1	1	1	2	0	0	5	2
	Reworked palynomorphs	36	41	24	26	39	34	17	29	20	16	29	29
Concentrations	Dinokysts/g	10069,6	13142,7	8522,1	15604,2	16128,8	19213,5	20552,5	18406,0	20794,6	20413,7	21937,1	14142,4
	Pollen+Spores/g	160,3	219,8	255,7	51,2	157,6	465,8	188,0	232,3	0,0	198,2	274,2	131,4
	Halodinium/g	2116,5	2901,1	2045,3	4195,2	2942,1	5181,8	3822,3	5225,7	6348,5	5615,4	5004,4	4115,7
	Foraminifera linings / g	1924,1	2153,8	994,3	2097,6	1260,9	1979,6	1691,8	3369,6	2785,6	2774,7	1645,3	2014,1
	Pediastrum / g	32,1	87,9	426,1	51,2	52,5	58,2	62,7	116,1	0,0	0,0	342,8	87,6
	Reworked palynomorphs / g	1154,5	1802,2	681,8	1330,2	2048,9	1979,6	1065,2	1683,8	1295,6	1057,0	1988,0	1269,8

Profondeur (cm)	119,5	124,5	129,5	134,5	139,5	144,5	149,5	154,5	159,5	164,5	169,5	174,5
Poids sec (g)	1,5414	2,3707	1,1379	2,7436	1,6449	2,0262	1,7435	2,5027	1,7971	1,8614	2,1554	1,5709
Fraction grossière (g)	0,0217	0,0265	0,0108	0,0388	0,0124	0,1115	0,0161	0,986	0,0172	0,0243	0,0207	0,0321
Lycopodes clavatum ajoutés	10679	10679	10679	10679	10679	10679	10679	10679	10679	10679	10679	10679
Dinokystes												
Bitectatodinium tepikiense	0	0	0	0	0	0	0	0	0	0	0	0
Impagidinium pallidum	9	9	3	5	6	7	10	4	2	6	4	1
Impagidinium paradoxum	0	0	0	0	0	0	0	0	0	0	0	0
Impagidinium sphearicum	2	1	0	0	0	0	0	0	0	0	1	0
Nematosphaeropsis labyrinthus	1	5	3	5	11	3	1	2	1	0	1	2
Operculodinium centrocarpum	5	6	12	18	16	17	11	14	16	10	16	9
Spiniferites elongatus	14	5	2	10	11	9	14	5	1	2	2	2
Spiniferites ramosus	0	0	0	0	0	2	0	0	0	0	0	0
Spiniferites spp	0	0	1	1	1	5	0	0	0	0	2	0
Cyst of Pentapharsodinium dalei	4	15	14	7	3	6	5	12	8	2	5	5
Islandinium minutum	230	238	243	238	229	280	236	230	215	224	256	251
Islandinium ? Cezare	1	4	0	0	0	0	1	0	0	0	2	0
Brigantedinium spp.	42	17	20	17	32	22	36	41	64	60	25	47
Selenopemphix quanta	0	0	0	0	0	0	0	0	0	0	0	0
PARC	0	0	0	0	0	0	0	0	0	0	0	0
Somme des dinokystes	308	300	298	301	309	351	314	308	308	305	314	317
Palynomorphes												
Lycopodes	104	81	221	90	103	119	160	140	118	105	74	80
Pollen / Spores	2	4	8	3	7	4	7	7	2	6	2	10
Halodinium	94	88	79	78	64	76	111	116	115	105	81	72
Foraminifera linings	61	45	41	44	48	24	37	48	63	52	52	56
Pediastrum	2	0	2	1	3	1	0	2	3	1	2	0
Reworked palynomorphs	26	24	33	25	31	18	24	24	30	32	34	29
Concentrations												
Dinokysts/g	20517,9	16683,6	12654,7	13017,7	19476,6	15545,6	12020,4	9387,4	15510,5	16664,9	21023,3	26937,1
Pollen+Spores/g	133,2	222,4	339,7	129,7	441,2	177,2	268,0	213,3	100,7	327,8	133,9	849,8
Halodinium/g	6262,0	4893,9	3354,8	3373,4	4034,0	3366,0	4249,2	3535,5	5791,3	5737,1	5423,2	6118,2
Foraminifera linings / g	4063,6	2502,5	1741,1	1902,9	3025,5	1062,9	1416,4	1463,0	3172,6	2841,2	3481,6	4758,6
Pediastrum / g	133,2	0,0	84,9	43,2	189,1	44,3	0,0	61,0	151,1	54,6	133,9	0,0
Reworked palynomorphs / g	1732,0	1334,7	1401,4	1081,2	1954,0	797,2	918,8	731,5	1510,8	1748,4	2276,4	2464,3

Profondeur (cm)	179,5	184,5	189,5	194,5	199,5	204,5	209,5	214,5	219,5	224,5	229,5	234,5
Poids sec (g)	2,2189	1,8015	1,7418	2,048	2,2726	1,9533	1,9466	2,491	2,372	2,5001	2,7052	2,5251
Fraction grossière (g)	0,0261	0,0187	0,0128	0,0226	0,0251	0,0158	0,0157	0,1976	0,0536	0,2061	0,0748	0,0245
Lycopodes clavatum ajoutés	10679	10679	10679	10679	10679	10679	10679	10679	10679	10679	10679	10679
Dinokystes												
Bitectatodinium tepikiense	0	0	0	0	0	0	0	0	0	0	0	0
Impagidinium pallidum	2	4	6	4	14	7	2	7	8	3	6	4
Impagidinium paradoxum	0	0	0	0	0	0	0	0	0	0	0	0
Impagidinium sphaericum	0	0	0	0	0	0	0	0	0	0	0	0
Nematosphaeropsis labyrinthus	1	0	1	0	1	0	2	1	1	3	0	0
Operculodinium centrocarpum	7	3	3	6	2	9	12	14	20	22	24	18
Spiniferites elongatus	1	3	2	2	3	2	4	10	3	3	6	16
Spiniferites ramosus	0	0	0	0	0	0	0	0	0	0	0	0
Spiniferites spp	0	0	0	1	0	0	0	0	1	0	0	0
Cyst of Pentapharsodinium dalei	2	4	10	5	6	3	4	2	0	0	2	0
Islandinium minutum	255	269	256	244	238	251	232	221	259	200	218	172
Islandinium ? Cezare	1	0	0	0	1	1	1	0	0	0	0	1
Brigantedinium spp.	39	19	30	36	38	37	57	50	21	73	63	94
Selenopemphix quanta	0	0	0	0	0	0	0	0	0	0	0	0
PARC	0	0	0	0	0	0	0	0	0	0	0	0
Somme des dinokystes	**308**	**302**	**308**	**298**	**303**	**310**	**314**	**305**	**313**	**304**	**328**	**305**
Palynomorphes												
Lycopodes	67	67	90	85	78	88	116	95	71	104	87	60
Pollen / Spores	3	2	4	5	3	1	8	5	3	5	9	2
Halodinium	83	66	65	55	70	70	83	65	62	127	130	116
Foraminifera linings	34	37	58	34	52	47	43	39	13	57	70	51
Pediastrum	1	0	0	0	0	1	1	0	0	0	2	1
Reworked palynomorphs	25	19	42	23	27	19	25	29	13	35	22	30
Concentrations												
Dinokysts/g	22124,3	26719,5	20981,7	18280,9	18253,9	19259,3	14850,0	13763,6	19847,3	12485,7	14882,8	21498,1
Pollen+Spores/g	215,5	177,0	272,5	306,7	180,7	62,1	378,3	225,6	190,2	205,4	408,4	141,0
Halodinium/g	5962,1	5839,4	4428,0	3374,0	4217,1	4348,9	3925,3	2933,2	3931,4	5216,1	5898,7	8176,3
Foraminifera linings / g	2442,3	3273,6	3951,1	2085,7	3132,7	2920,0	2033,6	1759,9	824,3	2341,1	3176,2	3594,8
Pediastrum / g	71,8	0,0	0,0	0,0	0,0	62,1	47,3	0,0	0,0	0,0	90,7	70,5
Reworked palynomorphs / g	1795,8	1681,0	2861,1	1410,9	1626,6	1180,4	1182,3	1308,7	824,3	1437,5	998,2	2114,6

	Profondeur (cm)	239,5	244,5	249,5	254,5	259,5	264,5	269,5	274,5	279,5	284,5	289,5	294,5
	Poids sec (g)	3,0089	2,5701	2,383	2,9685	2,2331	2,2966	2,3988	2,2001	2,0117	2,0445	0,7425	1,1515
	Fraction grossière (g)	0,0789	0,0594	0,024	0,033	0,1107	0,0341	0,0637	0,0641	0,0233	0,0342	0,007	0,0223
	Lycopodes clavatum ajoutés	10679	10679	10679	10679	10679	10679	10679	10679	10679	10679	10679	10679
Dinokystes	Bitectatodinium tepikiense	0	0	0	0	0	0	0	0	0	0	0	0
	Impagidinium pallidum	8	11	5	4	1	1	0	1	1	3	1	0
	Impagidinium paradoxum	0	0	0	0	0	0	0	0	0	0	0	0
	Impagidinium sphaericum	0	0	1	0	1	0	0	0	0	0	0	0
	Nematosphaeropsis labyrinthus	2	1	0	3	0	0	2	3	1	4	0	0
	Operculodinium centrocarpum	16	13	14	17	11	4	10	10	18	15	15	16
	Spiniferites elongatus	6	22	8	6	7	7	17	11	15	13	10	13
	Spiniferites ramosus	0	0	0	0	0	0	0	1	0	0	0	1
	Spiniferites spp	0	0	0	0	0	0	0	0	0	0	0	0
	Cyst of Pentapharsodinium dalei	1	0	3	1	2	1	0	2	0	1	3	1
	Islandinium minutum	217	151	175	200	168	185	161	136	194	180	168	231
	Islandinium ? Cezare	1	1	0	1	0	1	0	2	0	1	1	2
	Brigantedinium spp.	66	103	100	89	113	115	122	107	95	100	106	46
	Selenopemphix quanta	0	0	0	0	0	0	0	0	0	0	0	0
	PARC	0	0	0	0	0	0	0	0	0	0	0	0
	Somme des dinokystes	**317**	**302**	**306**	**321**	**303**	**314**	**312**	**273**	**324**	**317**	**304**	**310**
Palynomorphes	Lycopodes	106	60	74	99	75	78	79	59	109	84	215	132
	Pollen / Spores	5	4	8	4	4	5	5	6	4	10	8	6
	Halodinium	90	107	94	60	60	45	52	74	112	101	54	65
	Foraminifera linings	45	67	53	49	81	65	75	62	68	72	42	25
	Pediastrum	0	4	1	0	0	0	1	0	2	1	1	0
	Reworked palynomorphs	29	22	20	24	33	28	23	41	30	39	30	10
Concentrations	Dinokysts/g	10613,9	20914,0	18530,9	11664,4	19319,9	18718,9	17581,8	22459,4	15779,2	19711,7	20336,2	21779,8
	Pollen+Spores/g	167,4	277,0	484,5	145,4	255,0	298,1	281,8	493,6	194,8	621,8	535,2	421,5
	Halodinium/g	3013,4	7409,9	5692,5	2180,3	3825,7	2682,6	2930,3	6087,9	5454,5	6280,4	3612,3	4566,7
	Foraminifera linings / g	1506,7	4639,9	3209,6	1780,6	5164,7	3874,9	4226,4	5100,7	3311,7	4477,1	2809,6	1756,4
	Pediastrum / g	0,0	277,0	60,6	0,0	0,0	0,0	56,4	0,0	97,4	62,2	66,9	0,0
	Reworked palynomorphs / g	971,0	1523,5	1211,2	872,1	2104,1	1669,2	1296,1	3373,0	1461,0	2425,1	2006,9	702,6

Profondeur (cm)	299,5	304,5	309,5	314,5	319,5	324,5	329,5	334,5	339,5	344,5	349,5	354,5
Poids sec (g)	1,6371	1,8055	2,5939	2,4078	1,6566	2,7532	2,8263	2,6685	2,4016	2,8269	2,3885	2,4905
Fraction grossière (g)	0,0058	0,0222	0,0881	0,0289	0,0171	0,0218	0,0287	0,0566	0,0584	0,0374	0,0797	0,0227
Lycopodes clavatum ajoutés	10679	10679	10679	10679	10679	10679	10679	10679	10679	10679	10679	10679
Dinokystes												
Bitectatodinium tepikiense	0	0	0	0	0	0	0	0	0	0	0	0
Impagidinium pallidum	3	4	1	1	2	3	8	2	1	2	2	2
Impagidinium paradoxum	0	0	0	0	0	0	0	0	0	0	0	0
Impagidinium sphaericum	1	0	0	0	0	0	0	0	0	0	1	0
Nematosphaeropsis labyrinthus	1	5	0	3	0	3	0	2	2	2	1	0
Operculodinium centrocarpum	9	6	11	18	13	21	15	6	3	7	3	8
Spiniferites elongatus	15	16	12	11	9	8	9	7	2	10	10	6
Spiniferites ramosus	0	0	0	0	0	0	0	0	0	0	0	0
Spiniferites spp	0	0	0	0	0	0	1	0	0	0	0	0
Cyst of *Pentapharsodinium dalei*	4	1	1	0	3	0	0	0	0	0	0	0
Islandinium minutum	223	240	251	262	234	230	224	242	231	210	234	232
Islandinium ? Cezare	0	0	0	0	0	1	0	1	0	0	1	0
Brigantedinium spp.	55	51	46	44	49	50	53	60	69	80	57	54
Selenopemphix quanta	0	0	0	0	0	0	0	0	0	0	0	0
PARC	0	0	0	0	0	0	0	0	0	0	0	0
Somme des dinokystes	**311**	**323**	**322**	**339**	**310**	**316**	**310**	**320**	**308**	**311**	**309**	**302**
Palynomorphes												
Lycopodes	83	69	66	72	48	77	73	78	70	64	53	60
Pollen / Spores	6	3	4	6	5	3	3	4	5	5	4	6
Halodinium	52	51	58	58	49	63	57	62	67	93	57	83
Foraminifera linings	34	67	38	47	53	63	61	66	71	67	65	109
Pediastrum	0	1	1	2	0	1	0	0	1	0	2	1
Reworked palynomorphs	11	16	14	13	18	23	14	18	20	16	10	22
Concentrations												
Dinokysts/g	24442,1	27687,7	20085,8	20882,3	41632,6	15918,0	16045,4	16417,9	19565,1	18357,0	26066,8	21582,4
Pollen+Spores/g	471,6	257,2	249,5	369,6	671,5	151,1	155,3	205,2	317,6	295,1	337,4	428,8
Halodinium/g	4086,8	4371,7	3617,9	3572,8	6580,6	3173,5	2950,3	3181,0	4256,0	5489,4	4808,4	5931,6
Foraminifera linings / g	2672,1	5743,3	2370,4	2895,2	7117,8	3173,5	3157,3	3386,2	4510,1	3954,7	5483,3	7789,7
Pediastrum / g	0,0	85,7	62,4	123,2	0,0	50,4	0,0	0,0	63,5	0,0	168,7	71,5
Reworked palynomorphs / g	864,5	1371,5	873,3	800,8	2417,4	1158,6	724,6	923,5	1270,5	944,4	843,6	1572,2

Profondeur (cm)	359,5	364,5	369,5	374,5	379,5	384,5	389,5	394,5	399,5	404,5	409,5	414,5
Poids sec (g)	2,932	2,3375	2,4641	2,6667	2,4778	2,461	2,2433	2,5867	1,6071	2,4023	1,6145	1,2886
Fraction grossière (g)	0,0515	0,0427	0,0487	0,0745	0,0567	0,0243	0,0322	0,0235	0,009	0,0204	0,0167	0,0036
Lycopodes clavatum ajoutés	10679	10679	10679	10679	10679	10679	10679	10679	10679	10679	10679	10679
Dinokystes												
Bitectatodinium tepikiense	0	0	1	0	0	0	0	0	0	0	0	0
Impagidinium pallidum	1	2	10	1	3	6	11	17	5	10	4	3
Impagidinium paradoxum	0	0	0	0	0	0	0	0	0	0	0	0
Impagidinium sphaericum	0	0	0	0	0	0	0	0	0	0	0	0
Nematosphaeropsis labyrinthus	2	0	0	1	0	0	3	1	1	1	0	2
Operculodinium centrocarpum	13	8	10	5	8	10	10	10	17	13	5	8
Spiniferites elongatus	4	6	3	10	8	5	10	12	19	11	5	2
Spiniferites ramosus	0	0	0	0	0	0	1	0	0	0	0	0
Spiniferites spp	0	0	1	0	0	0	0	0	0	0	0	0
Cyst of Pentapharsodinium dalei	0	0	0	0	0	0	0	0	0	3	0	2
Islandinium minutum	243	238	268	228	232	247	244	228	215	211	228	243
Islandinium ? Cezare	2	1	0	0	0	1	0	0	0	0	0	0
Brigantedinium spp.	52	52	22	65	60	38	50	60	59	65	59	45
Selenopemphix quanta	0	1	0	0	1	0	0	0	0	0	0	0
PARC	0	0	0	0	0	0	0	0	0	0	1	1
Somme des dinokystes	317	308	315	310	312	307	329	328	316	314	302	306
Palynomorphes												
Lycopodes	65	57	65	52	74	54	73	70	79	55	91	66
Pollen / Spores	7	4	10	10	5	4	7	4	6	4	5	4
Halodinium	77	71	70	70	99	65	72	68	51	58	105	100
Foraminifera linings	52	92	41	64	61	39	45	48	51	44	38	35
Pediastrum	0	0	2	0	1	0	1	1	2	2	0	1
Reworked palynomorphs	22	23	23	10	16	16	22	16	22	25	22	22
Concentrations												
Dinokysts/g	17762,8	24686,2	21002,4	23873,4	18171,4	24669,7	21454,4	19344,6	26831,9	25378,8	21951,2	38422,9
Pollen+Spores/g	392,2	320,6	666,7	770,1	291,2	321,4	456,5	235,9	504,7	323,3	363,4	502,3
Halodinium/g	4314,6	5690,7	4667,2	5390,8	5765,9	5223,2	4695,2	4010,5	4289,7	4687,8	7632,0	12556,5
Foraminifera linings / g	2913,8	7373,8	2733,6	4928,7	3552,7	3133,9	2934,5	2830,9	4289,7	3556,3	2762,1	4394,8
Pediastrum / g	0,0	0,0	133,3	0,0	58,2	0,0	65,2	59,0	168,2	161,6	0,0	125,6
Reworked palynomorphs / g	1232,8	1843,5	1533,5	770,1	931,9	1285,7	1434,6	943,6	1850,5	2020,6	1599,1	2762,4

81

Profondeur (cm)	419,5	424,5	429,5	434,5	439,5	444,5	449,5	454,5	459,5
Poids sec (g)	2,4431	1,4349	2,0107	2,348	0,8783	2,2209	1,4405	2,3968	1,8154
Fraction grossière (g)	0,0128	0,008	0,0159	0,0203	0,0061	0,0118	0,0249	0,0367	0,021
Lycopodes clavatum ajoutés	10679	10679	10679	10679	10679	10679	9666	9666	9666
Bitectatodinium tepikiense	0	0	0	0	1	0	0	0	0
Impagidinium pallidum	2	6	5	5	2	0	0	3	8
Impagidinium paradoxum	0	0	0	0	0	0	0	0	0
Impagidinium sphearicum	0	0	0	0	0	0	0	0	0
Nematosphaeropsis labyrinthus	1	1	0	1	3	0	1	5	1
Operculodinium centrocarpum	6	15	6	2	1	5	6	4	9
Spiniferites elongatus	1	7	3	2	2	4	3	5	1
Spiniferites ramosus	1	0	0	0	0	0	0	0	0
Spiniferites spp	0	0	0	1	0	0	0	0	0
Cyst of *Pentapharsodinium dalei*	0	5	18	51	74	148	148	16	6
Islandinium minutum	248	207	231	200	193	127	127	186	212
Islandinium ? Cezare	0	0	0	1	0	0	1	2	1
Brigantedinium spp.	49	88	49	45	50	34	32	85	74
Selenopemphix quanta	0	0	0	0	0	0	0	0	0
PARC	0	0	0	0	0	0	0	0	0
Somme des dinokystes	**308**	**329**	**312**	**308**	**326**	**318**	**318**	**306**	**312**
Lycopodes	40	128	49	44	119	36	31	56	103
Pollen / Spores	1	10	7	9	10	5	3	3	7
Halodinium	59	141	75	84	60	59	44	45	69
Foraminifera linings	32	115	62	55	51	46	28	85	54
Pediastrum	2	3	0	1	1	2	0	2	2
Reworked palynomorphs	15	41	33	30	27	27	20	30	25
Dinokysts/g	33657,4	19129,1	33817,5	31836,9	33308,8	42474,3	68833,4	22036,8	16128,4
Pollen+Spores/g	109,3	581,4	758,7	930,3	1021,7	667,8	649,4	216,0	361,9
Halodinium/g	6447,4	8198,2	8129,2	8682,8	6130,4	7880,5	9524,1	3240,7	3566,9
Foraminifera linings / g	3496,9	6686,5	6720,1	5685,2	5210,9	6144,1	6060,8	6121,3	2791,5
Pediastrum / g	218,6	174,4	0,0	103,4	102,2	267,1	0,0	144,0	103,4
Reworked palynomorphs / g	1639,2	2383,9	3576,9	3101,0	2758,7	333,4	290,0	243,5	111,5

Row groups (left margin): Dinokystes · Palynomorphes · Concentrations

82

Tableau A2 : Reconstitutions des conditions des eaux de surface à partir des assemblages de dinokystes de la carotte HH16-1205-GC en utilisant la technique des analogues modernes (n=1968)

Profondeur (cm)	Température des eaux de surface en hiver (°C)	Température des eaux de surface en été (°C)	Salinité des eaux de surface en hiver (psu)	Salinité des eaux de surface en été (psu)	Couvert de glace de mer (mois/an)	Productivité primaire au printemps (gC/m²/an)	Productivité primaire en été (gC/m²/an)
0,5	-1,37	32,23	33,14	2,34	6,84	581,76	651,87
4,5	-1,65	31,22	33,32	0,35	9,62	423,01	597,00
9,5	-1,53	31,02	33,76	0,00	9,45	318,97	510,60
14,5	-1,54	30,82	34,04	-0,47	10,05	241,06	435,27
19,5	-0,88	31,56	34,14	1,22	7,83	411,88	618,26
24,5	-0,76	32,25	34,24	1,58	6,97	484,59	644,29
29,5	-0,78	32,58	33,52	2,63	6,37	615,41	909,97
34,5	-0,73	32,20	34,45	1,05	7,54	446,70	617,51
39,5	-1,54	32,04	33,07	1,66	8,04	514,09	683,41
44,5	-0,83	31,74	34,20	1,17	7,28	409,88	647,12
49,5	-1,65	31,65	33,14	1,31	8,47	523,27	680,09
54,5	-1,02	31,93	33,89	1,29	7,25	421,08	546,97
59,5	-1,49	31,83	33,35	1,36	7,85	479,73	609,08
64,5	-1,02	32,98	32,94	4,37	5,09	645,82	608,64
69,5	-1,27	31,33	33,58	0,91	7,68	344,29	600,99
74,5	-1,35	32,03	33,10	1,43	7,73	459,28	591,44
79,5	-0,57	32,52	33,51	3,26	5,54	572,68	824,59
84,5	-1,44	31,94	33,27	1,48	7,70	499,98	612,66
89,5	-0,86	32,26	33,61	1,90	6,46	536,83	650,04
94,5	-1,61	32,15	32,81	2,05	7,86	581,21	724,93
99,5	-0,51	32,95	33,78	3,57	5,16	661,99	754,46
104,5	-1,23	32,28	32,99	2,85	6,84	591,72	815,85
109,5	-1,30	32,16	33,24	2,40	6,85	442,26	579,17
114,5	-0,71	32,28	33,84	2,13	6,21	499,01	633,72
119,5	-1,43	31,95	33,28	1,48	7,68	494,50	604,99
124,5	-1,29	31,81	33,78	0,92	8,08	398,74	502,71
129,5	-0,73	32,06	33,97	2,11	6,42	507,55	606,30
134,5	-0,59	32,59	33,59	2,98	5,32	500,95	630,43
139,5	-0,52	32,53	34,13	2,06	6,33	518,65	609,63
144,5	-1,04	32,28	33,54	2,61	6,57	540,83	672,12
149,5	-1,43	32,06	33,37	1,83	7,58	506,51	578,14
154,5	-0,50	32,45	33,66	3,06	5,34	536,79	798,79
159,5	-1,13	31,94	33,51	1,97	7,16	444,31	696,15
164,5	-1,58	31,87	32,83	1,27	8,45	507,51	663,21
169,5	-1,30	32,06	33,66	1,31	8,09	475,45	530,73
174,5	-0,81	32,28	33,68	2,07	6,13	557,35	673,13
179,5	-1,58	31,36	33,28	0,41	9,51	364,23	559,68
184,5	-1,27	31,26	32,28	2,03	7,56	550,04	809,66
189,5	-0,77	32,09	33,76	1,86	6,67	550,95	815,76
194,5	-0,79	32,32	33,23	2,69	6,28	629,36	901,92
199,5	-1,61	31,33	33,45	0,29	9,23	410,71	593,48
204,5	-1,48	32,10	32,61	1,80	7,99	551,61	752,87
209,5	-0,85	32,38	33,60	2,17	6,08	521,65	615,54

Profondeur (cm)	Température des eaux de surface en hiver (°C)	Température des eaux de surface en été (°C)	Salinité des eaux de surface en hiver (psu)	Salinité des eaux de surface en été (psu)	Couvert de glace de mer (mois/an)	Productivité primaire au printemps (gC/m²/an)	Productivité primaire en été (gC/m²/an)
214,5	-0,32	32,57	33,79	3,17	4,96	562,69	810,23
219,5	-0,62	32,47	33,89	2,09	5,75	502,40	713,31
224,5	-0,48	32,87	34,11	2,00	5,28	477,09	680,46
229,5	-0,25	32,75	34,22	2,39	4,72	546,82	666,48
234,5	-1,54	31,99	32,39	1,60	8,44	549,60	739,64
239,5	-0,68	32,56	33,37	2,49	5,66	549,41	695,54
244,5	-1,57	31,86	32,37	1,48	8,56	562,66	766,03
249,5	-1,20	32,46	33,14	2,17	7,60	537,67	810,49
254,5	-0,70	32,55	33,41	2,49	5,62	540,05	679,94
259,5	-1,32	32,29	32,79	2,35	7,42	579,87	842,63
264,5	-1,54	32,15	32,64	1,76	7,84	569,99	732,66
269,5	-1,13	32,71	33,04	3,27	6,74	528,11	708,31
274,5	-1,22	32,56	33,10	2,85	5,95	530,34	574,06
279,5	-1,12	32,83	33,17	2,38	7,06	553,46	680,15
284,5	-0,72	32,56	33,38	2,55	5,59	537,81	664,62
289,5	-1,52	32,06	32,64	1,73	7,85	561,17	761,20
294,5	-1,68	32,23	32,87	2,04	7,76	637,15	763,82
299,5	-0,54	32,57	33,43	3,19	5,40	608,83	832,37
304,5	-0,37	32,82	33,92	2,62	4,39	580,23	698,29
309,5	-1,06	32,48	32,98	2,53	6,82	614,75	827,14
314,5	-0,29	33,24	33,95	3,51	4,41	566,78	732,55
319,5	-1,27	32,47	33,01	2,22	7,63	570,00	811,54
324,5	-0,45	33,02	33,58	2,74	4,77	560,89	674,96
329,5	-1,03	32,38	33,24	2,31	7,09	506,91	696,61
334,5	-1,00	32,31	33,27	2,28	7,16	480,20	704,58
339,5	-1,60	31,77	33,34	1,19	8,70	436,64	607,26
344,5	-0,89	32,49	33,30	2,38	6,67	537,79	745,83
349,5	-1,50	32,21	32,81	2,09	8,00	515,45	689,43
354,5	-1,54	32,35	32,64	2,04	7,88	580,17	697,93
359,5	-1,52	32,20	32,84	2,08	7,98	534,07	695,80
364,5	-1,47	32,24	32,76	2,06	8,01	504,35	681,78
369,5	-0,95	32,27	33,34	2,22	7,12	455,10	737,66
374,5	-1,03	32,45	33,16	2,30	6,96	538,17	737,37
379,5	-1,02	32,59	33,03	2,49	6,75	588,46	734,11
384,5	-1,45	32,21	32,70	2,03	8,04	506,30	684,61
389,5	-0,57	32,56	33,91	2,10	5,52	507,56	709,15
394,5	-0,62	32,70	33,69	2,29	5,79	482,91	708,52
399,5	-0,67	32,86	33,51	2,53	5,64	552,68	698,08
404,5	-0,41	32,49	33,74	3,09	5,18	549,63	812,33
409,5	-1,51	32,20	32,85	1,87	8,05	496,98	682,61
414,5	-0,64	32,39	33,84	2,39	5,56	559,91	731,57
419,5	-1,59	31,75	33,38	1,20	8,66	430,29	616,06
424,5	-0,43	32,46	33,70	3,12	5,25	546,84	832,35
429,5	-1,18	31,97	33,04	2,52	7,24	534,25	880,86
434,5	-1,17	31,68	33,44	2,08	7,16	473,34	662,42
439,5	-1,41	31,62	33,31	1,81	7,27	509,53	584,20
444,5	-1,39	30,45	32,07	3,91	7,31	928,83	1082,70
449,5	-1,27	30,57	31,80	4,74	6,94	765,91	1114,18
454,5	-1,36	31,67	33,62	1,39	7,31	421,95	530,01
459,5	-1,62	31,07	33,75	-0,12	9,78	308,55	504,20

APPENDICE B

RÉSULTATS DES ANALYSES SÉDIMENTOLOGIQUES

Tableau B1 : Résultats des propriétés physiques et chimiques de la carotte HH16-1205-GC mesurés par les intruments Multi Sensor Core Logger et scanneur X-Ray Fluoresecence Avaatech respectivement

Tableau B2 : Résultats de la granulométrie de la carotte HH16-1205-GC

Tableau B1 : Résultats des propriétés physiques et chimiques de la carotte HH16-1205-GC mesurés par les intruments Multi Sensor Core Logger et scanneur X-Ray Fluoresecence Avaatech respectivement

| Prof. (cm) | MSCL | | Résultats XRF (cps) | | | | | | | | | | |
	Densité (g/cc)	S.M. (SI* 10⁵)	Al	Si	Cl	K	Ca	Ti	Mn	Fe	Rb	Sr	Zr
1		10,3	10662	103010	68622	87833	44402	32577	9765	367912	3373	3637	6650
2	1,456	12	17030	155984	83826	120906	58947	43522	11905	491438	4506	4611	8086
3	1,482	12,8	17024	154978	90264	119021	57198	43609	13095	506047	4665	4678	8508
4	1,492	13,4	15310	138947	100722	112024	57200	41628	8472	497152	4431	4949	8812
5	1,492	13,8	15638	141992	90376	114053	56913	41821	9184	497924	4333	4824	7723
6	1,473	14,1	16225	146345	85779	115909	55361	41991	9315	495747	4230	4613	8384
7	1,477	14,4	16698	150672	84626	115735	55972	41331	7721	476066	4133	4491	7590
8	1,477	15	15014	136670	93929	112791	55012	41894	6476	474390	4314	4540	7980
9	1,479	15,8	14860	135540	99287	111390	55037	41083	6274	470156	4395	4832	7855
10	1,465	16,7	9350	91444	134259	89421	54794	35115	5342	425053	3873	4823	8335
11	1,460	17	10726	101034	133813	98150	51533	39090	4619	452818	4745	4942	8865
12	1,482	16,2	15992	145766	100641	119729	60100	44284	4769	482958	4373	5033	8360
13	1,492	15,3	17844	158849	89613	126562	62238	45373	4831	462865	4574	5002	8677
14	1,505	14,8	16726	152331	87524	119807	59536	43246	3868	442270	4275	4873	7622
15	1,490	14,5	14872	134330	92445	109895	55873	40520	3492	441882	4221	5035	7568
16	1,488	14,4	17187	154512	79750	117441	58382	42080	4967	439141	4076	5352	7729
17	1,479	14,5	16901	150825	84956	118713	58987	42780	4849	452310	4484	5145	8079
18	1,544	14,7	16146	143010	95629	117821	58555	42514	4440	467093	4350	5134	8221
19	1,491	14,8	17131	155845	84483	122828	58781	45185	6506	485356	5034	5151	9018
20	1,494	15,1	18652	166700	90368	129080	62260	47039	7308	508321	4812	5184	8949
21	1,494	15,3	18959	171558	91024	133488	62567	48878	9148	519235	4898	5305	9394
22	1,514	15,6	16125	148221	95247	121948	59120	45305	7446	497224	4934	5324	9084
23	1,501	15,5	16627	147245	99965	118048	56647	44098	7544	486309	4331	5010	8177
24	1,509	15,3	17461	158301	91858	122230	58498	44939	6298	496616	4530	4882	8939
25	1,506	15,3	19781	179125	83401	131838	65157	47636	5781	501730	4671	5106	8450
26	1,515	15,2	17501	159982	92928	126952	60345	45819	5835	499757	5019	5048	8757
27	1,514	15,1	20541	181808	80219	134260	63139	47705	6312	505573	4846	5127	9062
28	1,509	15,3	18973	173269	82502	129232	61075	46312	7198	495329	4590	4805	8112
29	1,505	15,4	17321	155662	86875	120966	56762	44244	7763	481177	4547	4663	7827
30	1,517	15,7	17507	156201	83738	119642	57460	43125	6785	468389	4204	4607	7564
31	1,537	16,2	18150	163578	81505	121714	56689	43843	6962	474121	4284	4740	8364
32	1,588	16,7	16080	146414	92107	114053	53960	42431	9184	482845	4156	4568	8767
33	1,556	16,9	18680	168199	84844	125810	58566	45439	10152	510691	4624	4812	8384
34	1,555	16,6	18606	165951	92622	127342	58982	46644	13496	560724	4797	4811	7775
35	1,546	16,2	20585	185328	84577	134924	60767	48450	15514	552809	4700	5073	8740
36	1,541	15,9	20026	179712	88661	133440	61328	48171	12521	539894	4962	5164	9193
37	1,516	15,6	17121	158793	94424	125018	58184	46419	12904	545757	4720	5102	9252
38	1,501	15,3	17775	166123	90289	127551	58003	46457	9401	554520	4639	5000	8402
39	1,492	15,1	17274	161875	91782	125942	57394	45768	6256	538576	4300	4969	8216
40	1,498	14,7	17720	161787	91074	122720	57193	43911	5606	533775	4357	4940	8794
41	1,490	14,5	16270	153532	94752	120789	56657	44614	5459	535106	4484	4857	8744
42	1,488	14,3	17192	156266	92633	122358	56625	44769	7465	522207	4081	4955	9380
43	1,474	14,2	17896	161974	89819	124938	57151	45761	9892	531075	4802	5294	8114
44	1,467	14	14965	141667	103534	117613	53620	43671	18645	564258	4242	4929	8686
45	1,452	13,8	19337	174633	86035	130550	56814	46569	19543	569470	4729	4923	8304
46	1,441	13,6	17260	160981	93465	128156	55489	46242	18862	579451	4828	5074	8490
47	1,432	13,5	17336	161210	93719	127356	56088	46375	16904	576556	4520	5034	8157
48	1,425	13,4	16962	156808	97667	123992	55134	45328	16263	575788	4639	4874	7967
49	1,406	13,3	17338	157131	95923	122163	55713	44650	11585	563270	4621	4938	8225
50	1,434	13,2	15705	147863	97724	120669	55467	44590	10160	552889	4229	4899	8676
51	1,431	13,2	17908	165152	90584	126771	58214	45571	12807	570332	4335	5008	9186

Prof. (cm)	MSCL		Résultats XRF (cps)										
	Densité (g/cc)	S.M. (SI*10⁻⁵)	Al	Si	Cl	K	Ca	Ti	Mn	Fe	Rb	Sr	Zr
52	1,413	13,4	15966	150996	96036	123935	63400	45407	12056	565758	4323	5202	7954
53	1,406	14	17118	158619	93837	127625	56006	46631	14220	575520	4500	5015	8417
54	1,393	13,7	18139	167873	89051	130718	56266	46817	12486	594557	4482	5057	8204
55	1,377	13	15899	154363	99039	125149	55905	45531	15728	610181	4394	5213	8552
56	1,398	12,6	16088	156096	94894	123536	57375	45730	13427	585901	4372	5156	8657
57	1,378	12,4	14057	132621	101800	111990	52136	41895	15747	581804	4421	4841	8626
58	1,363	12,4	10575	104871	115156	99195	48074	38738	16873	549222	4151	4753	7643
59	1,368	12,4	13808	131962	102852	110193	51828	41343	19489	549108	4242	4685	7936
60	1,402	12,4	14997	142607	94444	111185	53640	40546	9599	525518	4100	4741	8190
61	1,413	12,3	15051	138577	86837	105791	52554	38938	8284	481347	4267	4491	7804
62	1,400	12,1	11704	113785	98753	96223	48431	36409	10113	462542	4162	4628	7480
63	1,391	11,9	13235	124378	88011	96224	46775	35468	11699	460796	3926	4222	7876
64	1,391	11,8	12294	112813	86130	91208	44419	33766	11388	435702	3767	4207	6699
65		12	7777	73602	72345	66575	34363	26706	7997	342198	2730	3430	5683
66		12,5	15320	146309	87241	112859	54693	40803	7360	496257	4314	4485	7083
67	1,483	13,2	23352	209897	83001	146066	66748	52006	9657	598854	5085	5579	10114
68	1,479	13,7	22342	202763	83793	143022	66713	51505	9888	575388	4937	5373	8994
69	1,481	13,9	20470	186564	88079	134320	66924	49277	6533	518023	5016	5302	8732
70	1,497	14,2	19015	171275	87943	128736	65139	47148	4259	504468	4788	5095	8737
71	1,521	14,3	21913	195517	76733	137081	67018	49088	3214	495724	4974	5181	9158
72	1,503	14,4	21578	191553	76592	134507	67770	48731	3816	504272	4813	5313	9657
73	1,498	14,4	20296	182778	80836	130560	62502	47511	3644	481653	4947	5165	8876
74	1,489	14,6	19711	181598	83237	131610	60942	47704	4030	491973	5025	4984	9339
75	1,492	14,9	20414	185775	83077	132866	59210	47351	4648	504230	4908	5175	8570
76	1,485	15,1	20768	189424	83474	133880	61354	48124	3702	511080	4716	5123	9270
77	1,476	14,8	20546	187438	81208	133682	61003	47727	4496	493474	4965	5170	8787
78	1,498	14,8	19828	180619	83778	130815	57848	46347	4703	491950	4715	5080	8649
79	1,494	14,7	21422	192115	74644	133473	61180	47251	3214	466452	4935	4976	8881
80	1,504	14,7	19767	181105	80362	130261	62518	46269	4148	441298	4872	5063	9169
81	1,532	14,7	19979	178823	82718	131236	62627	46322	3129	425494	4739	5042	8779
82	1,526	14,7	20271	180361	82006	133455	64047	47938	2149	417321	5037	5218	9290
83	1,537	14,6	21123	187162	82605	135323	63469	47866	3596	442851	4693	5288	9226
84	1,522	14,5	18527	167386	94198	130130	61240	46629	3610	434267	5034	5495	9409
85	1,529	14,5	20217	180563	86987	133915	62061	48294	2936	431202	4914	5249	9303
86	1,525	14,5	20284	180514	84905	132786	62395	47310	2407	430429	5061	5281	8739
87	1,534	14,4	21631	190565	83418	137252	63043	48894	3029	424997	5519	5517	9328
88	1,526	14,4	22713	196861	79339	139660	63897	48621	3103	421914	5276	5273	9858
89	1,537	14,4	22165	191805	81977	137941	61601	49008	2845	425126	4797	5425	9964
90	1,515	14,3	20942	183635	87011	136342	59154	48569	3429	443653	5048	5186	9666
91	1,510	14,3	20770	188054	87884	138049	60423	49399	4450	462336	5319	5346	9435
92	1,541	14,4	21422	191673	84020	139672	60085	49355	3754	459025	5496	5366	9460
93	1,540	14,4	19054	171113	93343	129968	56128	46641	3764	446004	4623	5121	9399
94	1,542	14,4	17309	153308	96044	120644	56427	43971	3933	429685	4827	4983	8544
95	1,513	14,4	17977	159570	85361	121486	52417	43690	4801	427394	4111	4736	7858
96	1,496	14,4	16722	151335	90266	116876	50473	41891	5141	436964	4453	4798	8167
97	1,504	14,4	17134	155179	90019	116622	50637	41726	3961	450552	4232	4815	8140
98	1,519	14,3	16589	151332	92288	117013	50921	42104	4718	420672	4332	4611	7758
99	1,520	14,3	16371	156131	87928	118598	51914	42297	4143	422570	4156	4608	8020
100	1,517	14,5	15613	145992	89546	114952	50170	41198	4569	443169	4174	4695	8414
101	1,503	14,5	16798	155165	87582	118196	52268	42387	4458	422647	4095	4736	7906
102	1,515	14,6	18407	168905	84719	124794	56656	43808	3987	446030	4396	5320	8469

Prof. (cm)	Densité (g/cc)	S.M. (SI*10⁵)	Al	Si	Cl	K	Ca	Ti	Mn	Fe	Rb	Sr	Zr
103	1,516	14,7	17651	161836	93611	122189	56929	43647	5707	474845	4092	5225	8197
104	1,513	14,8	14998	141495	105356	116138	53336	43029	8528	473380	4566	5232	8324
105	1,501	15,1	18079	163772	93581	125009	54697	44663	8600	485436	4367	5089	8769
106	1,524	15,3	16050	150726	102082	118674	51879	42946	7346	474310	4488	5031	8583
107	1,506	15,6	18670	172206	90006	127630	55760	44835	5718	453810	4785	5179	8907
108	1,519	15,8	16258	153942	97236	120822	53830	43771	7917	473431	4405	4998	8162
109	1,502	15,6	15690	147313	97961	118464	52229	42840	8106	488395	4360	4920	8291
110	1,520	15,2	14727	138624	106367	112360	50899	41723	9104	466075	4525	5023	8794
111	1,537	15,1	15572	144468	101511	115226	51772	41429	8543	508375	4106	5038	8072
112	1,540	15	15724	147570	98121	117762	51151	42574	8677	463374	4369	4829	8337
113	1,525	15	17298	159263	91515	121314	52485	43773	6498	473762	4655	5014	7998
114	1,526	14,9	12799	123478	106816	103322	47858	39074	5586	438555	4271	4491	8275
115	1,532	14,8	14529	139853	107332	111701	53589	41339	4948	484437	4616	4606	8702
116	1,515	14,7	18207	169601	90095	126818	55268	46059	7870	479760	4393	5022	9299
117	1,522	14,5	17851	166946	97305	124387	64304	45409	9160	488172	4758	5212	8860
118	1,510	14,2	18206	166972	97178	128364	57041	46196	6786	486435	4969	5355	8894
119	1,505	14	18124	165118	97267	126624	55512	46230	5752	472531	4805	5294	8790
120	1,496	14	17385	160423	98176	123899	52835	45534	5936	460488	4596	5252	9218
121	1,506	13,9	17863	164032	92592	123269	52203	44200	5947	452683	4796	4930	8796
122	1,500	13,9	16034	148564	95018	116075	50057	41994	5634	456984	4348	4696	8664
123	1,492	13,9	16387	152006	96226	117234	51108	42337	6582	455703	4487	4752	7914
124	1,496	13,9	16258	149597	98966	115816	51342	43235	6879	475544	4585	4916	7517
125	1,504	13,9	16466	152368	95706	118430	50424	42608	6990	465144	4438	4872	8308
126	1,509	13,9	16625	156233	87320	119533	51004	42790	6744	462531	4073	4875	8250
127	1,507	14	17243	157855	88533	121240	51395	43436	6857	467271	4397	4777	7805
128	1,508	14,2	17767	165597	84589	122997	52448	43951	8100	467139	4257	4927	7869
129	1,516	14,3	15021	145171	93010	115607	51181	41699	6787	459860	4295	4755	8149
130	1,509	14,4	17081	158896	84540	120806	51957	43350	6359	458504	4702	4727	9024
131	1,549	14,6	14083	136034	93946	112145	49300	41512	5296	438333	4431	4652	7716
132	1,546	14,8	13039	129260	94761	109966	50641	39608	6103	441617	4159	4686	8016
133	1,554	15,2	14563	141854	90242	115153	50138	42079	7203	464710	4238	4852	8556
134	1,554	15,1	15794	148529	87044	117284	51688	42861	6144	458067	4464	4822	8379
135	1,548	15,1	15034	143144	90311	117530	51312	42932	5622	459262	4664	4905	8312
136	1,531	15,2	14321	135538	94941	111709	51607	40965	7902	465400	4231	4787	8062
137	1,538	15,3	14566	142468	87854	111065	56179	39989	7497	484377	3992	4977	7454
138	1,558	15,4	13815	132116	88754	106173	49523	38397	4553	501198	3906	4486	7760
139	1,564	15,5	15978	148692	82529	112555	50393	40074	6655	461044	4096	4481	7200
140	1,562	15,5	15302	144394	86004	111346	49185	40174	5195	457817	4050	4622	7618
141	1,572	15,5	14271	138306	89409	110385	48524	40716	5884	450999	4323	4749	8089
142	1,537	15,4	15999	154099	82371	114054	47838	40543	5576	436153	4101	4699	8515
143	1,533	15,4	16741	155182	80146	113250	47836	40323	6257	459221	4055	4588	8018
144	1,537	15,4	12563	120860	90224	98313	43063	36106	7329	497685	3411	4240	6932
145	1,551	15,4	13943	133696	82412	103532	44816	37271	7332	456595	4110	4264	6999
146	1,535	15,3	14803	138514	82599	106532	44977	38151	8313	461681	3706	4428	6909
147	1,562	15,3	14517	135923	86206	106761	44982	38388	5248	452216	4063	4594	7484
148	1,546	15,2	15385	144960	83348	110408	46153	40063	5617	445684	3645	4526	7829
149	1,528	15,2	16493	152133	79592	113411	47224	40587	6139	457797	3843	4577	8120
150	1,537	15,3	16787	155885	76354	114883	46379	40433	5291	452709	4057	4600	7472
151	1,520	15,3	17554	160016	73695	116652	46913	41528	4738	465615	4070	4577	7787
152	1,529	15,4	16505	151320	74419	112775	46357	40366	5133	462155	4367	4636	7774
153	1,530	15,3	16818	155413	76725	114378	46703	40848	8054	484518	4196	4398	7856

88

Prof. (cm)	MSCL		Résultats XRF (cps)										
	Densité (g/cc)	S.M. (SI*10⁵)	Al	Si	Cl	K	Ca	Ti	Mn	Fe	Rb	Sr	Zr
154	1,544	15,5	16297	148655	80612	112739	46330	40851	6425	475378	3745	4648	8366
155	1,571	15,6	10204	100819	92093	95267	40624	35589	7107	438593	3833	4413	7186
156	1,533	15,5	11908	118374	82742	98549	41652	36927	6400	436054	3619	4621	8356
157	1,514	15,7	14754	139153	85082	110452	45032	39606	7486	468293	4178	5670	9419
158	1,534	15,7	14623	136830	90737	110273	45781	40284	7935	495628	4084	4732	8167
159	1,528	15,8	16009	151836	85774	114984	47833	41694	6174	489180	4355	4838	8476
160	1,551	15,9	13605	130624	96714	107942	46013	40299	7043	495032	4047	4850	8074
161	1,575	15,9	18478	168760	79709	121820	52074	43776	9071	487818	4297	5030	8318
162	1,576	15,7	17880	164269	81915	120594	49996	42578	7502	475500	4707	5019	8058
163	1,571	15,5	16667	152994	85770	117596	47411	43233	8104	487273	4441	4975	7663
164	1,542	15,1	18194	167458	79388	121761	48506	43096	7642	487112	4222	4974	8732
165		15	8311	80630	54717	64044	30469	26627	4482	274151	2445	2955	5213
166		14,9	14785	134652	68445	101595	40163	37099	2363	434617	3561	4091	7285
167	1,600	15,2	16142	150776	77325	113714	43873	40229	7166	500728	3880	4517	7567
168	1,562	15,5	20159	180799	69706	125376	47795	44055	14018	475805	4142	4752	7465
169	1,552	15,7	19498	175112	76533	124881	48905	44278	14081	490263	4566	4815	8256
170	1,543	15,8	17476	164507	81286	121793	48191	42627	8765	494467	4357	5022	8559
171	1,550	15,9	18699	170649	78228	123614	48717	43671	13185	469611	4394	4781	8388
172	1,540	16	17360	159417	85322	119658	47107	42519	12214	485095	4192	4987	8245
173	1,542	16	18634	169601	75491	120381	47054	42785	9540	487264	4273	4721	7901
174	1,567	15,9	19433	174657	70788	122677	46849	42640	8698	466192	4231	4634	8004
175	1,536	16	18739	166472	71698	117791	46357	41379	5820	457526	4071	4413	7692
176	1,551	16	14073	135832	79883	105286	42943	37984	8116	425964	3978	4276	6834
177	1,541	16	15225	142126	79311	110349	44479	39015	4815	467641	4099	4395	7698
178	1,553	16	18406	168440	73741	119879	48069	42494	6888	454319	4047	4677	8265
179	1,544	16	17596	162175	81507	119037	52488	42158	5219	497116	4344	4719	8348
180	1,539	16	17834	166572	83641	122082	46702	43310	4397	542851	4554	4957	8572
181	1,543	16	19359	179457	82442	131804	50113	46105	7637	516682	4731	5223	8576
182	1,539	15,9	18816	175018	85186	130438	50051	46335	7486	524016	4462	5257	8913
183	1,533	16	17199	160319	92296	123513	44551	44635	8368	507085	4755	5208	9050
184	1,530	16	15074	143719	95297	117667	44676	42401	11639	486281	4376	5050	8722
185	1,528	16	16766	153605	91170	117238	46269	42578	11946	462532	4451	4924	8652
186	1,516	15,9	16538	153276	87477	118660	46210	42511	13018	471960	4377	4847	8065
187	1,512	15,9	17711	165862	81220	122518	48278	43903	13605	473463	4565	5007	7717
188	1,535	15,8	17497	163086	84915	121040	49714	43873	13135	498525	4199	4882	7643
189	1,555	15,8	17789	165586	86149	123466	48737	44163	7814	490556	4395	4899	8797
190	1,518	15,8	16938	155780	87876	121722	48306	44077	7630	481021	4645	5000	9062
191	1,499	15,8	16935	154742	91032	118849	47721	42227	12707	511950	4133	5122	8794
192	1,513	15,8	16504	153548	87983	118525	48112	42337	14300	511192	4214	4896	7971
193	1,568	15,9	15466	146166	93416	116940	48438	41961	11891	478074	4570	4986	8379
194	1,564	16	16358	154771	84040	116743	48061	41744	12087	492278	4270	4754	8161
195	1,543	16	16630	155826	82873	116954	46366	41578	9186	481075	4327	4847	8292
196	1,552	16,1	17729	163490	78052	120306	47980	42989	9451	462615	4341	4847	8387
197	1,555	16,1	16448	150885	84339	115743	46215	41371	9779	455917	4314	4908	8084
198	1,535	16,2	15009	141468	88886	109873	44875	40310	8887	457425	3887	4626	7816
199	1,511	16,3	13885	131271	90081	106550	44896	38703	8466	444948	4243	4550	8384
200	1,516	16,4	16596	152524	74762	112482	46403	39558	7376	404625	4064	4401	7857
201	1,567	16,6	14952	136755	76589	103891	42122	37351	4809	388944	4042	4162	7213
202	1,558	16,8	12376	113442	75394	90317	38042	33729	4530	374989	3480	4058	6490
203	1,549	16,8	9948	93990	67509	78062	33929	29133	4310	338005	3369	3693	6495
204	1,552	16,8	9003	88544	58359	73703	31464	27803	4887	312795	2991	3297	5934

Prof. (cm)	MSCL Densité (g/cc)	S.M. (SI*10⁵)	Al	Si	Cl	K	Ca	Ti	Mn	Fe	Rb	Sr	Zr
							Résultats XRF (cps)						
205	1,535	16,8	9475	89934	45174	70399	30244	26802	6127	288760	2743	2938	5087
206	1,543	16,7	5263	52127	30805	44492	20316	18241	4994	210924	1740	2193	3807
207	1,538	16,6	6194	63441	41266	57613	25959	22677	5725	247651	1983	2584	4425
208	1,551	16,6	12953	118189	56640	89686	40481	32899	4228	324556	3324	3957	6581
209	1,557	16,6	13741	127056	67211	97997	40852	35094	4756	387342	3752	4234	7200
210	1,542	16,5	14427	136218	79787	106859	45510	38026	7381	422969	3750	4721	8291
211	1,548	16,5	14618	137794	80368	107241	43458	38100	4484	449710	3801	4629	7782
212	1,541	16,4	13664	131282	86438	103163	42775	38133	7047	432592	4148	4623	7383
213	1,538	16,4	14217	136041	87030	106542	44372	39435	9858	450464	3969	4873	8585
214	1,526	16,3	14736	139471	80967	108680	45625	40450	5234	487030	4179	4831	8293
215	1,523	16,2	14026	132077	87124	105227	43418	38969	10818	464854	4147	5051	8189
216	1,510	16,2	14480	133317	76950	103698	42565	38663	10996	448774	3848	4552	8162
217	1,535	16,4	14126	135246	80244	106112	42486	38830	11633	440010	4033	4759	8375
218	1,533	16,5	14187	135700	84928	107047	42892	39170	10481	440635	3961	4468	8429
219	1,541	16,6	16281	151190	78040	111561	44889	39654	9405	454746	4053	4661	7635
220	1,568	16,8	12456	121777	85413	99616	40346	36006	7308	410628	3759	4492	7899
221	1,554	16,8	13388	127728	81778	100590	44266	36090	6656	409315	3714	4899	7204
222	1,597	16,8	14784	136568	83647	107949	43416	39566	6122	443126	3871	4914	9046
223	1,570	16,8	16876	158055	76868	117711	46284	41886	7441	470148	3981	4578	7428
224	1,570	16,8	12891	125216	91621	104715	43511	37940	9070	459135	3766	4597	8268
225	1,571	16,8	15943	148155	77645	110665	43438	39409	10357	464066	4041	4597	7475
226	1,531	16,8	13254	128684	86107	102463	42157	38051	8623	478706	3550	4376	7605
227	1,534	16,7	12811	122447	89708	102731	40873	37323	9489	459781	4124	4543	7298
228	1,541	16,7	14183	136090	85093	106251	43205	38647	8969	456041	3899	4519	7692
229	1,542	16,8	14845	143888	83689	109909	44722	39046	6586	463556	3844	4541	7500
230	1,567	16,8	10910	108513	79849	84928	270171	31005	3926	388146	3774	10427	5843
231	1,508	16,8	16403	135837	79622	101401	130698	36192	5959	439776	3889	6838	7353
232	1,512	16,8	16842	158232	83021	119313	47414	41318	9524	503873	4129	4846	8231
233	1,515	16,7	17763	166845	78634	120551	47254	42612	10431	517140	4024	4744	8125
234	1,495	16,8	17044	162046	82058	120229	47373	42619	10336	509052	4258	5025	8612
235	1,511	16,8	16226	155339	83373	116442	46177	42108	12862	495733	4089	4908	7783
236	1,539	16,9	16006	150277	83383	113187	45856	40040	11894	476058	4119	4820	8235
237	1,557	16,9	15958	152772	78765	112691	44496	40141	8751	472920	3731	4776	8134
238	1,562	16,9	14876	147438	81098	111519	43877	39113	8687	448815	4178	4527	8068
239	1,554	16,9	8280	90922	111864	94905	40524	37466	8448	448203	4056	4712	7317
240	1,529	17	14138	136609	90600	106283	43021	39693	5427	518513	3765	4687	8084
241	1,596	16,9	16699	157843	82812	117698	45687	42606	5580	462962	4248	4804	7780
242	1,638	16,9	16551	158303	83796	118461	45898	42181	7472	492981	4236	4842	8708
243	1,593	17	13646	135857	89012	104848	41427	38100	6695	494641	3968	4508	8430
244	1,538	16,9	15351	146456	77301	107844	41316	37991	8622	463838	3530	4355	7893
245	1,511	17	14711	139118	73281	100568	40210	36442	5806	427534	3646	4181	7738
246	1,542	16,9	14561	137144	74140	102031	40383	36507	6275	417389	3539	4230	7130
247	1,594	16,9	15136	142720	75824	105603	42457	38247	6152	409297	4063	4512	7966
248	1,570	16,8	13346	126655	88187	100417	41530	36665	5588	410141	3897	4258	7102
249	1,592	16,9	15151	144087	78509	106525	42514	38477	7783	434037	3945	4397	7871
250	1,562	16,8	12870	123890	85206	99142	39929	36748	5312	402776	3703	4332	7572
251	1,549	16,9	12733	121237	69039	92957	36440	33484	4244	374200	3411	3953	6983
252	1,532	17	10838	103086	70425	82766	34170	30589	5902	350153	3048	3763	6159
253	1,544	16,9	11786	112724	67752	86782	38267	31655	5885	360048	3013	3713	6565
254	1,534	16,9	13928	133089	67764	97955	39277	35302	4937	390187	3328	3868	6658
255	1,546	17	15903	148291	68202	105884	42554	38030	5940	402924	3714	4131	7291

	MSCL		Résultats XRF (cps)										
Prof. (cm)	Densité (g/cc)	S.M. (SI*10⁷ s)	Al	Si	Cl	K	Ca	Ti	Mn	Fe	Rb	Sr	Zr
256	1,539	16,9	15125	142065	76678	105873	42713	38803	5939	418359	3866	4434	7417
257	1,555	17	14010	135636	84747	105778	42280	38491	6692	415579	3704	4773	7646
258	1,553	16,8	14660	136975	78362	104395	41625	38571	5873	388373	3887	4383	7545
259	1,544	16,8	14118	131286	81362	102133	40927	37364	5852	393634	3947	4416	6940
260	1,576	16,7	15834	145152	69834	104676	39914	37371	3492	367041	3746	4184	7633
261	1,565	16,6	14349	132141	58408	93417	41709	33449	1641	327135	3368	4041	7127
262	1,586	16,5	6277	66848	49011	62525	29440	25587	2902	272116	2733	3211	5190
263	1,562	16,6	10482	106487	59020	92377	39241	34441	2106	345638	3622	4021	7719
264	1,567	16,4	12810	129613	54352	108053	43090	39489	2024	340935	4016	4334	8425
265	1,565	15,8	11412	113215	63629	99621	39544	37162	1775	341268	3904	4449	7806
266	1,536	15,1	11642	123896	80616	111961	45773	41117	5145	469558	3999	4948	8249
267		15,1	9980	101492	78291	95071	40648	36048	4802	498970	3464	4539	7005
268		16	8534	89318	62004	81390	35316	30514	2891	378548	3175	3917	6324
269	1,532	16,8	10566	105363	57544	91792	38261	33912	3007	373701	3171	4154	6589
270	1,563	17,4	10063	106795	76658	100084	43562	38530	2845	449854	4264	5381	8654
271	1,574	17,7	9180	95569	73339	87893	163506	33197	2651	360679	3588	14694	7838
272	1,588	18	9736	104811	79170	101837	43147	38883	3506	477362	4450	4971	8487
273	1,609	18,3	10401	110921	82441	105377	45947	39872	4692	447759	4176	4866	8384
274	1,570	18,6	10480	109678	76972	98510	40937	36556	3819	433887	3374	4637	7004
275	1,562	18,8	10513	109563	73204	99198	40284	36827	3479	425029	3706	4408	8251
276	1,544	18,9	14820	138892	74895	101625	43987	37042	3005	415751	3655	4554	7337
277	1,538	19	13017	124330	77318	93536	46178	34648	3368	432706	3391	4784	7095
278	1,558	19	13534	128239	82584	99967	42719	36077	2939	425017	3634	4370	8569
279	1,529	19	13877	132391	79673	103305	42830	37399	2838	425163	3779	4495	7474
280	1,544	18,9	12233	119311	87156	98277	39719	36880	3529	434965	3467	4653	7599
281	1,541	18,8	12418	119073	89673	96759	40429	37041	4415	432916	3631	4524	7053
282	1,538	18,7	13708	127055	86837	99077	40295	37293	3776	446976	3573	4412	7115
283	1,534	18,5	14018	132669	82078	99590	40071	37282	3810	433495	3560	4350	7106
284	1,527	18,3	14339	136424	75151	99662	39412	36348	4232	433341	3487	4273	7284
285	1,507	18,3	13983	129294	71446	95801	36957	35060	3328	392662	3463	4129	6997
286	1,513	18,3	8748	83002	63607	69094	26510	27071	2256	293988	2999	3370	5693
287	1,527	18,3	15198	139486	75215	106276	35928	39195	2513	403117	3848	4314	8339
288	1,654	18,4	14316	130361	83588	105694	37556	40315	1684	441620	4391	4634	8292
289	1,914	18,3	14268	130332	91801	109073	38933	41543	3191	448718	4670	5079	8967
290	1,866	18,3	13838	131767	102480	112875	40869	42922	4024	494316	5059	5417	9543
291	1,557	18,3	14535	139789	110677	117525	46197	45084	3966	567384	4785	5762	9389
292	1,520	18,4	18414	172690	93793	130262	48891	47453	5319	520417	5241	5829	9587
293	1,533	18,4	16977	159132	90643	121259	49023	44945	3753	496075	4566	5439	8863
294	1,513	18,4	14064	134395	84953	104920	44497	39327	2962	447558	4264	4933	7963
295	1,521	18,4	12783	122247	69447	91188	37446	32906	1758	373169	3239	4041	7203
296	1,525	18,3	9424	91030	72379	74269	31595	28490	2706	341744	2984	3468	6560
297	1,507	18,1	8763	86883	70382	71790	30173	27741	1660	345926	2857	3260	5654
298	1,534	18,2	9215	89922	56096	67788	28451	26437	3023	293401	2508	3088	4961
299	1,520	18	5523	57640	48734	49063	22094	20319	1532	226621	1865	2495	4459
300	1,528	18,1	7955	78670	63040	66985	27979	26008	2132	325215	2331	2985	5296
301	1,529	18,1	13446	127261	82313	102558	43429	38424	2709	422362	3876	4612	7737
302	1,490	18	15693	145486	91652	117233	48074	43030	2917	449622	4743	5505	9193
303	1,492	18,4	14176	137036	101098	115640	49554	43665	3227	444515	5013	5500	9476
304	1,517	18,5	13961	136269	100932	116121	48570	43890	3269	447402	5095	5812	10576
305	1,569	18,3	13706	133576	98094	114770	49403	42518	3221	462299	4979	5516	9301
306	1,589	18,3	14579	140042	86175	109638	46044	39948	3476	443348	4407	4955	7851

Prof. (cm)	MSCL		Résultats XRF (cps)										
	Densité (g/cc)	S.M. (SI*10⁵)	Al	Si	Cl	K	Ca	Ti	Mn	Fe	Rb	Sr	Zr
307	1,537	18,3	14397	133320	73370	99355	41201	36216	3005	383816	3906	4504	7129
308	1,561	18,3	14321	133909	70326	98288	39167	35652	2149	371930	3367	4130	7210
309	1,529	18,3	13714	126380	74877	95268	37644	34709	2317	355603	3291	3974	7022
310	1,523	18,3	12600	119844	78775	93590	35889	35377	2026	378624	3558	4155	6482
311	1,539	18,3	8612	84676	94454	75176	32040	29566	1677	352666	3318	3925	7213
312	1,580	18,2	12671	122502	86431	99531	39323	37528	1837	434557	3417	4394	7857
313	1,631	18,2	12320	123174	95823	105664	38165	38939	2771	477293	4072	4662	8052
314	1,563	18,1	14552	140609	91117	112969	42022	41947	2433	461445	4383	4687	8518
315	1,547	18,1	11872	117380	106972	102038	39711	39176	3397	474017	3909	4739	8214
316	1,531	18	12645	123986	108891	107516	45198	40640	4787	481055	4466	5243	8946
317	1,517	18,1	15425	150676	100723	121177	50604	43800	5716	501880	4425	5373	9189
318	1,543	18,1	14303	138574	108326	113003	49889	41934	4859	486941	4352	5220	9167
319	1,525	18,2	13858	135506	94774	108289	47815	39840	4504	469938	4130	5030	8198
320	1,513	18,3	11129	114117	101700	99940	44170	37487	4826	436852	3765	4998	8090
321	1,506	18,3	10841	114059	100339	101119	47257	37351	3948	436696	3796	4775	8216
322	1,507	18,4	11181	114870	97062	97023	44613	36511	2680	444096	3955	4655	6917
323	1,513	18,6	14076	136776	77597	101889	47363	37280	3131	421064	3818	4428	7787
324	1,516	18,8	14691	142480	67843	101422	44689	36202	2259	420554	3450	4184	6970
325	1,506	18,9	12600	121495	75077	92667	41473	34341	2703	389739	3240	4172	6451
326	1,518	19	13719	134579	80495	101940	44612	37333	3332	434538	3286	4464	7649
327	1,530	19,2	14366	140433	82887	104593	46688	38732	3717	433577	3730	4763	7302
328	1,507	19,2	12552	125145	98115	102013	45372	38476	3096	453408	4164	4863	8002
329	1,528	19,4	14131	141532	92882	111023	48480	41418	3270	481515	4247	5027	8513
330	1,567	19,5	14270	141551	94698	110919	54771	41791	3239	475113	4220	5124	7713
331	1,528	19,6	15812	147373	91101	111835	50753	41110	3258	459431	4383	5123	8837
332	1,548	19,6	15430	148546	87649	108053	52896	39624	4028	446582	3943	4931	8886
333	1,546	19,6	12767	120831	91590	95016	43670	35877	4007	431602	3857	4871	7981
334	1,545	19,7	13507	127801	85718	100012	43281	37382	5010	404907	4203	4958	8437
335	1,573	19,7	12967	125358	80473	96632	45341	35411	3360	405874	3707	4553	7859
336	1,532	19,6	13377	127141	73400	97661	40610	36120	3437	412954	3642	4475	7265
337	1,588	19,4	11178	107926	72112	88700	37245	33949	4224	399588	3609	4193	7199
338	1,536	19,2	11873	115033	70584	89207	37058	33150	3837	384983	3418	4217	6730
339	1,544	19,1	12117	116260	60054	87808	34566	31992	2530	365440	2917	3773	6141
340	1,524	19	10180	100470	52071	76089	30105	29215	2038	323466	2881	3295	5699
341	1,529	19	8255	80330	49563	62813	27723	25006	1681	277693	2472	3052	5242
342	1,519	19,1	8404	84177	52043	67709	30854	25847	2300	298652	2383	3173	5333
343	1,541	19,4	7733	81361	50435	69012	32303	25808	2706	297764	2442	3195	5510
344	1,592	19,6	8623	89140	48566	69330	32678	26465	3261	300575	2491	3184	5235
345	1,542	19,9	8957	92110	47993	70924	33255	26872	2878	301054	2482	3096	5352
346	1,536	20,3	10018	99258	50744	73742	34707	28650	2205	313358	2620	3408	5736
347	1,537	21	9828	97132	53343	74867	35189	27954	2152	324503	2683	3253	5751
348	1,532	22	9960	102108	52944	75107	34684	28186	1989	318433	2549	3359	5753
349	1,529	22,8	10273	101133	48644	73981	36679	28268	2168	303759	2529	3245	5640
350	1,534	22,7	9157	93089	54450	71765	37011	26708	1821	321113	2635	3478	5502
351	1,534	21,6	10497	103478	59439	77990	44836	29434	3460	344809	2757	3690	5841
352	1,546	20,4	12164	117853	59815	84069	42128	31966	2712	362322	3225	3945	6658
353	1,541	19,6	12594	122167	59671	87165	39707	31821	2880	359388	3156	3794	7157
354	1,541	19,2	11156	108987	66912	81219	36732	30914	2854	382902	2849	3762	6274
355	1,554	18,9	12922	123287	60533	87120	39121	32022	2530	352074	3056	3858	6044
356	1,559	18,8	11856	119823	62155	87038	40108	32287	2361	349165	3272	4007	6766
357	1,563	18,7	10539	106887	66542	80538	38631	29684	2079	344803	2909	3692	6016

Prof. (cm)	MSCL Densité (g/cc)	S.M. (SI*10⁵)	Al	Si	Cl	K	Ca	Ti	Mn	Fe	Rb	Sr	Zr
358	1,539	18,6	9116	95406	60800	76936	36655	28675	2381	316019	2863	3513	5970
359	1,536	18,6	8882	90331	59198	72024	33353	26767	2125	314486	2887	3518	6085
360	1,541	18,6	7678	81538	62173	68453	32710	26274	1778	331178	2698	3507	5527
361	1,534	18,5	9856	98715	60508	77398	34903	29152	2965	329993	2610	3649	5875
362	1,550	18,4	11607	112018	55988	81415	38213	30694	2135	319622	3271	3621	6514
363	1,551	18,3	6661	66502	38284	56951	22258	22423	1302	253131	2325	2780	6105
364	1,554	18	5118	56511	30960	45802	25792	19327	1175	189925	1932	2483	5095
365	1,590	17,7	3559	39945	20958	32809	23251	14856	1067	135203	1469	1845	3642
366	1,548	17,7	17023	166730	99930	127563	60324	47382	2351	510712	4974	6089	10370
367		17,5	11960	126033	100092	109213	52880	41826	3072	488539	3885	5409	8825
368		17,4	15055	143866	85302	106507	48945	38657	4404	422805	4246	4804	7915
369	1,528	17,7	11753	114405	80537	91818	44535	33782	3557	355674	3588	4478	7205
370	1,521	18,1	13722	130014	73177	95481	45961	34883	2675	357346	3791	4596	7099
371	1,551	18,5	14998	143110	82280	106854	50754	39829	3504	462443	3897	5307	7663
372	1,638	18,8	14196	138961	91513	113922	54923	42282	3602	470426	4366	5730	8986
373	1,634	19	15257	147418	86301	115815	55760	42669	3465	464168	4642	5546	9516
374	1,556	19,1	13162	135084	95204	115201	51569	42634	3442	460547	4281	5603	9861
375	1,575	19,1	8546	96327	105629	96211	54994	36199	2743	514329	4299	5688	8984
376	1,589	19,3	17119	163664	87531	124915	55058	46440	3614	487120	5073	5645	10183
377	1,667	19,5	17830	169494	85481	126638	54745	46210	2390	484892	4832	5693	9802
378	1,595	19,6	18564	173897	81048	129846	58825	47164	3503	467655	4546	5582	9617
379	1,663	19,7	16431	157727	86868	120896	57267	44458	3300	462715	4916	5626	10140
380	1,619	19,7	16717	158786	89103	119093	61980	44203	2912	500110	4592	5983	9102
381	1,581	19,5	17303	166798	84744	121217	67576	44401	3341	505018	4541	5755	8585
382	1,557	19,4	18194	171433	82912	123433	69616	45038	3321	481737	4517	5691	8305
383	1,549	19,4	16650	159286	81220	118836	90429	42788	3496	471421	4262	5925	8946
384	1,539	19,3	14785	146868	84427	114479	99153	41679	3281	465608	4075	6220	7648
385	1,527	19,3	18763	171885	77546	117406	111334	41208	2822	457124	4048	8222	7719
386	1,544	19,5	18609	170783	71323	117503	88535	42267	2185	439126	4184	5501	8543
387	1,551	19,5	17302	163122	68626	110733	101308	38824	2014	426352	3755	5340	7496
388	1,541	19,6	17284	160691	65191	107987	112402	38260	1475	388434	3966	5544	7819
389	1,567	19,7	17206	163076	69433	111146	144507	38126	1966	414720	3862	5717	8422
390	1,568	19,6	20274	186628	68413	124370	67729	43934	2914	423465	4274	5116	8596
391	1,568	19,5	18435	173038	73163	120400	64755	43361	3778	446303	4368	5132	8110
392	1,546	19,2	16952	162600	77092	117829	67402	42112	4023	452121	4178	5093	8020
393	1,526	19,1	17366	164795	75577	118224	64275	41596	3604	440086	4405	5142	8640
394	1,508	18,9	17302	162550	75466	114645	58731	41085	3124	448142	4064	5104	8327
395	1,543	18,8	18991	175219	66666	121180	62686	43266	2419	401888	4492	5193	8090
396	1,543	18,9	16224	154815	74409	116968	61415	41252	3030	410822	4449	4954	8222
397	1,547	18,9	15544	151351	74966	111495	55995	39994	2460	399848	4046	5013	8449
398	1,621	18,8	17334	162854	70575	114989	63479	40853	2166	386166	4238	5007	8314
399	1,586	18,7	19543	176979	67530	119804	71907	42521	2046	398896	4017	5103	8562
400	1,593	18,6	18727	170584	75029	119793	63087	43210	2659	420237	4102	5221	8652
401	1,612	18,5	18972	176498	71858	123166	62410	43586	2110	424256	4404	5151	9120
402	1,592	18,6	17348	163958	72279	122367	64598	42653	2093	414358	4118	5146	8678
403	1,596	18,6	13632	135416	77942	110923	60509	39678	2307	405168	4044	5275	8640
404	1,571	18,6	14457	139093	68657	107585	78198	37323	2691	345395	4200	5234	9060
405	1,565	18,5	19104	176612	68907	123589	94400	42861	2843	364289	4673	5590	9404
406	1,568	18,5	17120	163356	78100	114463	151565	40080	2103	403301	4180	6170	8364
407	1,605	18,5	17026	165410	80995	116289	124204	40995	2787	410724	4448	5914	8117
408	1,587	18,5	16805	161542	83684	116176	97401	41810	2899	414187	4067	5606	8891

Prof. (cm)	MSCL		Résultats XRF (cps)										
	Densité (g/cc)	S.M. (SI* 10^5)	Al	Si	Cl	K	Ca	Ti	Mn	Fe	Rb	Sr	Zr
409	1,560	18,4	16405	157560	88601	115285	93187	41764	3077	423138	4361	5665	8764
410	1,568	18,3	17186	166393	81723	119094	105500	41680	2586	425915	4630	5949	8457
411	1,565	18,3	17851	173011	76847	120257	140718	41009	2470	412791	4374	6140	9140
412	1,552	18,2	17043	161565	81197	117042	133631	40592	2314	419311	4129	5846	8367
413	1,562	18	14897	151574	81578	112066	186502	37995	1875	395280	4584	6294	8797
414	1,546	18	15584	152245	80093	111866	224901	38299	3109	384871	4763	6912	8353
415	1,558	17,9	14924	145886	81903	110099	247551	36544	2768	383355	4351	8039	8360
416	1,548	17,8	16358	158166	78035	117581	193939	38585	2970	394935	4662	6638	8159
417	1,549	17,8	18128	174056	74762	121638	133903	42703	2294	420860	4477	6384	8608
418	1,530	17,9	18926	178302	76021	122361	117771	42555	2149	443338	4796	6654	8632
419	1,537	17,8	18177	171142	79532	118866	141014	40957	1848	437297	4582	8641	8066
420	1,530	17,8	18162	173779	76518	119917	165938	41114	1771	419344	4655	10033	8446
421	1,546	17,9	16583	163388	78802	114050	237791	38289	2147	398657	4259	9821	8086
422	1,547	17,9	16787	165115	77287	114217	226823	39029	2461	401605	4312	7910	8490
423	1,523	17,9	16055	158433	79437	111560	202022	38094	2838	401432	4353	6770	7980
424	1,525	17,9	18068	174183	74106	117573	123225	40806	3165	429004	4071	6674	8103
425	1,532	17,9	17008	166153	72420	112431	100721	39455	2228	405439	4075	5945	8102
426	1,527	17,9	11612	115459	75317	88211	84351	32288	2159	338643	3591	5492	7067
427	1,545	18	17223	161635	70090	106668	103817	37417	1805	361667	3983	7169	7825
428	1,558	18	19119	184121	68832	120253	117517	41318	2268	393938	4316	6200	8127
429	1,606	18	19367	185193	75160	123268	122855	42535	2633	423586	4108	6569	8852
430	1,550	18,2	19798	188183	74880	123216	140947	42105	2376	418682	4677	9675	8765
431	1,536	18,2	17147	169246	80116	114656	163046	40155	2093	436303	4232	17265	7282
432	1,524	18,2	17644	170145	76335	113318	140231	39430	2261	436621	4153	11581	7927
433	1,509	18,2	18381	176531	72805	116189	106880	40816	1996	399344	4264	7232	8100
434	1,527	18,3	17246	167746	71030	110473	134828	38706	2759	386774	4248	6220	8598
435	1,523	18,4	14238	144218	78587	105295	156484	37513	2377	374565	3888	6437	7868
436	1,525	18,5	14900	152823	77589	106862	202762	37336	2371	370131	4085	6404	8042
437	1,526	18,5	16475	163031	76889	113498	162340	39527	1707	388424	4216	7922	8529
438	1,529	18,4	14993	153182	85171	110892	129921	39068	1962	384554	4575	7717	8219
439	1,570	18,3	15413	150351	80920	106680	129994	37791	1719	384817	4119	7586	7571
440	1,555	18,2	17108	166489	71489	109805	112096	38800	3143	384951	3898	9570	7871
441	1,527	17,9	16403	159407	71931	107643	124412	38531	2188	402200	3759	7727	8364
442	1,530	17,8	17047	164853	72852	111883	116510	38697	2473	370385	4176	5692	8005
443	1,503	17,9	17522	170501	72058	112708	147146	39449	1768	375845	4483	11596	7734
444	1,543	17,9	17041	164954	74987	109888	126315	39032	1929	407330	3771	10438	7274
445	1,552	18	16690	161889	72253	109330	124132	37970	2213	415511	3939	8042	7011
446	1,540	17,9	16070	154308	70076	104481	116382	36500	1829	423463	3525	9511	6686
447	1,534	17,8	15518	148794	69520	102769	126564	35859	1272	359677	3842	9261	7540
448	1,561	17,6	14254	142986	69947	99015	137336	34393	2113	353957	3693	12151	6349
449	1,548	17,4	14663	146239	73378	100255	166566	34003	1444	373811	3537	12180	6495
450	1,546	17,1	15898	153182	74102	104664	124572	36863	2947	398104	3736	7988	6438
451	1,515	16,9	14297	141158	79995	98980	220295	34122	1103	377597	3904	16195	6800
452	1,521	16,7	14400	140759	78032	99257	193661	34569	1975	368641	3816	13114	6876
453	1,521	16,7	13531	134314	80883	97131	207505	33610	1878	346844	3875	14599	7244
454	1,511	16,8	13152	128777	82586	95790	150646	34506	2198	358515	4064	8199	7620
455	1,519	16,8	12979	129506	92395	96154	186353	33789	2450	358164	3853	15385	7023
456	1,519	16,9	13825	138788	90697	101943	196253	36034	2044	392736	4003	17863	7637
457	1,543	16,8	14706	148216	84920	108088	204392	37989	2274	388101	4158	11694	8124
458	1,515	16,6	13433	136580	91222	100992	277763	35104	2430	372420	4231	17634	8079
459	1,523	16,4	14966	153145	79440	105327	276170	35754	2754	374555	4359	12371	7591
460	1,525	16,1	15934	157885	75504	107362	203844	37064	1986	425956	4153	11438	7734
461	1,513	15,6	16706	161224	73855	108371	138259	38613	1658	412543	4113	8350	7985
462	1,513	15	10401	107285	54628	75836	73639	28811	1037	304391	2961	4271	6168

Tableau B2 : Résultats de la granulométrie de la carotte HH16-1205-GC

Grain size (µm) \ Prof. (cm)	0	4	9	14	19	24	29	34	39	44	49	54	59	64	69
0,316	0,018	0,020	0,012	0,014	0,009	0,008	0,011	0,011	0,011	0,008	0,010	0,014	0,010	0,015	0,000
0,363	0,175	0,186	0,121	0,140	0,105	0,092	0,114	0,117	0,114	0,088	0,107	0,140	0,106	0,146	0,078
0,417	0,538	0,548	0,458	0,489	0,442	0,415	0,446	0,450	0,443	0,414	0,441	0,493	0,445	0,497	0,402
0,479	0,884	0,891	0,783	0,825	0,769	0,728	0,765	0,770	0,761	0,731	0,763	0,830	0,773	0,834	0,728
0,550	1,207	1,211	1,091	1,140	1,079	1,026	1,067	1,072	1,060	1,033	1,065	1,149	1,083	1,151	1,040
0,631	1,490	1,489	1,364	1,417	1,353	1,288	1,333	1,338	1,324	1,301	1,330	1,427	1,357	1,430	1,319
0,724	1,700	1,695	1,572	1,625	1,561	1,488	1,535	1,540	1,523	1,507	1,529	1,636	1,565	1,641	1,536
0,832	1,849	1,837	1,725	1,773	1,713	1,633	1,681	1,685	1,667	1,660	1,671	1,784	1,717	1,793	1,700
0,955	1,942	1,924	1,830	1,868	1,815	1,731	1,777	1,782	1,761	1,767	1,764	1,878	1,818	1,893	1,815
1,096	2,011	1,987	1,917	1,940	1,897	1,811	1,855	1,859	1,835	1,856	1,837	1,948	1,899	1,971	1,912
1,259	2,091	2,060	2,017	2,023	1,991	1,904	1,944	1,947	1,919	1,959	1,923	2,028	1,993	2,060	2,020
1,445	2,216	2,181	2,166	2,152	2,133	2,044	2,080	2,083	2,049	2,109	2,054	2,153	2,133	2,195	2,173
1,660	2,406	2,368	2,380	2,345	2,341	2,249	2,281	2,283	2,242	2,325	2,249	2,344	2,339	2,394	2,390
1,905	2,662	2,623	2,662	2,606	2,618	2,523	2,549	2,550	2,501	2,607	2,511	2,602	2,613	2,659	2,672
2,188	2,960	2,923	2,987	2,912	2,942	2,842	2,864	2,863	2,805	2,933	2,817	2,909	2,932	2,968	2,996
2,512	3,274	3,243	3,329	3,238	3,286	3,182	3,201	3,197	3,133	3,277	3,143	3,237	3,271	3,294	3,338
2,884	3,583	3,560	3,664	3,562	3,629	3,522	3,537	3,531	3,461	3,614	3,466	3,568	3,606	3,615	3,675
3,311	3,872	3,860	3,975	3,869	3,952	3,845	3,857	3,847	3,775	3,928	3,771	3,884	3,921	3,913	3,991
3,802	4,129	4,130	4,250	4,147	4,241	4,139	4,147	4,132	4,062	4,203	4,044	4,171	4,201	4,175	4,272
4,365	4,346	4,359	4,475	4,384	4,483	4,390	4,394	4,374	4,308	4,428	4,274	4,418	4,433	4,386	4,504
5,012	4,516	4,543	4,647	4,575	4,673	4,594	4,592	4,565	4,507	4,596	4,454	4,615	4,611	4,543	4,684
5,754	4,634	4,672	4,760	4,713	4,802	4,744	4,732	4,700	4,652	4,703	4,579	4,754	4,728	4,641	4,803
6,607	4,695	4,743	4,811	4,793	4,868	4,836	4,813	4,775	4,741	4,748	4,647	4,829	4,783	4,678	4,858
7,586	4,690	4,747	4,796	4,807	4,864	4,861	4,825	4,784	4,766	4,726	4,653	4,831	4,771	4,652	4,841
8,710	4,611	4,676	4,709	4,747	4,784	4,812	4,763	4,721	4,721	4,634	4,590	4,753	4,686	4,559	4,746
10,000	4,455	4,526	4,547	4,607	4,626	4,685	4,624	4,584	4,602	4,474	4,459	4,592	4,528	4,399	4,571
11,482	4,219	4,292	4,307	4,381	4,383	4,472	4,401	4,367	4,403	4,242	4,254	4,343	4,293	4,169	4,312
13,183	3,916	3,987	4,001	4,078	4,069	4,183	4,108	4,082	4,133	3,955	3,988	4,024	3,997	3,884	3,987
15,136	3,554	3,616	3,632	3,704	3,688	3,821	3,748	3,734	3,795	3,616	3,664	3,641	3,643	3,549	3,604
17,378	3,163	3,211	3,230	3,289	3,268	3,415	3,350	3,348	3,413	3,251	3,305	3,227	3,259	3,189	3,196
19,953	2,754	2,785	2,808	2,847	2,826	2,979	2,928	2,936	2,999	2,870	2,921	2,796	2,856	2,813	2,776

Prof. (cm)	0	4	9	14	19	24	29	34	39	44	49	54	59	64	69
Grain size (µm) 22,909	2,357	2,371	2,395	2,415	2,395	2,547	2,511	2,528	2,584	2,495	2,534	2,378	2,460	2,445	2,371
26,303	1,980	1,979	2,003	2,005	1,987	2,131	2,109	2,132	2,178	2,132	2,151	1,981	2,078	2,087	1,987
30,200	1,638	1,627	1,647	1,638	1,620	1,752	1,740	1,766	1,803	1,791	1,786	1,621	1,723	1,752	1,638
34,674	1,331	1,314	1,328	1,313	1,295	1,411	1,404	1,431	1,463	1,476	1,444	1,300	1,398	1,439	1,322
39,811	1,063	1,043	1,047	1,034	1,013	1,113	1,107	1,134	1,164	1,192	1,134	1,022	1,107	1,154	1,045
45,709	0,835	0,811	0,804	0,797	0,773	0,856	0,849	0,875	0,908	0,941	0,863	0,788	0,853	0,899	0,807
52,481	0,646	0,619	0,598	0,599	0,573	0,642	0,633	0,658	0,695	0,726	0,639	0,596	0,639	0,680	0,609
60,256	0,493	0,463	0,431	0,438	0,413	0,468	0,459	0,484	0,525	0,549	0,466	0,445	0,467	0,499	0,450
69,183	0,372	0,339	0,298	0,309	0,288	0,331	0,325	0,349	0,391	0,406	0,340	0,327	0,332	0,354	0,325
79,433	0,276	0,241	0,201	0,212	0,198	0,226	0,224	0,247	0,288	0,292	0,254	0,234	0,231	0,244	0,229
91,201	0,201	0,167	0,122	0,128	0,126	0,150	0,152	0,173	0,207	0,204	0,198	0,163	0,158	0,164	0,156
104,713	0,132	0,100	0,079	0,081	0,087	0,084	0,092	0,109	0,147	0,126	0,162	0,095	0,098	0,097	0,092
120,226	0,088	0,034	0,020	0,020	0,025	0,028	0,058	0,070	0,090	0,080	0,138	0,032	0,066	0,061	0,031
138,038	0,028	0,000	0,000	0,000	0,000	0,000	0,016	0,020	0,056	0,024	0,121	0,000	0,022	0,018	0,000
158,489	0,000	0,000	0,000	0,000	0,000	0,000	0,000	0,000	0,018	0,000	0,107	0,000	0,000	0,000	0,000
181,970	0,000	0,000	0,000	0,000	0,000	0,000	0,000	0,000	0,000	0,000	0,096	0,000	0,000	0,000	0,000
208,930	0,000	0,000	0,000	0,000	0,000	0,000	0,000	0,000	0,000	0,000	0,090	0,000	0,000	0,000	0,000
239,883	0,000	0,000	0,000	0,000	0,000	0,000	0,000	0,000	0,000	0,000	0,090	0,000	0,000	0,000	0,000
275,423	0,000	0,000	0,000	0,000	0,000	0,000	0,000	0,000	0,000	0,000	0,099	0,000	0,000	0,000	0,000
316,228	0,000	0,000	0,000	0,000	0,000	0,000	0,000	0,000	0,000	0,000	0,119	0,000	0,000	0,000	0,000
363,078	0,000	0,000	0,000	0,000	0,000	0,000	0,000	0,000	0,000	0,000	0,149	0,000	0,000	0,000	0,000
416,869	0,000	0,000	0,000	0,000	0,000	0,000	0,000	0,000	0,000	0,000	0,179	0,000	0,000	0,000	0,000
478,630	0,000	0,000	0,000	0,000	0,000	0,000	0,000	0,000	0,000	0,000	0,194	0,000	0,000	0,000	0,000
549,541	0,000	0,000	0,000	0,000	0,000	0,000	0,000	0,000	0,000	0,000	0,188	0,000	0,000	0,000	0,000
630,957	0,000	0,000	0,000	0,000	0,000	0,000	0,000	0,000	0,000	0,000	0,125	0,000	0,000	0,000	0,000
724,436	0,000	0,000	0,000	0,000	0,000	0,000	0,000	0,000	0,000	0,000	0,052	0,000	0,000	0,000	0,000
Median size (µm)	5,343	5,377	5,402	5,467	5,461	5,722	5,629	5,639	5,769	5,581	5,788	5,435	5,501	5,389	5,427
Classif. clay	40,581	40,313	39,926	39,674	39,499	38,057	38,633	38,637	38,002	38,924	38,044	39,793	39,387	40,235	39,688
silt	58,453	58,927	59,463	59,689	59,884	61,245	60,617	60,521	60,941	60,088	59,379	59,473	59,827	58,955	59,596
sand	0,966	0,759	0,611	0,637	0,618	0,699	0,750	0,842	1,057	0,988	2,578	0,735	0,787	0,810	0,716

Prof. (cm)	74	79	84	89	94	99	104	109	114	119	124	129	134	139	144
0,316	0,010	0,010	0,008	0,006	0,006	0,007	0,006	0,000	0,007	0,000	0,000	0,000	0,000	0,008	0,009
0,363	0,110	0,108	0,095	0,078	0,078	0,081	0,074	0,065	0,083	0,062	0,049	0,061	0,047	0,089	0,098
0,417	0,450	0,450	0,431	0,410	0,403	0,409	0,389	0,369	0,406	0,381	0,347	0,363	0,337	0,406	0,411
0,479	0,780	0,782	0,758	0,736	0,721	0,730	0,697	0,672	0,721	0,700	0,646	0,665	0,628	0,716	0,715
0,550	1,093	1,098	1,071	1,048	1,026	1,037	0,992	0,962	1,023	1,006	0,934	0,955	0,908	1,011	1,004
0,631	1,371	1,377	1,348	1,327	1,297	1,311	1,253	1,220	1,291	1,279	1,191	1,214	1,158	1,273	1,261
0,724	1,584	1,590	1,562	1,543	1,507	1,523	1,454	1,420	1,498	1,491	1,392	1,414	1,352	1,475	1,458
0,832	1,740	1,745	1,720	1,703	1,663	1,681	1,603	1,569	1,653	1,650	1,544	1,565	1,498	1,625	1,603
0,955	1,845	1,848	1,829	1,814	1,773	1,791	1,707	1,674	1,761	1,762	1,654	1,672	1,602	1,729	1,704
1,096	1,929	1,929	1,917	1,905	1,864	1,883	1,795	1,764	1,853	1,856	1,751	1,764	1,693	1,816	1,788
1,259	2,022	2,020	2,017	2,006	1,969	1,987	1,898	1,871	1,959	1,963	1,866	1,872	1,801	1,918	1,888
1,445	2,161	2,155	2,163	2,152	2,120	2,140	2,049	2,029	2,113	2,116	2,033	2,029	1,959	2,068	2,035
1,660	2,362	2,354	2,373	2,360	2,337	2,358	2,267	2,254	2,333	2,333	2,268	2,253	2,184	2,283	2,248
1,905	2,630	2,618	2,650	2,633	2,622	2,644	2,554	2,549	2,618	2,616	2,574	2,545	2,480	2,568	2,527
2,188	2,942	2,928	2,973	2,951	2,952	2,976	2,887	2,891	2,947	2,943	2,928	2,884	2,826	2,898	2,851
2,512	3,275	3,258	3,315	3,290	3,303	3,327	3,241	3,254	3,291	3,288	3,303	3,244	3,195	3,248	3,193
2,884	3,607	3,586	3,653	3,627	3,651	3,674	3,589	3,612	3,627	3,628	3,672	3,600	3,563	3,593	3,530
3,311	3,922	3,895	3,971	3,947	3,980	3,997	3,915	3,947	3,938	3,944	4,015	3,932	3,909	3,914	3,843
3,802	4,205	4,170	4,253	4,235	4,274	4,281	4,200	4,242	4,210	4,220	4,312	4,224	4,217	4,195	4,117
4,365	4,443	4,399	4,487	4,477	4,519	4,510	4,432	4,484	4,430	4,442	4,549	4,462	4,469	4,421	4,339
5,012	4,630	4,575	4,666	4,666	4,708	4,678	4,605	4,667	4,596	4,604	4,721	4,640	4,659	4,587	4,506
5,754	4,758	4,691	4,781	4,794	4,833	4,780	4,715	4,786	4,703	4,703	4,823	4,753	4,781	4,688	4,614
6,607	4,822	4,745	4,831	4,857	4,890	4,816	4,763	4,843	4,754	4,740	4,858	4,803	4,837	4,728	4,665
7,586	4,817	4,730	4,807	4,846	4,872	4,784	4,749	4,834	4,745	4,715	4,829	4,789	4,824	4,708	4,659
8,710	4,733	4,641	4,705	4,755	4,773	4,680	4,670	4,756	4,674	4,625	4,734	4,710	4,743	4,625	4,594
10,000	4,568	4,477	4,523	4,582	4,593	4,506	4,527	4,609	4,536	4,471	4,575	4,566	4,596	4,483	4,471
11,482	4,319	4,235	4,260	4,326	4,331	4,259	4,314	4,389	4,326	4,250	4,349	4,353	4,380	4,278	4,286
13,183	4,002	3,932	3,934	4,003	4,006	3,953	4,043	4,105	4,053	3,972	4,067	4,081	4,107	4,020	4,048
15,136	3,624	3,573	3,554	3,623	3,626	3,595	3,714	3,761	3,716	3,641	3,728	3,751	3,780	3,711	3,758
17,378	3,219	3,189	3,153	3,220	3,224	3,211	3,352	3,381	3,341	3,280	3,355	3,387	3,422	3,370	3,436
19,953	2,798	2,793	2,743	2,806	2,812	2,813	2,965	2,973	2,937	2,897	2,955	2,995	3,041	3,002	3,087

Grain size (µm)

	Prof. (cm)	74	79	84	89	94	99	104	109	114	119	124	129	134	139	144
Grain size (μm)	22,909	2,391	2,408	2,350	2,407	2,412	2,426	2,577	2,565	2,531	2,516	2,554	2,601	2,657	2,627	2,728
	26,303	2,004	2,042	1,979	2,028	2,029	2,054	2,195	2,163	2,132	2,141	2,159	2,212	2,276	2,251	2,362
	30,200	1,651	1,707	1,641	1,680	1,674	1,711	1,836	1,785	1,758	1,787	1,787	1,845	1,913	1,886	2,003
	34,674	1,332	1,403	1,336	1,363	1,350	1,396	1,504	1,439	1,415	1,458	1,444	1,504	1,570	1,540	1,653
	39,811	1,052	1,136	1,070	1,081	1,062	1,116	1,206	1,133	1,112	1,161	1,138	1,198	1,258	1,223	1,324
	45,709	0,813	0,906	0,841	0,835	0,815	0,870	0,946	0,871	0,853	0,901	0,873	0,930	0,981	0,942	1,024
	52,481	0,614	0,710	0,651	0,627	0,611	0,661	0,725	0,655	0,640	0,682	0,652	0,703	0,744	0,703	0,762
	60,256	0,454	0,549	0,497	0,458	0,447	0,489	0,543	0,483	0,472	0,504	0,475	0,516	0,550	0,510	0,544
	69,183	0,330	0,418	0,374	0,323	0,320	0,350	0,395	0,350	0,341	0,361	0,338	0,366	0,394	0,358	0,370
	79,433	0,234	0,312	0,274	0,223	0,224	0,238	0,276	0,246	0,241	0,252	0,234	0,249	0,273	0,241	0,244
	91,201	0,163	0,224	0,197	0,137	0,154	0,155	0,185	0,169	0,167	0,170	0,158	0,162	0,183	0,156	0,139
	104,713	0,103	0,156	0,126	0,090	0,094	0,083	0,107	0,103	0,104	0,111	0,094	0,093	0,110	0,084	0,084
	120,226	0,068	0,091	0,084	0,023	0,058	0,027	0,065	0,066	0,067	0,072	0,058	0,059	0,072	0,027	0,019
	138,038	0,022	0,036	0,028	0,000	0,016	0,000	0,018	0,020	0,021	0,049	0,016	0,019	0,023	0,000	0,000
	158,489	0,000	0,000	0,000	0,000	0,000	0,000	0,000	0,000	0,000	0,036	0,000	0,000	0,000	0,000	0,000
	181,970	0,000	0,000	0,000	0,000	0,000	0,000	0,000	0,000	0,000	0,034	0,000	0,000	0,000	0,000	0,000
	208,930	0,000	0,000	0,000	0,000	0,000	0,000	0,000	0,000	0,000	0,033	0,000	0,000	0,000	0,000	0,000
	239,883	0,000	0,000	0,000	0,000	0,000	0,000	0,000	0,000	0,000	0,036	0,000	0,000	0,000	0,000	0,000
	275,423	0,000	0,000	0,000	0,000	0,000	0,000	0,000	0,000	0,000	0,036	0,000	0,000	0,000	0,000	0,000
	316,228	0,000	0,000	0,000	0,000	0,000	0,000	0,000	0,000	0,000	0,035	0,000	0,000	0,000	0,000	0,000
	363,078	0,000	0,000	0,000	0,000	0,000	0,000	0,000	0,000	0,000	0,038	0,000	0,000	0,000	0,000	0,000
	416,869	0,000	0,000	0,000	0,000	0,000	0,000	0,000	0,000	0,000	0,006	0,000	0,000	0,000	0,000	0,000
	478,630	0,000	0,000	0,000	0,000	0,000	0,000	0,000	0,000	0,000	0,000	0,000	0,000	0,000	0,000	0,000
	549,541	0,000	0,000	0,000	0,000	0,000	0,000	0,000	0,000	0,000	0,000	0,000	0,000	0,000	0,000	0,000
	630,957	0,000	0,000	0,000	0,000	0,000	0,000	0,000	0,000	0,000	0,000	0,000	0,000	0,000	0,000	0,000
	724,436	0,000	0,000	0,000	0,000	0,000	0,000	0,000	0,000	0,000	0,000	0,000	0,000	0,000	0,000	0,000
	Median size (μm)	5,452	5,493	5,426	5,479	5,498	5,463	5,701	5,705	5,579	5,591	5,661	5,736	5,876	5,666	5,799
Classif.	clay	39,646	39,515	39,733	39,393	39,180	39,473	38,177	37,988	38,939	38,849	38,127	37,872	36,974	38,435	37,854
	silt	59,553	59,396	59,317	59,929	60,069	59,801	60,920	61,184	60,242	60,011	61,098	61,313	62,113	60,830	61,427
	sand	0,801	1,089	0,950	0,678	0,751	0,726	0,903	0,829	0,819	1,140	0,775	0,815	0,912	0,735	0,719

Grain size (µm)

Prof. (cm)	149	154	159	164	169	174	179	184	189	194	199	204	209	214	219
0,316	0,010	0,000	0,010	0,012	0,000	0,012	0,009	0,000	0,007	0,010	0,016	0,018	0,007	0,014	0,000
0,363	0,109	0,054	0,103	0,124	0,070	0,126	0,098	0,068	0,079	0,103	0,157	0,172	0,083	0,140	0,065
0,417	0,430	0,351	0,406	0,452	0,370	0,459	0,413	0,359	0,390	0,423	0,487	0,511	0,387	0,460	0,355
0,479	0,740	0,649	0,699	0,769	0,672	0,780	0,719	0,650	0,695	0,734	0,804	0,835	0,686	0,768	0,645
0,550	1,034	0,936	0,977	1,068	0,960	1,085	1,010	0,929	0,987	1,030	1,101	1,139	0,972	1,059	0,922
0,631	1,294	1,192	1,223	1,332	1,218	1,354	1,267	1,178	1,247	1,292	1,362	1,406	1,228	1,316	1,169
0,724	1,491	1,393	1,410	1,533	1,419	1,559	1,464	1,372	1,448	1,493	1,559	1,607	1,426	1,512	1,360
0,832	1,634	1,545	1,546	1,678	1,569	1,709	1,608	1,517	1,599	1,642	1,699	1,750	1,575	1,655	1,503
0,955	1,729	1,654	1,638	1,775	1,675	1,809	1,706	1,622	1,704	1,744	1,791	1,841	1,681	1,751	1,604
1,096	1,804	1,749	1,715	1,852	1,766	1,890	1,787	1,713	1,793	1,828	1,862	1,910	1,770	1,828	1,689
1,259	1,888	1,858	1,806	1,941	1,869	1,983	1,881	1,821	1,893	1,924	1,945	1,988	1,872	1,919	1,784
1,445	2,015	2,014	1,943	2,076	2,019	2,122	2,021	1,979	2,039	2,067	2,073	2,109	2,018	2,054	1,920
1,660	2,201	2,234	2,144	2,275	2,232	2,326	2,226	2,202	2,246	2,272	2,265	2,293	2,226	2,253	2,112
1,905	2,449	2,521	2,411	2,540	2,511	2,597	2,497	2,493	2,516	2,543	2,520	2,542	2,497	2,516	2,362
2,188	2,740	2,851	2,722	2,849	2,835	2,914	2,814	2,830	2,829	2,857	2,819	2,834	2,808	2,823	2,648
2,512	3,048	3,202	3,052	3,176	3,179	3,251	3,151	3,188	3,159	3,188	3,134	3,147	3,137	3,148	2,949
2,884	3,355	3,548	3,379	3,498	3,521	3,584	3,486	3,542	3,484	3,514	3,445	3,459	3,461	3,467	3,245
3,311	3,643	3,873	3,687	3,799	3,842	3,895	3,801	3,875	3,789	3,819	3,736	3,754	3,764	3,765	3,521
3,802	3,900	4,161	3,961	4,063	4,127	4,169	4,083	4,170	4,060	4,087	3,993	4,019	4,033	4,028	3,767
4,365	4,114	4,399	4,188	4,280	4,362	4,391	4,316	4,412	4,285	4,308	4,205	4,242	4,256	4,243	3,974
5,012	4,279	4,582	4,366	4,444	4,542	4,555	4,497	4,595	4,460	4,478	4,371	4,419	4,430	4,409	4,141
5,754	4,392	4,703	4,489	4,553	4,662	4,658	4,619	4,715	4,580	4,592	4,486	4,543	4,552	4,521	4,265
6,607	4,452	4,763	4,562	4,608	4,726	4,700	4,683	4,772	4,647	4,650	4,551	4,615	4,624	4,582	4,348
7,586	4,458	4,761	4,583	4,608	4,732	4,681	4,687	4,765	4,657	4,650	4,564	4,631	4,641	4,587	4,386
8,710	4,408	4,693	4,551	4,552	4,679	4,599	4,627	4,692	4,608	4,588	4,521	4,586	4,600	4,532	4,374
10,000	4,301	4,561	4,466	4,438	4,567	4,455	4,505	4,555	4,496	4,463	4,418	4,476	4,498	4,414	4,306
11,482	4,134	4,360	4,324	4,262	4,391	4,247	4,314	4,349	4,318	4,270	4,251	4,297	4,328	4,227	4,177
13,183	3,920	4,103	4,132	4,032	4,158	3,984	4,067	4,089	4,082	4,022	4,028	4,056	4,099	3,982	3,991
15,136	3,660	3,791	3,888	3,748	3,864	3,670	3,765	3,777	3,790	3,720	3,751	3,755	3,813	3,682	3,749
17,378	3,376	3,448	3,608	3,429	3,529	3,325	3,431	3,436	3,465	3,389	3,440	3,417	3,491	3,351	3,469
19,953	3,074	3,078	3,291	3,080	3,155	2,956	3,072	3,074	3,113	3,036	3,101	3,048	3,142	3,002	3,160

Prof. (cm)	149	154	159	164	169	174	179	184	189	194	199	204	209	214	219
22,909	2,770	2,703	2,953	2,718	2,762	2,582	2,708	2,709	2,751	2,681	2,752	2,671	2,787	2,658	2,841
26,303	2,465	2,324	2,593	2,348	2,358	2,206	2,343	2,344	2,384	2,326	2,396	2,291	2,431	2,323	2,516
30,200	2,165	1,957	2,224	1,983	1,962	1,844	1,990	1,989	2,025	1,981	2,044	1,922	2,085	2,008	2,195
34,674	1,870	1,604	1,852	1,629	1,584	1,500	1,651	1,648	1,676	1,649	1,699	1,571	1,750	1,708	1,880
39,811	1,582	1,278	1,493	1,299	1,240	1,185	1,335	1,328	1,349	1,337	1,370	1,248	1,431	1,425	1,576
45,709	1,307	0,985	1,159	1,003	0,939	0,907	1,047	1,036	1,052	1,049	1,066	0,959	1,131	1,156	1,286
52,481	1,052	0,734	0,864	0,748	0,687	0,672	0,794	0,779	0,792	0,793	0,797	0,711	0,856	0,904	1,016
60,256	0,822	0,529	0,617	0,540	0,487	0,483	0,580	0,563	0,576	0,575	0,570	0,506	0,612	0,676	0,774
69,183	0,621	0,365	0,421	0,374	0,330	0,334	0,403	0,386	0,401	0,393	0,386	0,340	0,406	0,478	0,568
79,433	0,454	0,245	0,271	0,253	0,218	0,225	0,270	0,254	0,264	0,257	0,249	0,218	0,251	0,317	0,406
91,201	0,317	0,143	0,166	0,149	0,124	0,128	0,151	0,139	0,165	0,138	0,132	0,114	0,124	0,199	0,284
104,713	0,214	0,087	0,080	0,090	0,072	0,073	0,085	0,076	0,078	0,072	0,069	0,030	0,032	0,105	0,200
120,226	0,127	0,021	0,025	0,020	0,015	0,014	0,017	0,014	0,024	0,012	0,011	0,000	0,000	0,034	0,143
138,038	0,080	0,000	0,000	0,000	0,000	0,000	0,000	0,000	0,000	0,000	0,000	0,000	0,000	0,000	0,105
158,489	0,044	0,000	0,000	0,000	0,000	0,000	0,000	0,000	0,000	0,000	0,000	0,000	0,000	0,000	0,084
181,970	0,023	0,000	0,000	0,000	0,000	0,000	0,000	0,000	0,000	0,000	0,000	0,000	0,000	0,000	0,082
208,930	0,000	0,000	0,000	0,000	0,000	0,000	0,000	0,000	0,000	0,000	0,000	0,000	0,000	0,000	0,100
239,883	0,000	0,000	0,000	0,000	0,000	0,000	0,000	0,000	0,000	0,000	0,000	0,000	0,000	0,000	0,139
275,423	0,000	0,000	0,000	0,000	0,000	0,000	0,000	0,000	0,000	0,000	0,000	0,000	0,000	0,000	0,197
316,228	0,000	0,000	0,000	0,000	0,000	0,000	0,000	0,000	0,000	0,000	0,000	0,000	0,000	0,000	0,263
363,078	0,000	0,000	0,000	0,000	0,000	0,000	0,000	0,000	0,000	0,000	0,000	0,000	0,000	0,000	0,321
416,869	0,000	0,000	0,000	0,000	0,000	0,000	0,000	0,000	0,000	0,000	0,000	0,000	0,000	0,000	0,348
478,630	0,000	0,000	0,000	0,000	0,000	0,000	0,000	0,000	0,000	0,000	0,000	0,000	0,000	0,000	0,322
549,541	0,000	0,000	0,000	0,000	0,000	0,000	0,000	0,000	0,000	0,000	0,000	0,000	0,000	0,000	0,258
630,957	0,000	0,000	0,000	0,000	0,000	0,000	0,000	0,000	0,000	0,000	0,000	0,000	0,000	0,000	0,111
724,436	0,000	0,000	0,000	0,000	0,000	0,000	0,000	0,000	0,000	0,000	0,000	0,000	0,000	0,000	0,028
Median size (μm)	6,067	5,844	6,138	5,739	5,853	5,549	5,845	5,885	5,878	5,763	5,784	5,662	5,953	5,816	6,535
clay	37,007	37,377	36,347	38,363	37,434	39,217	37,604	37,104	37,515	38,131	38,293	38,870	37,171	38,013	35,057
silt	61,333	61,897	62,845	60,887	61,928	60,130	61,617	62,170	61,700	61,141	61,001	60,553	62,167	61,028	61,189
sand	1,660	0,726	0,808	0,750	0,638	0,652	0,779	0,726	0,785	0,728	0,706	0,577	0,661	0,959	3,754

Row group labels: Grain size (μm); Classif.

Prof. (cm)	224	229	234	239	244	249	254	259	264	269	274	279	284	289	294	299
0,316	0,007	0,009	0,007	0,000	0,000	0,006	0,008	0,000	0,000	0,000	0,000	0,000	0,000	0,000	0,000	0,000
0,363	0,081	0,095	0,085	0,071	0,060	0,074	0,088	0,057	0,066	0,048	0,006	0,007	0,049	0,006	0,007	0,007
0,417	0,380	0,391	0,392	0,362	0,341	0,357	0,395	0,349	0,348	0,298	0,227	0,269	0,335	0,227	0,281	0,288
0,479	0,672	0,679	0,694	0,654	0,624	0,635	0,696	0,642	0,630	0,549	0,454	0,529	0,624	0,468	0,543	0,565
0,550	0,952	0,953	0,983	0,936	0,897	0,900	0,983	0,923	0,901	0,789	0,675	0,782	0,904	0,703	0,799	0,827
0,631	1,202	1,197	1,242	1,189	1,142	1,136	1,240	1,173	1,143	1,004	0,875	1,013	1,156	0,916	1,031	1,054
0,724	1,396	1,385	1,446	1,388	1,336	1,319	1,439	1,366	1,331	1,170	1,033	1,194	1,354	1,084	1,216	1,221
0,832	1,541	1,525	1,601	1,539	1,483	1,456	1,589	1,511	1,473	1,294	1,155	1,336	1,506	1,213	1,359	1,338
0,955	1,643	1,622	1,713	1,648	1,591	1,553	1,696	1,612	1,574	1,382	1,247	1,442	1,617	1,309	1,468	1,413
1,096	1,729	1,704	1,811	1,743	1,685	1,636	1,786	1,697	1,662	1,455	1,330	1,538	1,712	1,395	1,567	1,475
1,259	1,827	1,798	1,921	1,849	1,792	1,734	1,890	1,793	1,766	1,537	1,428	1,650	1,820	1,494	1,683	1,551
1,445	1,968	1,937	2,077	2,000	1,943	1,877	2,039	1,931	1,916	1,655	1,567	1,809	1,970	1,634	1,846	1,672
1,660	2,168	2,135	2,294	2,210	2,152	2,082	2,250	2,127	2,129	1,822	1,757	2,029	2,180	1,828	2,072	1,854
1,905	2,429	2,394	2,574	2,480	2,421	2,349	2,524	2,382	2,406	2,039	2,000	2,313	2,450	2,077	2,363	2,098
2,188	2,730	2,694	2,894	2,791	2,731	2,658	2,841	2,676	2,727	2,288	2,278	2,640	2,760	2,365	2,698	2,384
2,512	3,050	3,010	3,230	3,118	3,058	2,984	3,175	2,987	3,067	2,551	2,571	2,988	3,088	2,673	3,055	2,693
2,884	3,366	3,324	3,559	3,440	3,382	3,306	3,505	3,294	3,404	2,811	2,860	3,336	3,415	2,984	3,411	3,008
3,311	3,665	3,620	3,864	3,741	3,689	3,609	3,815	3,586	3,724	3,057	3,134	3,668	3,725	3,287	3,749	3,318
3,802	3,936	3,888	4,132	4,011	3,966	3,880	4,091	3,850	4,012	3,281	3,384	3,973	4,007	3,573	4,057	3,614
4,365	4,166	4,117	4,348	4,237	4,200	4,110	4,322	4,076	4,258	3,474	3,600	4,238	4,251	3,834	4,320	3,891
5,012	4,355	4,305	4,509	4,416	4,388	4,297	4,503	4,263	4,458	3,634	3,782	4,460	4,454	4,070	4,535	4,147
5,754	4,496	4,447	4,610	4,544	4,525	4,440	4,631	4,405	4,607	3,759	3,927	4,634	4,610	4,274	4,696	4,378
6,607	4,591	4,545	4,653	4,623	4,610	4,543	4,706	4,502	4,704	3,850	4,036	4,760	4,717	4,447	4,802	4,583
7,586	4,634	4,592	4,636	4,648	4,640	4,604	4,725	4,548	4,745	3,904	4,104	4,834	4,770	4,579	4,849	4,752
8,710	4,618	4,583	4,557	4,616	4,611	4,621	4,684	4,539	4,725	3,921	4,130	4,852	4,763	4,664	4,833	4,877
10,000	4,539	4,512	4,418	4,522	4,519	4,589	4,580	4,468	4,638	3,899	4,105	4,807	4,689	4,688	4,750	4,940
11,482	4,390	4,374	4,216	4,361	4,361	4,500	4,407	4,329	4,479	3,835	4,023	4,690	4,539	4,644	4,592	4,928
13,183	4,177	4,173	3,963	4,140	4,144	4,351	4,172	4,125	4,254	3,734	3,886	4,501	4,318	4,525	4,366	4,829
15,136	3,902	3,912	3,664	3,860	3,872	4,138	3,874	3,858	3,963	3,602	3,692	4,235	4,026	4,331	4,072	4,633
17,378	3,587	3,611	3,340	3,543	3,569	3,868	3,534	3,546	3,628	3,451	3,459	3,905	3,681	4,071	3,728	4,347
19,953	3,242	3,278	3,001	3,197	3,241	3,541	3,158	3,197	3,258	3,285	3,193	3,515	3,292	3,750	3,342	3,973

Grain size (μm)

Prof. (cm)	224	229	234	239	244	249	254	259	264	269	274	279	284	289	294	299
22,909	2,888	2,934	2,663	2,842	2,907	3,171	2,769	2,832	2,873	3,112	2,915	3,089	2,884	3,388	2,937	3,532
26,303	2,531	2,582	2,330	2,482	2,569	2,763	2,372	2,460	2,481	2,928	2,636	2,638	2,465	2,993	2,521	3,038
30,200	2,182	2,234	2,008	2,129	2,236	2,337	1,983	2,097	2,098	2,730	2,370	2,187	2,054	2,587	2,113	2,522
34,674	1,840	1,891	1,695	1,784	1,903	1,906	1,608	1,749	1,729	2,510	2,123	1,751	1,658	2,179	1,720	2,005
39,811	1,509	1,557	1,394	1,454	1,575	1,493	1,259	1,428	1,385	2,266	1,905	1,352	1,293	1,789	1,358	1,518
45,709	1,193	1,239	1,107	1,145	1,256	1,116	0,947	1,143	1,074	2,000	1,721	1,004	0,970	1,429	1,037	1,085
52,481	0,899	0,945	0,843	0,862	0,955	0,794	0,679	0,901	0,804	1,720	1,571	0,717	0,697	1,111	0,766	0,726
60,256	0,639	0,685	0,608	0,613	0,684	0,537	0,463	0,704	0,582	1,439	1,452	0,495	0,481	0,841	0,548	0,451
69,183	0,420	0,468	0,410	0,405	0,452	0,342	0,294	0,548	0,405	1,168	1,351	0,331	0,317	0,619	0,379	0,262
79,433	0,258	0,300	0,262	0,249	0,277	0,209	0,176	0,429	0,271	0,920	1,253	0,214	0,202	0,441	0,252	0,128
91,201	0,128	0,183	0,143	0,124	0,135	0,107	0,082	0,336	0,174	0,700	1,141	0,135	0,112	0,302	0,161	0,066
104,713	0,065	0,097	0,084	0,033	0,067	0,059	0,021	0,264	0,096	0,516	1,007	0,076	0,067	0,200	0,088	0,010
120,226	0,010	0,058	0,019	0,000	0,010	0,012	0,000	0,208	0,032	0,372	0,849	0,048	0,015	0,129	0,029	0,000
138,038	0,000	0,016	0,000	0,000	0,000	0,000	0,000	0,167	0,000	0,272	0,682	0,015	0,000	0,091	0,000	0,000
158,489	0,000	0,000	0,000	0,000	0,000	0,000	0,000	0,139	0,000	0,213	0,522	0,000	0,000	0,079	0,000	0,000
181,970	0,000	0,000	0,000	0,000	0,000	0,000	0,000	0,122	0,000	0,195	0,391	0,000	0,000	0,089	0,000	0,000
208,930	0,000	0,000	0,000	0,000	0,000	0,000	0,000	0,113	0,000	0,212	0,297	0,000	0,000	0,113	0,000	0,000
239,883	0,000	0,000	0,000	0,000	0,000	0,000	0,000	0,108	0,000	0,259	0,247	0,000	0,000	0,136	0,000	0,000
275,423	0,000	0,000	0,000	0,000	0,000	0,000	0,000	0,105	0,000	0,332	0,238	0,000	0,000	0,144	0,000	0,000
316,228	0,000	0,000	0,000	0,000	0,000	0,000	0,000	0,100	0,000	0,418	0,260	0,000	0,000	0,130	0,000	0,000
363,078	0,000	0,000	0,000	0,000	0,000	0,000	0,000	0,090	0,000	0,501	0,297	0,000	0,000	0,080	0,000	0,000
416,869	0,000	0,000	0,000	0,000	0,000	0,000	0,000	0,072	0,000	0,554	0,314	0,000	0,000	0,015	0,000	0,000
478,630	0,000	0,000	0,000	0,000	0,000	0,000	0,000	0,054	0,000	0,536	0,302	0,000	0,000	0,000	0,000	0,000
549,541	0,000	0,000	0,000	0,000	0,000	0,000	0,000	0,015	0,000	0,458	0,180	0,000	0,000	0,000	0,000	0,000
630,957	0,000	0,000	0,000	0,000	0,000	0,000	0,000	0,000	0,000	0,224	0,061	0,000	0,000	0,000	0,000	0,000
724,436	0,000	0,000	0,000	0,000	0,000	0,000	0,000	0,000	0,000	0,067	0,000	0,000	0,000	0,000	0,000	0,000
Median size (µm)	6,158	6,261	5,757	6,044	6,221	6,422	5,839	6,369	6,176	8,241	8,267	6,492	6,106	7,486	6,319	7,134
clay	36,248	35,850	38,095	36,702	35,813	35,038	37,615	35,431	35,820	30,285	29,281	34,045	36,209	30,617	34,764	31,781
silt	63,028	63,200	61,138	62,638	63,415	64,362	61,923	61,889	63,351	62,203	61,776	65,257	63,195	67,036	64,466	67,856
sand	0,724	0,949	0,767	0,660	0,771	0,600	0,462	2,680	0,829	7,512	8,943	0,697	0,596	2,346	0,770	0,363

Grain size (µm)

Classif.

Prof. (cm)	304	309	314	319	324	329	334	339	344	349	354	359	364	369	374	379
0,316	0,000	0,000	0,000	0,000	0,000	0,000	0,000	0,000	0,000	0,000	0,000	0,000	0,000	0,000	0,000	0,000
0,363	0,039	0,051	0,006	0,039	0,000	0,034	0,064	0,008	0,036	0,055	0,008	0,008	0,051	0,008	0,038	0,007
0,417	0,332	0,335	0,252	0,324	0,212	0,311	0,329	0,290	0,315	0,330	0,297	0,297	0,321	0,308	0,316	0,280
0,479	0,630	0,620	0,516	0,613	0,452	0,592	0,595	0,556	0,598	0,607	0,563	0,576	0,594	0,590	0,598	0,560
0,550	0,918	0,894	0,774	0,892	0,693	0,863	0,849	0,815	0,872	0,874	0,823	0,849	0,857	0,868	0,871	0,834
0,631	1,179	1,138	1,008	1,145	0,912	1,108	1,076	1,050	1,120	1,112	1,059	1,098	1,093	1,121	1,116	1,084
0,724	1,384	1,327	1,195	1,344	1,088	1,301	1,253	1,234	1,316	1,298	1,246	1,295	1,277	1,322	1,309	1,282
0,832	1,541	1,469	1,341	1,496	1,227	1,449	1,385	1,376	1,468	1,438	1,390	1,450	1,416	1,479	1,456	1,438
0,955	1,655	1,570	1,452	1,608	1,334	1,559	1,479	1,481	1,581	1,537	1,498	1,565	1,515	1,596	1,563	1,553
1,096	1,751	1,654	1,552	1,707	1,434	1,657	1,559	1,575	1,680	1,622	1,595	1,669	1,599	1,699	1,654	1,655
1,259	1,857	1,750	1,669	1,821	1,551	1,771	1,651	1,685	1,794	1,721	1,708	1,786	1,694	1,814	1,757	1,769
1,445	2,005	1,888	1,833	1,981	1,714	1,931	1,783	1,843	1,952	1,862	1,866	1,950	1,829	1,973	1,902	1,927
1,660	2,212	2,084	2,060	2,205	1,938	2,155	1,968	2,064	2,170	2,063	2,085	2,175	2,019	2,189	2,105	2,144
1,905	2,481	2,338	2,354	2,495	2,225	2,444	2,207	2,350	2,449	2,324	2,366	2,464	2,265	2,465	2,369	2,421
2,188	2,791	2,633	2,695	2,830	2,556	2,777	2,479	2,680	2,768	2,626	2,688	2,794	2,548	2,779	2,673	2,740
2,512	3,122	2,945	3,060	3,187	2,910	3,130	2,764	3,032	3,103	2,948	3,028	3,143	2,847	3,107	2,993	3,076
2,884	3,453	3,256	3,427	3,544	3,267	3,479	3,042	3,382	3,434	3,270	3,365	3,486	3,143	3,427	3,309	3,408
3,311	3,770	3,552	3,780	3,882	3,611	3,806	3,300	3,715	3,744	3,577	3,681	3,807	3,423	3,724	3,602	3,720
3,802	4,059	3,820	4,103	4,187	3,928	4,097	3,529	4,018	4,022	3,858	3,966	4,090	3,680	3,984	3,860	3,999
4,365	4,307	4,050	4,382	4,444	4,207	4,339	3,722	4,278	4,257	4,103	4,208	4,326	3,905	4,198	4,072	4,235
5,012	4,510	4,235	4,613	4,647	4,442	4,528	3,877	4,491	4,446	4,309	4,407	4,510	4,098	4,366	4,236	4,425
5,754	4,661	4,372	4,785	4,790	4,629	4,661	3,994	4,652	4,586	4,471	4,559	4,641	4,259	4,485	4,350	4,569
6,607	4,757	4,459	4,899	4,872	4,769	4,740	4,075	4,764	4,678	4,592	4,668	4,724	4,390	4,562	4,421	4,671
7,586	4,793	4,495	4,948	4,890	4,856	4,764	4,120	4,823	4,720	4,667	4,731	4,756	4,490	4,596	4,449	4,728
8,710	4,763	4,474	4,927	4,841	4,890	4,731	4,129	4,825	4,707	4,691	4,744	4,736	4,555	4,587	4,437	4,738
10,000	4,663	4,397	4,831	4,722	4,863	4,638	4,098	4,765	4,634	4,658	4,701	4,658	4,576	4,529	4,382	4,693
11,482	4,487	4,259	4,655	4,527	4,769	4,480	4,023	4,635	4,493	4,559	4,591	4,512	4,544	4,414	4,278	4,581
13,183	4,243	4,068	4,407	4,265	4,604	4,259	3,906	4,436	4,285	4,393	4,412	4,298	4,449	4,239	4,127	4,396
15,136	3,932	3,826	4,089	3,934	4,362	3,972	3,747	4,163	4,008	4,156	4,158	4,009	4,282	3,997	3,923	4,131
17,378	3,576	3,553	3,723	3,558	4,052	3,637	3,555	3,830	3,678	3,859	3,843	3,663	4,046	3,697	3,674	3,795
19,953	3,185	3,253	3,319	3,144	3,676	3,257	3,335	3,443	3,302	3,506	3,471	3,266	3,738	3,344	3,384	3,393

Grain size (µm)

Prof (cm)	304	309	314	319	324	329	334	339	344	349	354	359	364	369	374	379
22,909	2,784	2,942	2,902	2,719	3,254	2,856	3,097	3,023	2,903	3,119	3,065	2,847	3,375	2,959	3,065	2,955
26,303	2,379	2,623	2,479	2,291	2,794	2,444	2,844	2,581	2,491	2,705	2,637	2,419	2,964	2,553	2,723	2,496
30,200	1,988	2,305	2,070	1,880	2,323	2,040	2,581	2,139	2,085	2,284	2,209	2,008	2,529	2,147	2,372	2,050
34,674	1,615	1,985	1,680	1,494	1,857	1,653	2,306	1,709	1,693	1,866	1,790	1,621	2,084	1,755	2,017	1,631
39,811	1,273	1,672	1,322	1,145	1,420	1,298	2,023	1,313	1,330	1,471	1,400	1,272	1,655	1,392	1,670	1,259
45,709	0,968	1,372	1,002	0,844	1,034	0,986	1,736	0,965	1,008	1,113	1,052	0,968	1,260	1,072	1,343	0,945
52,481	0,708	1,092	0,728	0,600	0,719	0,728	1,456	0,682	0,739	0,809	0,760	0,716	0,920	0,806	1,051	0,698
60,256	0,498	0,843	0,505	0,415	0,486	0,527	1,192	0,469	0,529	0,569	0,531	0,519	0,647	0,599	0,803	0,515
69,183	0,333	0,628	0,328	0,282	0,325	0,376	0,952	0,319	0,373	0,388	0,358	0,372	0,438	0,441	0,599	0,385
79,433	0,214	0,451	0,202	0,190	0,221	0,264	0,739	0,216	0,259	0,257	0,237	0,263	0,285	0,321	0,434	0,290
91,201	0,114	0,308	0,102	0,115	0,153	0,180	0,554	0,147	0,177	0,166	0,137	0,182	0,178	0,228	0,299	0,212
104,713	0,061	0,201	0,027	0,074	0,102	0,104	0,403	0,092	0,107	0,093	0,082	0,113	0,094	0,142	0,196	0,149
120,226	0,011	0,125	0,000	0,019	0,070	0,060	0,288	0,063	0,068	0,057	0,019	0,075	0,054	0,091	0,109	0,088
138,038	0,000	0,079	0,000	0,000	0,048	0,015	0,213	0,022	0,020	0,016	0,000	0,025	0,014	0,028	0,068	0,055
158,489	0,000	0,056	0,000	0,000	0,023	0,000	0,174	0,000	0,000	0,000	0,000	0,000	0,000	0,000	0,025	0,019
181,970	0,000	0,050	0,000	0,000	0,000	0,000	0,165	0,000	0,000	0,000	0,000	0,000	0,000	0,000	0,000	0,000
208,930	0,000	0,056	0,000	0,000	0,000	0,000	0,174	0,000	0,000	0,000	0,000	0,000	0,000	0,000	0,000	0,000
239,883	0,000	0,067	0,000	0,000	0,000	0,000	0,190	0,000	0,000	0,000	0,000	0,000	0,000	0,000	0,000	0,000
275,423	0,000	0,078	0,000	0,000	0,000	0,000	0,203	0,000	0,000	0,000	0,000	0,000	0,000	0,000	0,000	0,000
316,228	0,000	0,084	0,000	0,000	0,000	0,000	0,205	0,000	0,000	0,000	0,000	0,000	0,000	0,000	0,000	0,000
363,078	0,000	0,081	0,000	0,000	0,000	0,000	0,193	0,000	0,000	0,000	0,000	0,000	0,000	0,000	0,000	0,000
416,869	0,000	0,069	0,000	0,000	0,000	0,000	0,164	0,000	0,000	0,000	0,000	0,000	0,000	0,000	0,000	0,000
478,630	0,000	0,053	0,000	0,000	0,000	0,000	0,127	0,000	0,000	0,000	0,000	0,000	0,000	0,000	0,000	0,000
549,541	0,000	0,015	0,000	0,000	0,000	0,000	0,077	0,000	0,000	0,000	0,000	0,000	0,000	0,000	0,000	0,000
630,957	0,000	0,000	0,000	0,000	0,000	0,000	0,044	0,000	0,000	0,000	0,000	0,000	0,000	0,000	0,000	0,000
724,436	0,000	0,000	0,000	0,000	0,000	0,000	0,010	0,000	0,000	0,000	0,000	0,000	0,000	0,000	0,000	0,000
Median size (µm)	5,985	6,518	6,289	5,891	6,779	6,102	7,312	6,357	6,159	6,490	6,402	6,106	6,852	6,208	6,491	6,266
clay	36,735	34,789	34,657	36,904	32,569	36,034	32,660	34,700	35,960	34,604	34,754	36,067	33,583	35,973	34,966	35,430
silt	62,656	63,036	64,807	62,520	66,609	63,103	62,800	64,557	63,170	64,562	64,545	63,037	65,516	62,933	63,518	63,510
sand	0,609	2,175	0,535	0,576	0,822	0,863	4,541	0,743	0,870	0,835	0,701	0,896	0,901	1,094	1,517	1,060

Row group labels: Grain size (µm) · Classif.

Prof. (cm)	384	389	394	399	404	409	414	419	424	429	434	439	444	449	454	459
0,316	0,000	0,000	0,000	0,007	0,007	0,000	0,000	0,000	0,000	0,000	0,000	0,000	0,000	0,000	0,000	0,000
0,363	0,008	0,008	0,008	0,082	0,084	0,052	0,007	0,006	0,007	0,007	0,008	0,008	0,006	0,007	0,006	0,008
0,417	0,288	0,308	0,300	0,399	0,432	0,345	0,264	0,256	0,264	0,268	0,300	0,309	0,245	0,289	0,237	0,315
0,479	0,553	0,587	0,586	0,709	0,720	0,641	0,523	0,518	0,557	0,521	0,602	0,603	0,495	0,581	0,516	0,603
0,550	0,811	0,859	0,866	1,007	0,978	0,927	0,775	0,774	0,836	0,770	0,890	0,884	0,741	0,858	0,781	0,877
0,631	1,044	1,106	1,120	1,273	1,202	1,185	1,004	1,004	1,081	0,995	1,143	1,130	0,964	1,102	1,014	1,115
0,724	1,227	1,299	1,321	1,480	1,374	1,387	1,185	1,186	1,268	1,172	1,336	1,316	1,141	1,286	1,191	1,292
0,832	1,367	1,447	1,476	1,633	1,505	1,540	1,323	1,324	1,404	1,308	1,478	1,452	1,279	1,419	1,321	1,418
0,955	1,469	1,554	1,590	1,739	1,600	1,649	1,424	1,426	1,500	1,409	1,576	1,544	1,382	1,512	1,412	1,501
1,096	1,561	1,644	1,689	1,823	1,683	1,742	1,513	1,515	1,582	1,499	1,661	1,624	1,476	1,592	1,493	1,571
1,259	1,668	1,745	1,800	1,915	1,774	1,844	1,616	1,618	1,682	1,604	1,762	1,718	1,586	1,691	1,592	1,657
1,445	1,822	1,886	1,955	2,047	1,898	1,989	1,763	1,764	1,830	1,754	1,912	1,860	1,744	1,840	1,742	1,791
1,660	2,038	2,081	2,169	2,234	2,062	2,192	1,969	1,968	2,043	1,964	2,127	2,064	1,963	2,055	1,957	1,989
1,905	2,320	2,332	2,446	2,480	2,266	2,454	2,236	2,231	2,321	2,235	2,408	2,331	2,247	2,336	2,240	2,252
2,188	2,646	2,619	2,766	2,765	2,491	2,756	2,547	2,535	2,644	2,550	2,734	2,639	2,577	2,662	2,569	2,562
2,512	2,993	2,921	3,103	3,067	2,719	3,074	2,881	2,858	2,990	2,887	3,083	2,966	2,933	3,010	2,923	2,895
2,884	3,339	3,218	3,435	3,366	2,936	3,390	3,219	3,180	3,336	3,226	3,432	3,292	3,294	3,358	3,279	3,233
3,311	3,667	3,497	3,746	3,649	3,134	3,689	3,546	3,489	3,670	3,552	3,766	3,604	3,646	3,690	3,623	3,562
3,802	3,965	3,747	4,021	3,907	3,308	3,960	3,852	3,774	3,977	3,855	4,072	3,892	3,974	3,995	3,943	3,871
4,365	4,221	3,963	4,249	4,128	3,454	4,193	4,124	4,024	4,249	4,122	4,339	4,146	4,266	4,261	4,226	4,148
5,012	4,435	4,141	4,430	4,312	3,573	4,386	4,362	4,239	4,480	4,352	4,561	4,365	4,516	4,486	4,471	4,389
5,754	4,603	4,282	4,563	4,453	3,665	4,535	4,557	4,413	4,664	4,539	4,734	4,544	4,714	4,665	4,672	4,586
6,607	4,730	4,387	4,652	4,553	3,732	4,642	4,712	4,551	4,803	4,685	4,856	4,685	4,861	4,797	4,829	4,740
7,586	4,810	4,453	4,696	4,606	3,771	4,700	4,820	4,648	4,889	4,784	4,921	4,779	4,946	4,876	4,934	4,842
8,710	4,840	4,474	4,693	4,608	3,777	4,705	4,874	4,698	4,915	4,832	4,922	4,821	4,965	4,896	4,981	4,884
10,000	4,810	4,440	4,635	4,549	3,742	4,648	4,864	4,694	4,872	4,817	4,851	4,798	4,910	4,845	4,958	4,856
11,482	4,707	4,341	4,510	4,421	3,658	4,518	4,779	4,623	4,750	4,729	4,696	4,697	4,772	4,712	4,851	4,747
13,183	4,526	4,173	4,314	4,224	3,523	4,316	4,613	4,480	4,546	4,564	4,460	4,516	4,554	4,499	4,658	4,557
15,136	4,259	3,930	4,040	3,956	3,333	4,039	4,362	4,260	4,257	4,319	4,139	4,248	4,256	4,201	4,374	4,284
17,378	3,920	3,627	3,700	3,636	3,101	3,704	4,039	3,972	3,901	4,008	3,755	3,909	3,900	3,839	4,015	3,944
19,953	3,514	3,273	3,301	3,270	2,833	3,318	3,651	3,620	3,487	3,636	3,319	3,507	3,495	3,422	3,590	3,547

Grain size (µm)

Prof (cm)	384	389	394	399	404	409	414	419	424	429	434	439	444	449	454	459
22,909	3,068	2,895	2,872	2,882	2,548	2,908	3,223	3,225	3,041	3,228	2,861	3,070	3,071	2,981	3,129	3,118
26,303	2,599	2,508	2,430	2,481	2,258	2,485	2,767	2,798	2,578	2,794	2,397	2,612	2,635	2,528	2,648	2,670
30,200	2,135	2,139	2,004	2,085	1,981	2,069	2,308	2,359	2,120	2,356	1,950	2,161	2,209	2,088	2,174	2,223
34,674	1,694	1,797	1,608	1,702	1,729	1,670	1,858	1,922	1,681	1,922	1,531	1,728	1,797	1,671	1,721	1,789
39,811	1,296	1,494	1,258	1,346	1,515	1,303	1,439	1,508	1,280	1,512	1,156	1,333	1,413	1,291	1,309	1,384
45,709	0,957	1,234	0,964	1,028	1,350	0,979	1,065	1,135	0,929	1,139	0,835	0,987	1,066	0,957	0,952	1,022
52,481	0,686	1,021	0,732	0,757	1,239	0,709	0,752	0,819	0,642	0,817	0,575	0,701	0,767	0,678	0,659	0,717
60,256	0,486	0,851	0,559	0,539	1,181	0,497	0,505	0,569	0,421	0,557	0,378	0,477	0,525	0,457	0,435	0,475
69,183	0,342	0,711	0,433	0,371	1,163	0,338	0,320	0,382	0,259	0,356	0,240	0,310	0,336	0,289	0,271	0,293
79,433	0,240	0,590	0,336	0,245	1,163	0,223	0,194	0,250	0,152	0,216	0,136	0,195	0,205	0,173	0,163	0,171
91,201	0,165	0,475	0,251	0,156	1,158	0,146	0,099	0,161	0,075	0,110	0,082	0,105	0,102	0,084	0,084	0,081
104,713	0,098	0,368	0,178	0,083	1,126	0,085	0,054	0,103	0,020	0,029	0,016	0,059	0,027	0,022	0,046	0,021
120,226	0,060	0,272	0,106	0,027	1,054	0,053	0,010	0,066	0,000	0,000	0,000	0,012	0,000	0,000	0,009	0,000
138,038	0,016	0,200	0,067	0,000	0,944	0,015	0,000	0,045	0,000	0,000	0,000	0,000	0,000	0,000	0,000	0,000
158,489	0,000	0,153	0,024	0,000	0,809	0,000	0,000	0,034	0,000	0,000	0,000	0,000	0,000	0,000	0,000	0,000
181,970	0,000	0,133	0,000	0,000	0,672	0,000	0,000	0,032	0,000	0,000	0,000	0,000	0,000	0,000	0,000	0,000
208,930	0,000	0,130	0,000	0,000	0,549	0,000	0,000	0,039	0,000	0,000	0,000	0,000	0,000	0,000	0,000	0,000
239,883	0,000	0,136	0,000	0,000	0,460	0,000	0,000	0,053	0,000	0,000	0,000	0,000	0,000	0,000	0,000	0,000
275,423	0,000	0,140	0,000	0,000	0,411	0,000	0,000	0,077	0,000	0,000	0,000	0,000	0,000	0,000	0,000	0,000
316,228	0,000	0,136	0,000	0,000	0,402	0,000	0,000	0,109	0,000	0,000	0,000	0,000	0,000	0,000	0,000	0,000
363,078	0,000	0,120	0,000	0,000	0,419	0,000	0,000	0,142	0,000	0,000	0,000	0,000	0,000	0,000	0,000	0,000
416,869	0,000	0,086	0,000	0,000	0,440	0,000	0,000	0,165	0,000	0,000	0,000	0,000	0,000	0,000	0,000	0,000
478,630	0,000	0,055	0,000	0,000	0,428	0,000	0,000	0,171	0,000	0,000	0,000	0,000	0,000	0,000	0,000	0,000
549,541	0,000	0,012	0,000	0,000	0,385	0,000	0,000	0,133	0,000	0,000	0,000	0,000	0,000	0,000	0,000	0,000
630,957	0,000	0,000	0,000	0,000	0,212	0,000	0,000	0,053	0,000	0,000	0,000	0,000	0,000	0,000	0,000	0,000
724,436	0,000	0,000	0,000	0,000	0,072	0,000	0,000	0,000	0,000	0,000	0,000	0,000	0,000	0,000	0,000	0,000
Median size (µm)	6,461	6,683	6,174	6,028	7,485	6,122	6,722	6,878	6,387	6,748	6,106	6,421	6,598	6,331	6,600	6,536
clay	34,307	34,293	35,933	37,078	33,425	36,333	33,133	32,881	34,524	33,063	35,857	34,733	33,230	34,821	33,362	34,008
silt	64,896	62,231	62,824	62,177	55,084	62,932	66,309	65,245	65,069	66,360	63,760	64,702	66,226	64,721	66,167	65,538
sand	0,797	3,475	1,242	0,745	11,491	0,736	0,557	1,874	0,407	0,577	0,383	0,565	0,544	0,458	0,470	0,454

APPENDICE C

PHOTOGRAPHIES DE LA CAROTTE HH16-1205-GC

Figure C1 : Photos de la carotte HH16-1205-GC

Figure C2 : Photographies aux rayons-X de la carotte HH16-1205-GC

Figure C1 : Photos de la carotte HH16-1205-GC

Figure C2 : Photographies aux rayons-X de la carotte HH16-1205-GC
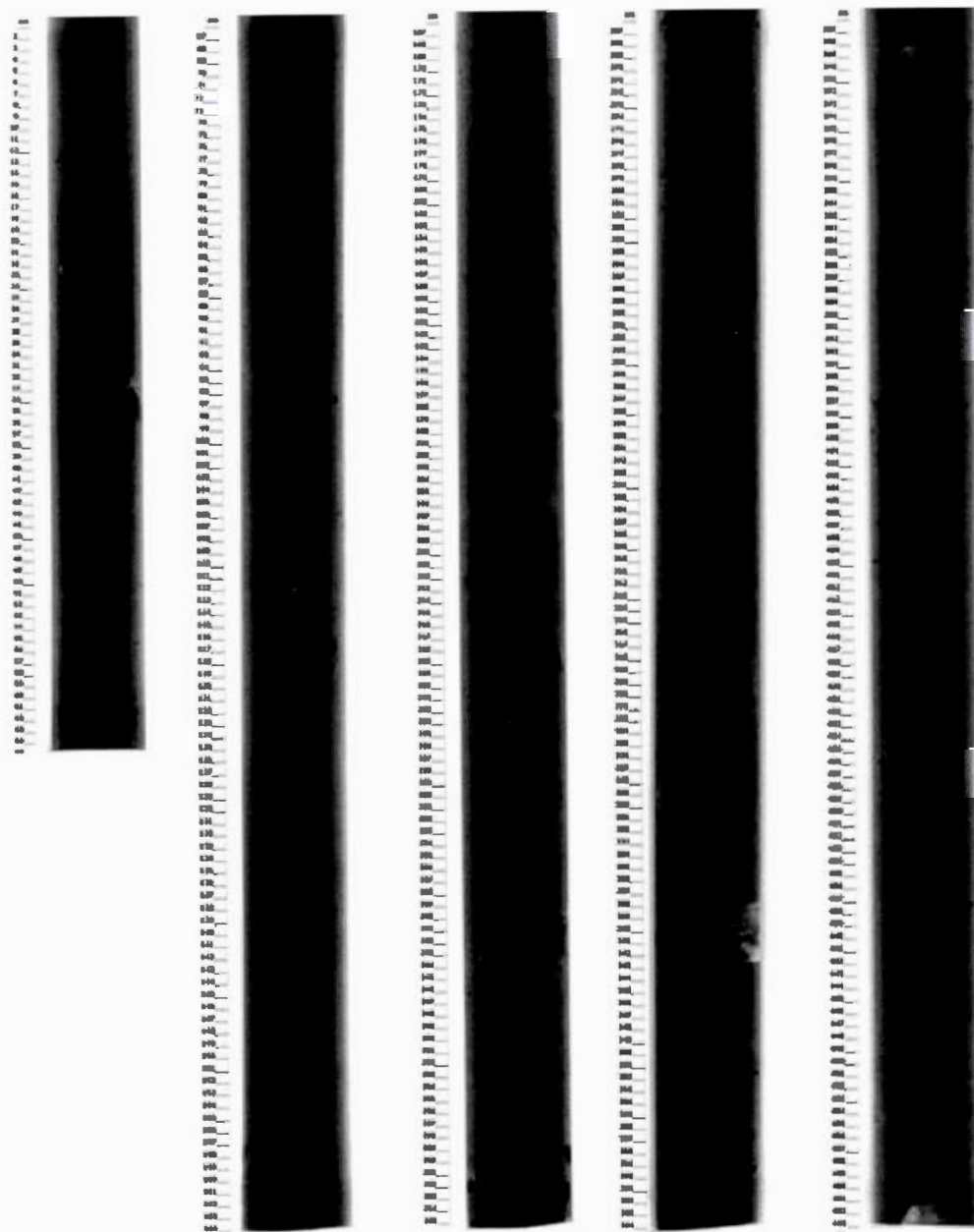
BIBLIOGRAPHIE GÉNÉRALE

Aagaard, K., Swift, J. et Carmack, E. (1985). Thermohaline circulation in the Arctic Mediterranean seas. *Journal of Geophysical Research: Oceans, 90*(C3), 4833-4846.

Baeten, N.J., Forwick, M., Vogt, C. et Vorren, T.O. (2010). Late Weichselian and Holocene sedimentary environments and glacial activity in Billefjorden, Svalbard. *Geological Society, London, Special Publications, 344*(1), 207-223. doi: 10.1144/sp344.15

Bartels, M., Titschack, J., Fahl, K., Stein, R. et Hebbeln, D. (2018). Wahlenbergfjord, eastern Svalbard: a glacier-surrounded fjord reflecting regional hydrographic variability during the Holocene? *Boreas, 47*(4), 1003-1021. doi: 10.1111/bor.12325

Bartels, M., Titschack, J., Fahl, K., Stein, R., Seidenkrantz, M.-S., Hillaire-Marcel, C. et Hebbeln, D. (2017). Atlantic Water advection vs. glacier dynamics in northern Spitsbergen since early deglaciation. *Climate of the Past, 13*(12), 1717-1749. doi: 10.5194/cp-13-1717-2017

Forwick, M. et Vorren, T.O. (2007). Holocene mass-transport activity and climate in outer Isfjorden, Spitsbergen: marine and subsurface evidence. *The Holocene, 17*(6), 707-716.

Forwick, M. et Vorren, T.O. (2009). Late Weichselian and Holocene sedimentary environments and ice rafting in Isfjorden, Spitsbergen. *Palaeogeography, Palaeoclimatology, Palaeoecology, 280*(1-2), 258-274. doi: 10.1016/j.palaeo. 2009.06.026

Forwick, M., Vorren, T.O., Hald, M., Korsun, S., Roh, Y., Vogt, C. et Yoo, K.-C. (2010). Spatial and temporal influence of glaciers and rivers on the sedimentary environment in Sassenfjorden and Tempelfjorden, Spitsbergen. *Geological Society, London, Special Publications, 344*(1), 163-193. doi: 10.1144/sp344.13

Grøsfjeld, K., Harland, R. et Howe, J. (2009). Dinoflagellate cyst assemblages inshore and offshore Svalbard reflecting their modern hydrography and climate. *Norwegian Journal of Geology/Norsk Geologisk Forening, 89.*

Guiot, J. et de Vernal, A. (2011). Is spatial autocorrelation introducing biases in the apparent accuracy of paleoclimatic reconstructions? *Quaternary Science Reviews, 30*(15-16), 1965-1972.

Hald, M., Ebbesen, H., Forwick, M., Godtliebsen, F., Khomenko, L., Korsun, S., Ringstad Olsen, L. et Vorren, T.O. (2004). Holocene paleoceanography and glacial history of the West Spitsbergen area, Euro-Arctic margin. *Quaternary Science Reviews, 23*(20-22), 2075-2088. doi: 10.1016/j.quascirev.2004.08. 006

Hald, M., Salomonsen, G., Husum, K. et Wilson, L. (2011). A 2000 year record of Atlantic Water temperature variability from the Malangen Fjord, northeastern North Atlantic. *The Holocene, 21*(7), 1049-1059.

IPCC. (2014). *Contribution of Working Groups I, II and III to the Fifth Assessment Report of the Intergovernmental Panel on Climate Change.* Dans [Core Writing Team, P., Rajendra K., Meyer, L. A.] (dir.). (IPCC). Geneva

Jorissen, F.J., Fontanier, C. et Thomas, E. (2007). Chapter seven paleoceanographical proxies based on deep-sea benthic foraminiferal assemblage characteristics. *Developments in Marine Geology, 1,* 263-325.

Koç, N., Klitgaard-Kristensen, D., Hasle, K., Forsberg, C.F. et Solheim, A. (2002). Late glacial palaeoceanography of Hinlopen Strait, northern Svalbard. *Polar Research, 21*(2), 307-314. doi: 10.1111/j.1751-8369.2002.tb00085.x

Kucera, M. (2007). Chapter six planktonic foraminifera as tracers of past oceanic environments. *Developments in marine geology, 1,* 213-262.

Ottesen, D., Dowdeswell, J.A., Landvik, J.Y. et Mienert, J. (2007). Dynamics of the Late Weichselian ice sheet on Svalbard inferred from high-resolution sea-floor morphology. *Boreas, 36*(3), 286-306. doi: 10.1111/j.1502-3885.2007.tb01251.x

Rasmussen, T.L., Forwick, M. et Mackensen, A. (2012). Reconstruction of inflow of Atlantic Water to Isfjorden, Svalbard during the Holocene: Correlation to climate and seasonality. *Marine Micropaleontology*, 94-95, 80-90. doi: 10.1016/j.marmicro.2012.06.008

Renssen, H., Goosse, H., Fichefet, T., Brovkin, V., Driesschaert, E. et Wolk, F. (2005). Simulating the Holocene climate evolution at northern high latitudes using a coupled atmosphere-sea ice-ocean-vegetation model. *Climate Dynamics, 24*(1), 23-43.

Serreze, M.C. et Barry, R.G. (2011). Processes and impacts of Arctic amplification: A research synthesis. *Global and planetary change, 77*(1-2), 85-96.

Skirbekk, K., Kristensen, D.K., Rasmussen, T.L., Koç, N. et Forwick, M. (2010). Holocene climate variations at the entrance to a warm Arctic fjord: evidence from Kongsfjorden trough, Svalbard. *Geological Society, London, Special Publications, 344*(1), 289-304. doi: 10.1144/sp344.20

Ślubowska-Woldengen, M., Rasmussen, T.L., Koç, N., Klitgaard-Kristensen, D., Nilsen, F. et Solheim, A. (2007). Advection of Atlantic Water to the western and northern Svalbard shelf since 17,500cala BP. *Quaternary Science Reviews, 26*(3-4), 463-478. doi: 10.1016/j.quascirev.2006.09.009

Svendsen, J.I., Mangerud, J., Elverhøi, A., Solheim, A. et Schüttenhelm, R.T. (1992). The Late Weichselian glacial maximum on western Spitsbergen inferred from offshore sediment cores. *Marine Geology, 104*(1-4), 1-17.

Werner, K., Spielhagen, R.F., Bauch, D., Hass, H.C. et Kandiano, E. (2013). Atlantic Water advection versus sea-ice advances in the eastern Fram Strait during the last 9 ka: Multiproxy evidence for a two-phase Holocene. *Paleoceanography, 28*(2), 283-295. doi: 10.1002/palo.20028